INFORMATION TO USERS

This manuscript has been reproduced from the microfilm master. UMI films the text directly from the original or copy submitted. Thus, some thesis and dissertation copies are in typewriter face, while others may be from any type of computer printer.

The quality of this reproduction is dependent upon the quality of the copy submitted. Broken or indistinct print, colored or poor quality illustrations and photographs, print bleedthrough, substandard margins, and improper alignment can adversely affect reproduction.

In the unlikely event that the author did not send UMI a complete manuscript and there are missing pages, these will be noted. Also, if unauthorized copyright material had to be removed, a note will indicate the deletion.

Oversize materials (e.g., maps, drawings, charts) are reproduced by sectioning the original, beginning at the upper left-hand corner and continuing from left to right in equal sections with small overlaps.

Photographs included in the original manuscript have been reproduced xerographically in this copy. Higher quality 6" x 9" black and white photographic prints are available for any photographs or illustrations appearing in this copy for an additional charge. Contact UMI directly to order.

Bell & Howell Information and Learning
300 North Zeeb Road, Ann Arbor, MI 48106-1346 USA
800-521-0600

DIRECTIONAL ANALYSIS OF AN A–TRAIN DOUBLE WITH DAMPED ARTICULATION

David Vazquez-Vega

A Thesis
in
The Department
of
Mechanical Engineering

Presented in partial Fulfillment of the Requirements
for
the Degree of Master of Applied Science
at
Concordia University
Montreal, Quebec, Canada

February 2000

Abstract

DIRECTIONAL ANALYSIS OF AN A–TRAIN DOUBLE WITH DAMPED ARTICULATION

David Vazquez–Vega

Owing to relaxations in weights and dimensional policies on freight vehicles, the population of heavier and longer articulated vehicles, often referred to as Long Combination Vehicles (LCVs), has steadily increased in North America. The directional stability and control limits of most combinations have been adversely affected by the increase in weights and dimensions, which has prompted many concerns related to operational safety of such vehicles. Particularly, A-trains doubles, which belong to the classification of LCVs, exhibit larger magnitude oscillations in both lateral and yaw motions under directional maneuvers, which limit their directional dynamic performance at highway speeds. Two concepts in damped articulations are formulated and their potential benefits or limitations in enhancing the dynamic behavior of A-train doubles are investigated in terms of different performance measures, which are evaluated under both open and closed-loop maneuvers. These concepts are based upon articulation dampers introduced between the first semitrailer (unit 2) and the A-dolly (unit 3), referred to as Case I, and between the first and second semitrailer (units 2 and 4), referred to as Case II. A nonlinear yaw-plane analytical model of the A-train double incorporating the articulation dampers is formulated. Damping forces and moments acting on each of the units involved are derived from a comprehensive kinematic analysis of the damped articulation mechanism. The strongly nonlinear cornering properties of tires are effectively characterized using the functional Magic Formula approach. An analytical function based upon the Magic Formula is further derived to describe the path coordinates for closed-loop directional maneuvers. A simple path-follower driver-vehicle model is formulated using the preview strategy in conjunction with the path coordinates function to perform the closed-loop maneuver.

A set of performance measures is selected for objective assessment of potential performance benefits of the proposed damped articulation concepts. The equations of motion obtained from the analytical model are numerically solved for different directional maneuvers to derive the suggested performance measures. The performance characteristics of an A-train double are initially analyzed to examine the feasibility of the proposed concepts and the influence of damping coefficients. The results of this preliminary analysis suggested that the damped articulation between units 2 and 3 (Case I) offers considerable potentials for enhancement of directional performance of an A-train double. Further parametric studies are performed to derive suitable geometric parameters of the connecting dampers.

The potential performance benefits of the proposed damped articulation concept are assessed by comparing the performance measures evaluated for an A-train double with damped articulation with those evaluated for the conventional vehicle. The comparison revealed that the transient directional dynamics of an A-train double, specifically the rearward amplification, peak lateral acceleration and transient off-tracking, can be considerably enhanced through the use of damped articulations.

Acknowledgment

This dissertation research is the result of collaborative efforts of CONCAVE Research Center, Concordia University, and Instituto Mexicano del Transporte (IMT), Querétaro, México. Special thanks are therefore due to Ing. Alfonso Rico for creating this opportunity. I would like to express my sincere thanks Drs. S. Rakheja, A.K.W. Ahmed, Alejandro Lozano, Miguel Martinez, and Mr. Francisco Carrion for providing me with continued technical support, guidance and motivation to carry out this work.

I would also like to thank all the graduate students, faculty members and staff at CONCAVE Research Center for providing me with a friendly working environment during the course of this research, and to my friends at IMT for their sustained moral support.

My sincere thanks to my family for their love and unconditional support during the pursuit of this work.

Contents

List of Figures

List of Tables

Nomenclature

a	Either projection along the longitudinal axis passing through CG of units 2 and 3 of the distance between damper mounts K and L or M and N (m), Case I (Figure 2.2), or projection along the longitudinal axis passing through CG of units 3 and 4 of the distance between damper mount L and joint C (m), Case II (Figure 2.3)
A	Articulation joint between units 1 and 2 of the A-train double
a_{yi}, A_{yi}	Lateral acceleration of unit i (m/s^2)
b	Distance between damper mounts L and N and the longitudinal axis passing through CG of unit 3 (m), Case I (Figure 2.2), or distance between damper mounts L and N and the longitudinal axis passing through CG of unit 4 (m), Case II (Figure 2.3)
B	Magic Formula coefficient: Stiffness factor
B	Articulation joint between units 2 and 3 of the A-train double
c	Distance between damper mounts K and M and the longitudinal axis passing through CG of unit 2 (m), Cases I and II (Figures 2.2 and 2.3)
C	Magic Formula coefficient: Shape factor
C	Articulation joint between units 3 and 4 of the A-train double
CG	Center of gravity
$\mathbf{C_{KL}}$, $\mathbf{C_{MN}}$	Viscous damping coefficients of dampers 1 and 2 (N-s/m)
C_{Sij}	Longitudinal stiffness of a tire on axle ij (N/unit slip)

D	Magic Formula coefficient: Peak factor
D1, D2	Instantaneous axial distances of dampers 1 and 2 (m)
E	Magic Formula coefficient: Curvature factor
F_{2X}, F_{3X}, F_{4X} F_{2Y}, F_{3Y}, F_{4Y}	Components of the constraints forces acting along the body-fixed axis system of the following units (N)
F_{AX}, F_{BX}, F_{CX} F_{AY}, F_{BY}, F_{CY}	Components of the constraints forces acting along the body-fixed axis system of the leading units (N)
F_{ij}	Lateral cornering force at the j-th axle of the i-th unit (N)
F_K, F_L, F_M, F_N	Forces developed by dampers at their corresponding mountings (N)
F_{KL}, F_{MN}	Damping forces developed by dampers 1 and 2 (N)
F_{Zij}	Normal load on the tire of the j-th axle of the i-th unit (N)
H(s)	Transfer function describing the driver dynamics in the driver-vehicle model
HOF	Steady-state high-speed offtracking (m)
g	Acceleration due to gravity (m/s^2)
G(s)	Function describing the dynamics of the A-train double vehicle
I_i	Yaw mass moment of inertia of i-th units ($kg\text{-}m^2$)
K_p	Constant gain of driver-vehicle model (rad./s)
K	Mounting of damper 1 on unit 2
Ku_i	Understeer coefficient of i-th unit (deg.)
$(Ku_{cr})_i$	Critical understeer coefficient of i-th unit (deg.)
L	Mounting of damper 1 on either unit 3, Case I, or unit 4, Case II
m_i	Mass of i-th unit (kg)

M	Mounting of damper 2 on unit 2
M_{ij}	Total aligning moment from the j-th axle of i-th unit (N-m)
$(M_{ij})_{DT}$	Aligning moment due to dual tire from the j-th axle of i-th unit (N-m)
$(M_{ij})_{PT}$	Self-aligning moment due to pneumatic trail from the j-th axle of i-th unit (N-m)
N	Mounting of damper 2 on either unit 3, Case I, or unit 4, Case II
P(s)	Preview control strategy used to estimate the future lateral position of unit 1 of the A-train in the driver-vehicle model
r_i	Yaw rate of i-th unit of the A-train double (deg./s)
RWA_{LA}	Rearward amplification of lateral acceleration
RWA_{YW}	Rearward amplification of yaw rate
s	Laplace operator
S_h	Offset in the input variable of the Magic Formula
S_v	Offset in the output variables of the Magic Formula
SP1, SP2 SP3, SP4	Parameters for defining piecewise linear approximation of desired path-change maneuvers (m)
TOF	Transient high-speed offtracking (m)
t	Time (s)
T	Preview interval for driver-vehicle model (s)
T_s	Simulation time (s)
U_i	Forward speed at the CG of i-th unit of the A-train double (km/h)
$(U_{cr})_i$	Critical forward speed of the i-th oversteer unit of the A-train double (km/h)
V_i	Lateral velocity at the CG of the i-th unit of the A-train double (m/s)
V_K, V_L,	Instantaneous resultant velocities along the axis of dampers 1 and 2, at the damper mounts, K, L, M, N, (m/s)

V_M, V_N	
V_{KL}, V_{MN}	Relative velocities across dampers 1 and 2, between damper mounts K and L for damper 1 and damper mounts M and N for damper 2, (m/s)
WB_i	Wheelbase of the i-th unit of the A-train double (m)
X_{ij}	Longitudinal distance between CG of unit i and its corresponding j-th axle (m)
X_{1A}, X_{2A}	Longitudinal distances between units 1 and 2 and articulation joint A (m)
X_{2B}, X_{3B}	Longitudinal distances between CG of units 2 and 3 and articulation joint B (m)
X_{3C}, X_{4C}	Longitudinal distances between CG of units 3 and 4 and articulation joint C (m)
YDR	Yaw Damping Ratio
$y_1(t)$	Current absolute lateral position of unit 1 (m)
$y_1(t+T)$	Estimated absolute lateral position of unit 1 in the driver-vehicle model (m)
y_{DT}	Half-spacing of dual tire set (m)
$Y_p(t+T)$	Desired absolute lateral position of CG of unit 1(m)
$\dot{y}_1(t)$	Current absolute lateral velocity of CG of unit 1 (m/s)
$\ddot{y}_1(t)$	Current absolute lateral acceleration of CG of unit 1 (m/s^2)
α_{ij}	Side-slip angle of the j-th axle of i-th unit of the A-train double (rad.)
β_1, β_2	Instantaneous angles defining the orientation of dampers 1 and 2 with respect to unit 2 for Case I (rad.)
γ_j	j-th articulation angles (rad.)
δ	Logarithmic decrement
δ_f	Steering angle at the front wheels of unit 1 of the A-train double (deg.)

$\varepsilon(t+T)$	Error function describing the estimated lateral deviation in the driver-vehicle model (m)
$\zeta_1,\ \zeta_2$	Instantaneous angles defining the orientation of dampers 1 and 2 with respect to either unit 3, for Case I, or unit 4, for Case II (rad.)
$\theta_1,\ \theta_2$	Instantaneous angles defining the orientation of dampers 1 and 2 with respect to unit 2 for Case I (rad.)
τ	Transport lag for driver-vehicle model (s)
$\psi_1(t)$	Heading angle of unit 1 (deg.)

Chapter 1

Introduction and Literature Review

1.1 General

The increasing demand on operating efficiency and productivity of heavy-duty vehicles has resulted in increasing allowable length and weight of such vehicles, which has raised concerns over highway safety and conservation of highway infrastructure. The size and weight policies related to these vehicles have been relaxed during the past three decades, thus allowing longer and heavier trucks. Numerous research and development efforts have thus been directed to realize effective design characteristics and configurations of heavy vehicles to address the concern related to their operational safety and potential infrastructure damage. For example, the use of multiple axle semitrailers has been increasing in order to carry heavier loads and to reduce the infrastructure damage. Moreover, long combination vehicles (LCVs), which consist of a tractor and trailer combination groups, have been growing considerably. A trailer combination group may consist of either a double or triple trailer combination, with an overall length up to 37 m (120ft) and a gross combination weight (GCW) up to 60840 kg (134,000lb).

The transportation efficiency and productivity is not only related to the load carrying capacity of the vehicle, but also its directional dynamic performance characteristics, which directly relate to the safety performance of the vehicle. It has been established that increase in trucks sizes and weights strongly influences the vehicle stability limits and directional dynamics performance in an adverse manner. The LCVs, specifically, are known to exhibit lower yaw and roll stability limits, and poor emergency maneuverability characteristics. Many studies on directional dynamics of heavy vehicle combinations have evolved into a number of performance measures for assessment of their dynamic safety characteristics. The proposed performance measures address the vehicle rollover, handling, yaw instability, offtracking, rearward amplification tendencies, etc.

The most common configuration of LCVs used in both North America is the so-called, A–train double. This combination uses a dolly with one drawbar to connect the two semitrailers, as shown in Figure 1.1. It is known that maneuverability of the tractor–semitrailer combination of an A–train double is practically unaffected by the presence of the full-trailer. In an emergency maneuver, however, the second semitrailer of the combination may significantly amplify the lateral motion of the tractor. This effect is known as the rearward amplification and is generally recognized as the most important property of the A–train double combination. High magnitude of rearward amplification may yield premature rollover of the second unit, and excessive dynamic off-tracking of the combination.

Apart from the significant rearward amplification, the A-train double combination exhibits considerable yaw oscillation of the second unit, primarily due to low articulation

damping. Under emergency maneuvers performed at highway speeds, such oscillations may cause yaw instabilities and rollover of the rearmost semitrailer. Such instabilities may also occur under extreme external disturbances.

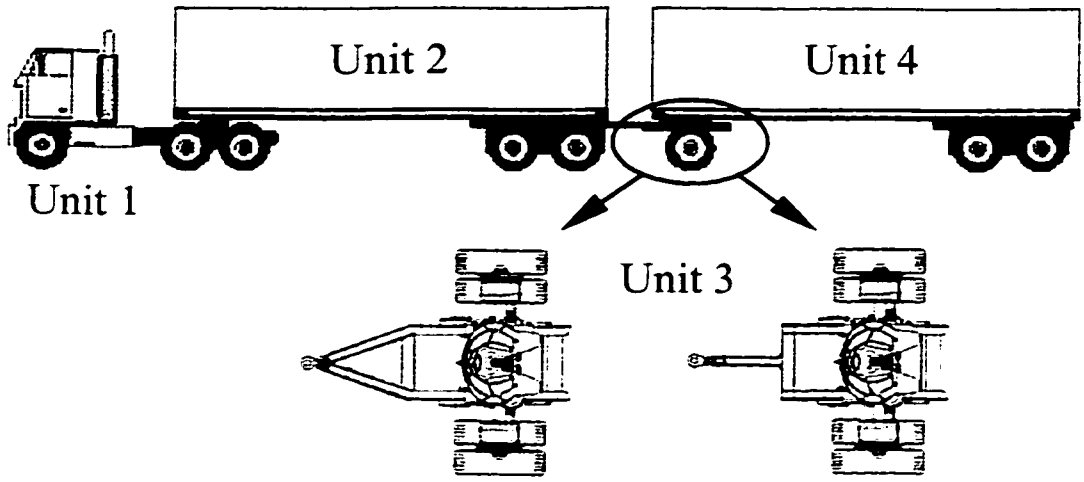

Figure 1.1: Schematic of an 8-axle A-train double combination and single-axle A-dollies [1].

This dissertation describes the potential yaw instabilities of an A-train double combination, specifically the rearward amplifications tendencies. A design concept based upon external articulation damping is proposed and investigated to enhance the directional dynamics performance of the combination. The potential performance benefits of the proposed concept are evaluated in terms of various performance measures, such as understeer coefficient (a measure of vehicle handling), rearward amplification, yaw damping ratio, and offtracking. Two different mechanisms, namely, damped articulation mechanism between first semitrailer and A–dolly (units 2 and 3), and damped articulation mechanism between first and second semitrailers (units 2 and 4), are

proposed. Analytical models of the combination vehicle with different damped articulation concepts are developed incorporating geometric nonlinearities of the damping mechanism and nonlinear cornering properties of the tire. A driver path follower model is developed and integrated within the vehicle model to permit directional dynamics analysis of the closed-loop driver-vehicle system.

1.2 Classification of LCVs and its Coupling Mechanisms

Long combination vehicles (LCVs) are heavy vehicle combinations that consist of a tractor–semitrailer combination that is attached to one full–trailer. The total vehicle combination is thus referred to as a double. LCV may also consist of a tractor–semitrailer combination and two full–trailers, which is often referred to as a triple. A full-trailer may consist of a semitrailer supported on a single or double-axle dolly via either a fifth wheel or a turntable. A full–trailer is frequently attached to the leading unit via either one or two pintle hooks. Each pintle hitch incorporates a draw bar and a hook–and–eye arrangement to couple the leading and following units.

LCVs can be identified with specific names such as A–train, B-train or C–train, based upon the type of coupling system used. For A-trains and C-trains, this coupling system is referred to as a "dolly". Two types of dollies are thus mainly used in the freight transportation industry, namely, A–dolly and C–dolly, which may be supported by either one or two axles. A schematic of single and double-axle C-dolly is illustrated in Figure 1.2. When a LCV, either double or triple, consists of A–dollies, the combination is referred to as an A–train, while the combination composed of C–dollies is referred to as a

C–train. An A–dolly attaches the following unit to the leading unit via one pintle hook-eye combination and a drawbar, whereas a C–dolly joins leading and following units via two pintle hook-eyes combinations and two drawbars. Figure 1.1 illustrates a schematic of an 8–axle A–train double together with two different designs of A-dollies.

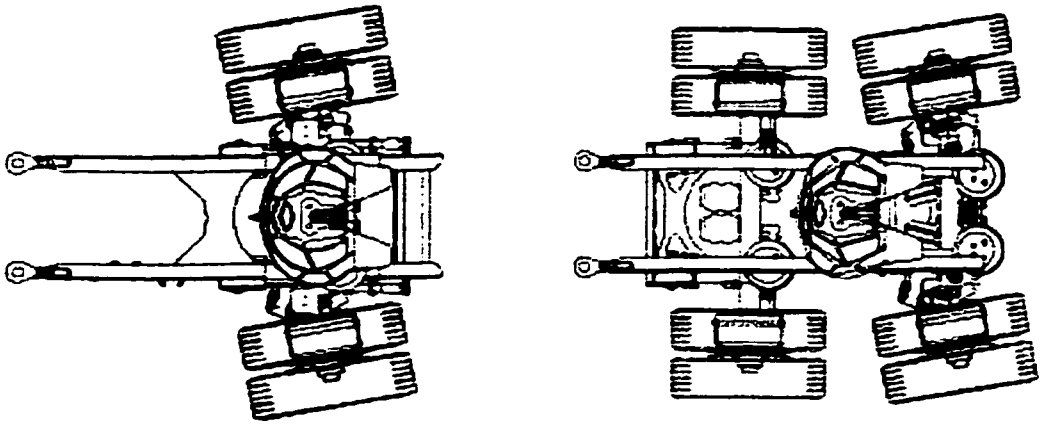

Figure 1.2: Schematic of an single and double-axle C-dollies.

The directional dynamic performance of a vehicle combination is strongly affected by the properties and motion constraints imposed by the coupling mechanism, and the degrees-of-freedom of motion allowed between the coupled units. These coupling mechanisms include fifth wheel, inverted fifth wheel, kingpin, turntable, and pintle hitches. Each of these mechanisms offers specific mechanical properties and constraints.

In A-train combinations, the unit leading the a-dolly is equipped with one pintle hook, whereas the unit leading the C-dolly, in C-train combinations, is equipped with two pintle hooks. Examples of pintle hooks are shown in Figure 1.3. In general, these hitches consist of a hook and a locking mechanism, which engages with the towing-eye attached

to the drawbar of the dolly. Figure 1.4 illustrates some examples of the towing-eyes. A pintle hook thus supports and tows the dolly via the towing-eye. A single hook–eye combination, employed in an A-dolly, results in a joint that allows articulation in all directions. An A–dolly is thus free to articulate in yaw (steering), pitch (fore–aft rotation), and roll (side–to–side rotation) with respect to the leading unit. On the contrary, a C–dolly, employing a double drawbar, provides articulation in pitch only, while the relative yaw and roll articulations with respect to the leading unit are eliminated.

Figure 1.3: A pictorial view of pintle hooks [1].

Figure 1.4: A pictorial view of towing-eyes [1].

An A–train double thus comprises of 3 articulation points, namely, two fifth wheels and the hook–eye combination, while a C–train double yields only two articulation points arising from two fifth wheels. The triple combinations of A– and C–trains posses five and three articulation points, respectively.

The fifth wheel and turntable type coupling mechanisms primarily allow relative yaw motion of the coupled units, with only minimal pitch and roll motions [2]. These coupling mechanisms are located on the frame of the leading unit (tractor or dolly), while

the following unit comprises a kingpin, which allow the both coupled units to yaw relative to each other. Turntables are rigidly attached to the dolly frame and thus allow only a yaw motion between the coupled units [3]. A dolly equipped with a turntable is frequently referred to as fixed dolly, while a dolly equipped with a fifth wheel is called a converter dolly [4].

1.3 Review of Previous Investigations

Dynamic performance of heavy vehicles, and in particular LCVs, involves various issues, such as stability, control, handling, and maneuverability. These dynamic performances are widely used to derive a number of direct performance measures related to highway safety performance, such as rearward amplification, load transfer ratio, rollover threshold and path-offtracking. Comprehensive studies on the dynamics of heavy vehicles have been conducted by a number of researchers during the past three decades. Vlk [5] presented an extensive review of reported studies that concern lateral dynamics of commercial vehicle combinations and concluded that only few studies address the directional dynamics concerns for such vehicles. Owing to the relaxation on policies on the sizes and weights of heavy vehicles, single units and tractor–semitrailer combinations have evolved into relatively more complex combinations, such as doubles and triples. These new vehicle combinations impose new challenges to designers concerning the safety–related performance of such vehicles. The directional dynamics analysis of LCVs, in general, involves characterization of vehicle components, vehicle configuration and coupling mechanisms, development of analytical models, analysis leading to directional

performance, field assessments, and interpretations. The reported studies related to these aspects are briefly reviewed and discussed in this section to formulate the scope of this dissertation research.

1.3.1 Directional Dynamic of LCVs

Directional dynamics of LCVs are investigated to derive their handling, directional control and directional stability characteristics under transient and steady steering maneuvers. During the application of a steering input and the achievement of steady–state motion, the vehicle undergoes a transient state. The overall handling quality of a vehicle depends, to a great extent, on its transient behavior. The inertial properties of the vehicle must be taken into consideration when the transient response is analyzed. Furthermore, the vehicle combination undergoes translational as well as rotational motions during a directional maneuver. The steady-state handling performance of a vehicle is concerned with its directional behavior during a turn under time invarying conditions. The steady–state directional dynamic response determines the vehicle handling and rollover immunity under steady turning maneuvers, whereas the transient directional dynamic response is concerned with roll and yaw instabilities under transient maneuvers, such as single path-change and double path-change maneuvers. Simultaneous applications of steering and breaking inputs may cause yaw instabilities of the vehicle, which are related to jackknife and trailer swing.

Huber and Dietz [6], and Dietz [7,8] perhaps performed the earliest documented research on the directional dynamic performance of tractor-semitrailer combination.

Their experimental studies involved testing of scale models of laterally constrained trailers, on an endless moving belt and was specially focused on the lateral stability of straight running vehicle configurations with two-axle trailers equipped with either turntable or Ackerman steering. The study concluded that the trailer yaw oscillations could be most effectively suppressed by introducing viscous damping within the turntable. Their experiments also showed that coulomb damping within the turntable had undesirable results; the same kind of damping, however, introduced within the hitch had quite favorable effects. This experimental study was followed by a complementary theoretical effort by Ziegler [9,10], which assumed the tire forces as coulomb damping alone. Almost two decades after Ziegler's research, Laurien [11] investigated the directional stability of tractor–semitrailer vehicles, and concluded that the trailer yaw oscillations could be most effectively suppressed by introducing coulomb damping at the hitch and at the trailer steering mechanism. A trailer with Ackerman steering was observed to be more prone to lateral oscillations than a trailer with the turntable steering.

Both static and dynamic stability of heavy articulated vehicles are important issues to be considered when evaluating the behavior of LCVs. Nalecz and Genin [12] presented a review of published literature on analytical modeling of heavy truck behavior, specifically addressing the dynamic stability of heavy articulated vehicles. The study presented a comprehensive review in terms of undesirable response characteristics of heavy commercial vehicles and modeling of pneumatic tire for dynamic simulations. The undesirable response characteristics of heavy vehicles were grouped in four different classes including loss of control during breaking, directional instability during cornering, roll instability, and amplified directional motions occurring with full–trailers. Fancher

[13] investigated the static stability of commercial vehicles, referred to as an aperiodic divergence such as that attained by an oversteer automobile operating above its critical speed.

The directional performance characteristics of LCVs are primarily analyzed with specific considerations of the multiple axles and articulation points. Fancher [14] presented an overview of technical considerations pertaining to the directional mechanics of multi–articulated heavy trucks employing multiple axle suspensions. The study analyzed the directional dynamics of B–train configurations as well as full–trailers with conventional dolly, specifically the A–dolly. The study reported various factors influencing the directional performance characteristics of heavy truck combinations, such as the tire cornering stiffness, wheel locations, suspension roll stiffness, steering system compliance, and frame stiffness. From the results, it was concluded that the lateral constraint force at the pintle hitch of a typical A–dolly is relatively small, and that the forced directional response of vehicles employing full–trailers can involve large amounts of rearward amplification.

In view of considerable rearward amplification tendencies of A–train doubles, a number of theoretical and experimental studies have been performed to study the directional behavior of A-train doubles. Billing [15] performed full–scale tests to compare the directional behavior of both A– and B–train double configurations. The test consisted in evaluating the roll stability due to single path-change and double path-change maneuvers. Parameters such as free play of trailer suspension springs and dolly hitch length were changed during the tests to study their contributions to the combination's roll stability. The study concluded that a B–train was dynamically more

stable than an A–train, when comparing the rollover threshold and rearward amplification tendencies of the vehicles. It was further concluded that variations in free play of trailer suspension springs and hitch length do not affect the rollover stability significantly. Winkler and Bogard [16] developed a series of simple equations, based upon linear regression techniques, to predict certain performance measures of A–train double combination vehicles based on descriptive parameters of the vehicle. Billing and Mercer [17] evaluated the directional dynamic performance of A–train double and concluded that the vehicle was quite responsive, with a rearward amplification of lateral acceleration of about 1.80. The directional stability of the combination was thus considered relatively poor. Furthermore, the stability of the combination clearly deteriorated at the highway speed limit. Therefore, the A–train double configuration is considered undesirable because of its low stability at highway speeds.

Nordstrom et al. [18] developed vehicle dynamic simulation programs to study the lateral and roll stability of heavy vehicles, including tank trucks. Several full–scale tests were performed to evaluate the dynamic performance of heavy vehicles and to validate the simulation programs. In addition, a comprehensive computer program was also developed to simulate the directional dynamics of LCVs, which had up to three articulation points and a maximum of nine axles [19]. The eight–degrees–of–freedom analytical model was developed assuming linear suspension springs, while the interactions between longitudinal tire forces, and pitch and lateral load transfer were neglected [20]. Based upon the simulation results for a lane change maneuver, it was concluded that LCVs with long wheelbase, low normal load on the tires, short distance between truck rear axle and the hook-eye combination (overhang) could achieve a

satisfactory lane change performance. A longer drawbar, however, yields large amplitudes of lateral oscillations.

El–Gindy [21] and Tong et al. [22] carried out full–scale tests and computer–based analysis of the dynamic performance of common Canadian log–hauling trucks. They evaluated performance measures such as rearward amplification ratio, load transfer ratio, transient high–speed offtracking, static rollover threshold, understeer coefficient, and low–speed friction demand. A nonlinear yaw–roll model was used to assess the dynamic performance, and a good agreement between the simulation results and measurements was obtained.

Owing to the increasing use of commercial articulated vehicles, concerns on their safety in operation have been growing. As a result, comprehensive studies, based on the development of various computer simulation models for the dynamic performance prediction of articulated vehicles, have been published. These comprehensive computer simulation models have taken into account nonlinear tire models since the directional dynamics of a vehicle configuration is strongly related to the forces and moments generated at the tire–road interface [23]. A comprehensive three–dimensional simulation program, referred to as yaw–roll model, was developed by the Road and Transportation Association of Canada (RTAC) and the University of Michigan Transportation Research Institute (UMTRI) to evaluate roll, yaw, and lateral directional response characteristics of heavy vehicle combinations, which include up to 4 units and 11–axle LCVs and different articulation mechanisms [24]. This simulation program incorporated nonlinear cornering characteristics of tires, nonlinear suspension forces, and closed–loop driver model, while the forward speed was assumed to be constant.

El–Gindy and Wong [25] performed a comprehensive study of different computer simulation programs involving different levels of complexity to predict the directional response of commercial articulated vehicles in steady–state and lane–change maneuvers. The study was focused on four of the better known simulation models, namely, linear yaw–plane model, the TBS[1] model, the yaw–roll model, and the Phase 4 model developed at UMTRI. The study concluded that a more sophisticated simulation model, such as the Phase 4 model, does not necessarily yield more accurate predictions, in quantitative terms, than a simpler model, such as the TBS or linear yaw–plane model, under certain circumstances. The study showed that the transient steering response characteristics of a tractor–semitrailer in a lane–change maneuver predicted using the four simulation models are qualitatively similar. Nevertheless, when compared with available measured data, all the simulation programs revealed discrepancies of varying degrees. The study proposed that in view of the complexities in simulation models and actual measures, it is important to select a simulation model appropriate for a specific task. The study further suggested that a comprehensive parametric sensitivity analysis of the sophisticated models may be useful.

It has been recognized that LCVs exhibit certain unique dynamic characteristics that can limit their stability and emergency maneuverability characteristics. A limited number of studies have attempted to enhance the performance characteristics of some of the LCV configurations. Winkler [26] proposed concepts in innovative dollies and evaluated their performance through computer simulation and full–scale tests. The need

[1] TBS is a simplified non-linear mathematical model, originally formulated by Leucht. The basic assumptions of this model are similar to those for the linear yaw plane model, but non-linear tire model and dynamic load transfers are introduced.

to develop commercial vehicle dollies that can significantly improve the dynamic performance of multi–trailer combination vehicle was emphasized. The study suggested the use of four innovative dollies, namely, the trapezoidal dolly, the linked–articulation dolly, the self–steering B–dolly, and the controlled–steering B–dolly. Although Rakheja et al. [27] introduced a concept of articulation damping that is applied to a tractor–semitrailer combination, the same concept has not been applied to study the potential performance benefits for LCVs. The study investigated the influence of damped articulations on the magnitudes of yaw and lateral oscillations of a tractor–semitrailer combination, which is subjected to directional maneuvers. Kageyama and Saito [28] proposed an active trailer steering system for enhancement of stability performance of articulated vehicles at high speeds. The study proposed a new trailer steering system with viscous coupling arms to be set between the tractor and the trailer, similar to that proposed by Rakheja et al. [27].

1.3.2 Performance Measures Related to Directional Dynamics

In view of the growing highway safety concerns related to directional dynamics performance of LCVs, many analytical and experimental studies have been performed in recent years to quantify and assess the safety performance of heavy vehicles [29, 30, 31, 32, 33]. Winkler et al. [29] concluded that rearward amplification is an effective performance measure for qualifying the vehicle performance in obstacle–avoidance maneuvers, which is strongly influenced by the roll characteristics of the vehicle. A

number of screening procedures have also been proposed for LCVs to provide weight limits based upon vehicle dimensions and articulation arrangements. El–Gindy [30] presented a review of some existing performance measures, and proposed additional performance measures to assess certain issues that had not previously addressed. Nix et al. [31] presented a summary of a workshop on performance–based regulations for truck size and weight. Three specific issues, namely, implementation of performance–based size and weight limits, vehicle stability and control, and vehicle–pavement interaction were addressed in the workshop. The vehicle stability and control performance is described through four essential performance attributes relevant to safety: roll stability, rearward amplification, low–speed offtracking, and high–speed offtracking. Sweatman [32] indicated that Australian road trains and North American long combination vehicles, such as doubles and triples, are the worst vehicles in view of rearward amplification performance. Sweatman [32] further stated that stability performance varies significantly between various countries' typical vehicles, and that stability performance has thus not been controlled in any effective way though the engineering performance of trucks has been researched extensively in Europe. A draft proposal has been prepared for the testing of lateral stability of trucks, which incorporates various criterions, including rearward amplification and yaw damping ratio. Blow et al. [33] utilized the analytical approach to evaluate the safety measures from the perspective of stability and control performance of several truck configurations. The performance measures evaluated, using simulation models, included static roll stability, rearward amplification, load transfer ratio, low–speed offtracking, high–speed steady–state offtracking, transient high–speed offtracking, and steering axle friction demand. El–Gindy [30] has summarized eight

different stability and control measures, which emerged from his general review. These performance measures are further summarized below:

1. Handling performance measure, to assess the relative handling quality of the vehicle.

2. Static rollover threshold (SRT), to assess the rollover limits of heavy vehicles under steady turns.

3. Dynamic rollover stability in terms of Load Transfer Ratio (LTR) and Rearward Amplification (RWA), to assess the dynamic roll stability limits under transient maneuvers.

4. Yaw Damping Ratio (YDR), to assess the rate of decay of yaw oscillations of the trailer.

5. Friction demand of the drive–axle tires, to assess the low and high–speed jackknife potentials of vehicle combinations.

6. Lateral friction utilization, to characterize the highest level of lateral friction utilization of a group of axles of a vehicle during low– and high–speed turn maneuvers.

7. Offtracking, including low–speed offtracking (LOF), steady–state high–speed offtracking (HOF), and transient high–speed offtracking (TOF), to assess the maneuverability at tight intersections, and safety risk on the highways.

8. Breaking performance, to assess the breaking efficiency, stopping distance, brake time response and jackknife potentials of LCVs.

1.4 Scope of the Thesis and Layout

From the literature review, it is apparent that extensive efforts have been made to enhance and to understand the directional stability and control performance of articulated vehicles. Some of the heavy vehicle configurations, mainly the LCVs, however, imply complex designs that directly affect the directional stability and control performance.

While the reported studies mostly focus on the dynamics of straight trucks and tractor-semitrailer combinations, the dynamics of LCVs, such as A-trains, have been addressed in few studies. Earlier studies have described the importance of articulation damping in reducing the yaw and lateral oscillations of tractor–semitrailer combinations, the potential performance benefits of damped articulations, however, have not been explored for LCVs. Although the A-train double configurations are considered undesirable due to their lower stability limits at highway speeds, they continue to remain popular due to their relatively good maneuverability [17]. It has been reported that approximately 74% of all LCVs used in Canada are A-trains, 22% are B-trains, and remaining are C-trains and triples [34], while in the U.S. over 99% of the LCVs are A-trains [1]. A transition from the existing A–train combination to any other configuration may not thus occur due to economical reasons. While comprehensive vehicle–dynamics analysis programs have been developed during the past few decades, the programs do not emphasize upon the contribution due to articulation damping.

The primary objective of this study is thus formulated to investigate the potential performance benefits of articulation damping in terms of directional control and maneuverability performance of an A–train double. Two different concepts in articulation damping are proposed and investigated, namely, damped articulation mechanism between the first semitrailer and the A–dolly, and damped articulation mechanism between first and second semitrailers. The specific objectives of the study are:

1. To develop an analytical model of an LCV (A–train double) with and without damped articulations to study its yaw and lateral dynamic response.

2. To formulate analytical models describing the nonlinear lateral force and alignment moment developed by the tires.

3. To formulate kinematic models of the proposed damped and undamped articulation mechanisms.

4. To investigate the yaw and lateral dynamics of the LCV under different steering maneuvers with and without damped articulations.

5. To investigate the dynamic performance measures of the LCV and quantify the potential performance enhancement due to damped articulations.

In Chapter 2, a nonlinear yaw-plane analytical model of an A-train double combination incorporating damped articulation is developed. Two concepts of damped articulations, namely, articulation dampers introduced between units 2 and 3 (Case I), and articulation dampers introduced between units 2 and 4 (Case II), are proposed to study their potential benefits in the response of an A-train double. A comprehensive kinematic model of the dampers is further developed. The nonlinear cornering forces and aligning moments developed by the tires are introduced in the yaw-plane model. The Magic Formula approach for predicting the cornering properties of the tire in terms of vertical load and side-slip angles is used. Geometric nonlinearities arising from the damped articulations are identified from the kinematic analysis and incorporated within the yaw-plane model of the A-train double combination for each of the proposed damped articulation concepts.

In Chapter 3, a set of performance measures are selected to evaluate the dynamic behavior of the fully-loaded A-train double combination. Each of these performance measures is described and specific methods of analysis are presented. Both open loop and closed-loop directional maneuvers to assess the performance measures are described.

Furthermore, a method to describe closed-loop maneuvers through continuos functions is proposed. A predictive/preview model is presented to compute the front wheel steer angle necessary in order to follow the required closed-loop maneuver. In addition, the parameters of the driver-vehicle model needed to perform the single path-change maneuver are computed and adjusted to achieve desired path tracking performance.

In chapter 4, a set of weights and dimensional parameter of the candidate A-train double vehicle is presented, and the Magic Formula approach is applied to predict lateral forces and self-aligning moments generated by tire as a function of vertical load and side-slip angles. A feasibility analysis of the two proposed concepts in damped articulations is performed to evaluate their relative potential performance benefits or limitations, which are assessed in terms of the selected performance measures.

Chapter 5 consists of a comprehensive parametric study, which is performed to identify appropriate damping coefficients and geometric parameters for the A-train double combination integrating damped articulation between units 2 and 3, Case I. A set of damping coefficient and geometric parameters is thus proposed and a performance assessment of the combination vehicle in terms of the selected performance measures is carried out. A comparison in term of potential gains is further performed between the A-train double with damped articulation and a conventional A-train double without damped articulation, under identical loading conditions and directional maneuvers.

The highlights of the dissertation research, major conclusions drawn and recommendations for the future work are finally presented in Chapter 6.

Chapter 2

Development of Analytical Models

2.1 General

Owing to the increasing concerns on the use of safer heavy articulated vehicles, and specially LCVs, on highways, intensive theoretical and experimental studies of the directional control and stability of such vehicles have been performed. Furthermore, a number of computer simulation models have been developed to predict the dynamic behavior of such vehicles [24, 25, 35]. For instance, in–plane and three–dimensional models have been developed to analyze yaw, lateral and roll motions of different combinations of heavy vehicles [24]. These analytical models vary from the simple linear yaw–plane model to the sophisticated 71 degrees–of–freedom Phase IV model [24, 36]. The comprehensive Phase IV model has been employed into the HVE (Human–Vehicle–Environment) simulation platform, which is a user–friendly interface between the user and the system, to realize a new simulation program called Engineering Dynamics Vehicle Dynamics Simulator (EDVDS) [37]. Although EDVDS is a user–friendly software, highly complex mathematical formulations are introduced in the new model.

A comparative study of some of the simulation programs revealed that more sophisticated models do not necessary yield more accurate predictions [25]. Furthermore, complex simulation programs, such as yaw/roll and phase IV, require extensive input data and computer time. A linear yaw–plane model provides a reasonable estimation of periodic or oscillatory yaw response. The aperiodic response characteristic, however, cannot be accurately estimated using the same model [27]. Both nonlinear lateral forces and alignment moments developed at the tire-road interface yield the aperiodic response characteristic. The lateral forces developed by radial truck tires, currently used in heavy vehicles, are strongly related to both normal loads and side-slip angles in a nonlinear manner. A nonlinear yaw–plane model incorporating nonlinear tire properties is thus considered adequate to accurately predict the yaw and lateral directional dynamics of LCVs, while neglecting roll dynamics and the influence of suspension forces. In this study, a nonlinear yaw–plane model is derived to investigate the directional dynamics of LCVs, specifically an A-train double combination with damped articulations.

The analytical model is initially derived for a conventional A-train without external articulation dampers. Two different concepts in articulation damping are presented; analytical models are derived and then integrated within the vehicle model.

2.2 Nonlinear Yaw–Plane Model of an A–train double with Damped Articulation

In the linear yaw–plane model reported in the literature [25, 38], the LCVs' tires only produce lateral forces and self–aligning moments that are linear with respect to both

vertical load and side-slip angle. In view of the strong non-linearities due to tire forces and moments, a nonlinear yaw–plane model has also been proposed by incorporating the nonlinear cornering forces and aligning moments due to tires. The yaw plane model has been extensively used to determine the lateral and yaw motions of the vehicle, while pitch and roll motions of the sprung masses are considered negligible. The model can effectively estimate the handling properties of the vehicle, with limited number of degrees-of-freedom for the vehicle model. For a two–axle vehicle, the model is represented by a single rigid body with freedom to move with respect to the ground-fixed axis system (X–Y) under the influence of external forces and moments, while the forward speed is assumed constant. Therefore, this system possesses only two degrees-of-freedom (d.o.f.), viz., lateral motion and yaw motion, which are required to evaluate the handling performance of the vehicle.

In this study, the directional analysis is performed for a LCV, which comprises four units coupled through different articulation mechanisms. The four units of the A-train double combination considered in this study include a three-axle tractor coupled to a two-axle semitrailer through a fifth-wheel type coupling. The two-axle semitrailer is coupled to a one-axle A-dolly through a hook-eye type coupling. The one-axle A-dolly is coupled to a one-axle semitrailer through another fifth-wheel type coupling. Yaw plane representation of the four units is formulated by neglecting vertical and roll compliance due to suspension and tires. Figure 2.1 illustrates the general yaw–plane model of an A–train double comprising a three–axle tractor, a three–axle semitrailer (trailer 1), a two–axle A–dolly, and a three–axle semitrailer (trailer 2). The different elements of the A–train double are identified as unit 1, unit 2, unit 3, and unit 4, as shown in Figure 2.1.

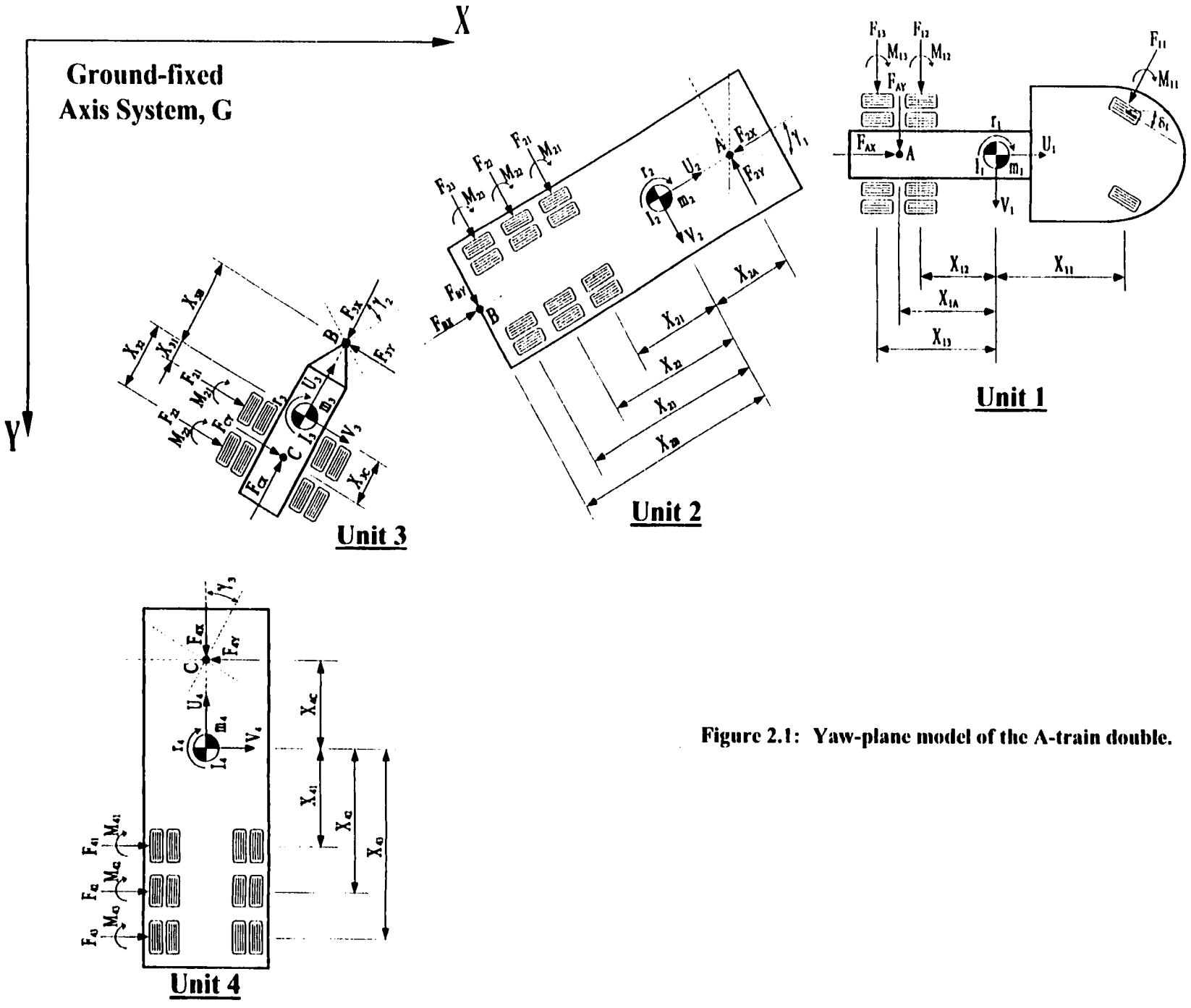

Figure 2.1: Yaw-plane model of the A-train double.

It should be noted that the combination of units 3 and 4 may also be referred to as a full-trailer. Each unit is considered to move longitudinally, laterally, and rotate about a vertical axis passing through its center of gravity (CG), subject to constraints posed by the coupling mechanism. The velocity vector for each unit thus consists of the longitudinal velocity (U_i), lateral velocity (V_i), and yaw rate (r_i), for i = 1, 2, 3, 4. Three articulation joints coupling the consecutive units are referred to as **'A'** (fifth wheel attached to unit 1), **'B'** (hook–eye combination attached to unit 2), and **'C'** (fifth wheel attached to the dolly or unit 3). The fifth wheel constraints permit relative yaw rotations of the coupled units, while the pintle hook (joint **B**) allows yaw, roll, and pitch rotations of units 2 and 3. An independent articulation angle, the angle formed by the longitudinal axes of the coupled units, is thus developed at each articulation joint. The articulation angles developed between units 1 and 2, 2 and 3, and 3 and 4 are denoted as γ_1, γ_2, and γ_3 respectively.

The articulation joints pose certain constraints and thus forces acting on the coupled units, as shown in Figure 2.1. F_{iX} and F_{iY} represent the longitudinal and lateral forces, respectively, acting on the unit i (i = 1, 2, 3, 4) along the body-fixed axis system of the unit. F_{qX} and F_{qY} represent the longitudinal and lateral forces acting at the joint q (q = **A**, **B**, **C**), which depend of the type of coupling and are derived from the kinematic analysis. In the absence of breaking torque, the pneumatic tires impose lateral forces (F_{ij}) and aligning moments (M_{ij}) on the vehicle units, as shown in Figure 2.1. The lateral force developed by tires on axle j (j = 1, 2, 3 for units 1, 2, and 4, and j = 1, 2 for unit 3) of unit i (i = 1, 2, 3, 4) strongly depends on the side-slip angle developed at the tire-road interface and the normal load acting on the tire. The aligning moment M_{ij} developed by

tires on axle j of unit i arises from two phenomena: (1) side-slip angle of the tire; and (2) longitudinal slip caused by dual tire combination. Those phenomena are described in details in later sections. The yaw-plane model of the A-train double combination is formulated to incorporate nonlinear cornering characteristics of the tires as a function of the normal load and side-slip angle.

The dynamics of the steering mechanism is neglected on the basis that the natural frequency of the wheel masses, which are constrained by the stiffness of the steering mechanism and the aligning stiffness of the tires, is considerably higher than the frequency of yaw motion.

The fifth wheel coupling mechanisms provide certain damping due to coulomb friction between the fifth wheel plates. This damping force, however, is considered to be small when the fifth wheel plates are adequately lubricated. The damping developed at the fifth wheel joints is thus assumed negligible. Many earlier studies, however, have emphasized the important significance of coulomb and viscous damping within the hitch and towbar in reducing the yaw oscillations of the vehicle [6–11]. More recently, Rakheja et al. [27] introduced a concept of external articulation damping that is applied to tractor-semitrailer combinations. The study showed that the directional control performance of such a combination can be considerably enhanced with external articulation dampers. Kageyama and Saito [28] also presented a similar study with objective to enhance lateral stability of articulated vehicles at highway speeds. Apart from articulation damping, some studies have explored potential performance benefits of an electronic braking system to control the lateral snaking motions of multiple articulated heavy vehicles [39]. The concept of introducing viscous damping between different units

of an A–train double combination, however, has not been addressed. This dissertation thus addresses the dynamics associated with viscous damped articulations between the units of an A-train double and the analysis of potential performance benefits.

2.2.1 Major Assumptions

The set of nonlinear differential equations of motion applicable to the A–train double, shown in Figure 2.1, is derived based on the following assumptions [38]:

1. Each element of the A-train double is a rigid body constrained to move on a horizontal plane.

2. The longitudinal component of the translational velocity, i.e., forward speed, of the vehicle is constant.

3. The tractor is free to yaw and sideslip, and each trailing element can articulate with respect to its leading element. Pitch and roll motions are small and hence neglected.

4. The nonlinear dependence of the cornering force and aligning torque on the slip angles for tires is represented by a function that is derived using the Magic Formula [40].

5. Longitudinal forces at the tire–road interface are very small relative to the lateral forces and thus neglected.

6. The articulation angles, γ_i, defined in Figure 2.1, are small such that $\sin \gamma_i \cong \gamma_i$ and $\cos \gamma_i \cong 1$.

7. All joints are frictionless, and the articulations take place about vertical axis.

8. Gyroscopic moments due to rotating elements such as wheels and tires are small and, therefore, neglected.

9. Simulations can be performed in the open–loop or closed–loop modes. In the open–loop mode, the time history of the steering angle is provided as input to the

model. In the closed–loop mode, the trajectory to be followed by the vehicle is specified, and a driver-vehicle model is implemented to compute the appropriate front wheel steer angle.

10. Steering system dynamics are neglected, and steering input is characterized by the angular displacement of the front wheels about a vertical axis.

11. In view of the negligible roll motion of the units, lateral transfer of load on the tires is neglected.

2.3 Articulation Damping Concept

Two concepts in articulation damping for A-train doubles are presented. The first concept involves introduction of two hydraulic dampers between the first semitrailer (unit 2) and the A-dolly (unit 3), and is referred to as 'Case I'. Figure 2.2 illustrates a possible arrangement of the dampers between units 2 and 3. The second concept of articulation damping comprises two hydraulic dampers introduced between the first semitrailer (unit 2) and the second semitrailer (unit 4), and is referred to as 'Case II'. Figure 2.3 illustrates a possible configuration of dampers for Case II.

The damping forces and moments imposed on the coupled units are derived from the forces developed at the ends of each damper, such as points **K** and **L** for damper 1, and points **M** and **N** for damper 2. These forces and moments are strongly related to the geometry and kinematics of each damper links, damping coefficients and motion coordinates of the coupled units. The damping forces incorporating geometric non-linearities due to damper links are derived and integrated into the yaw–plane model. A comprehensive study on the geometry and kinematics of each damper link for each articulation damping configuration is carried out and presented in subsection 2.3.1.

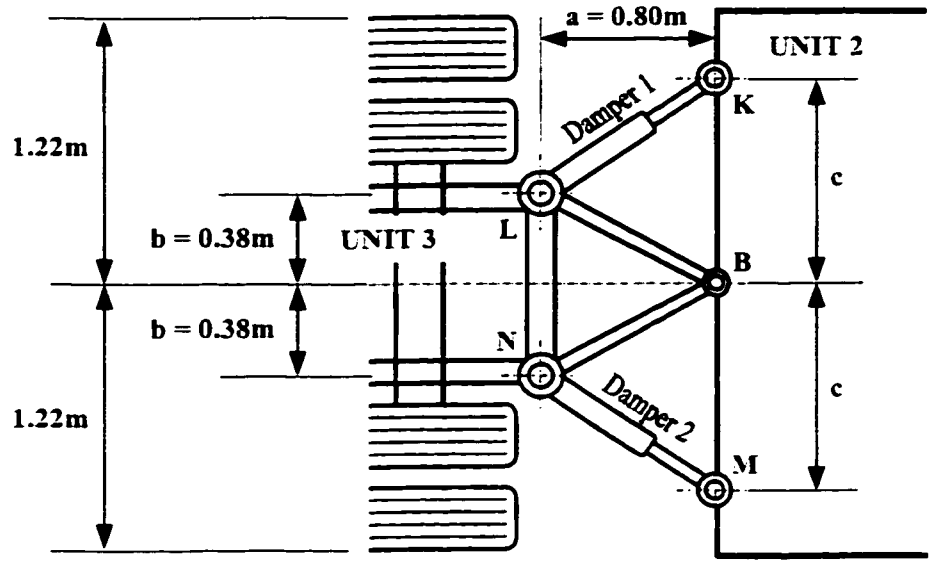

Figure 2.2: Scheme of articulation damping mechanism between units 2 and 3 (Case I).

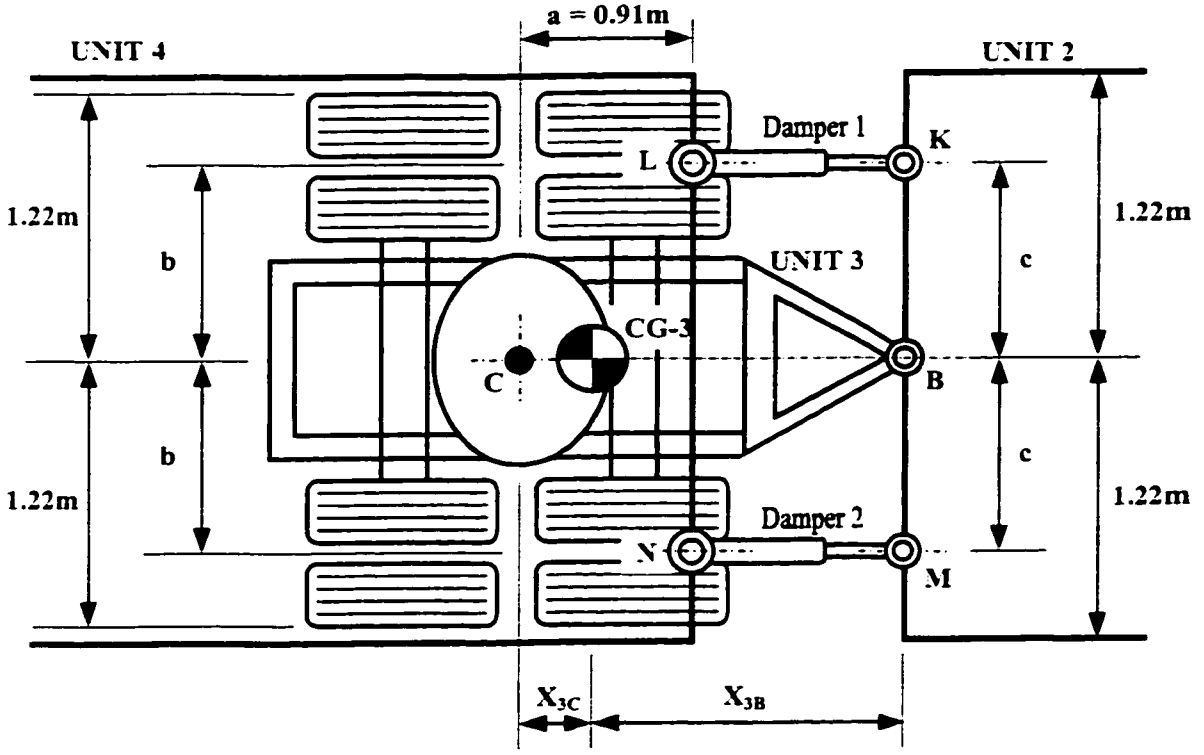

Figure 2.3: Scheme of articulation damping mechanism between units 3 and 4 (Case II).

2.3.1 Kinematic Analysis

A kinematic analysis of the proposed damping concepts is carried out to derive the forces and moments developed by externally mounted dampers. The kinematic analysis is performed to evaluate the relative velocities along the dampers axes as functions of motion coordinates of different units. The velocity functions are then used to derive the damping forces and moments imposed on the coupled units.

Case I: Articulation Damping between Units 2 and 3

Figure 2.4 illustrates a schematic layout of dampers between units 2 and 3, when both units are moving along a straight path. The articulation angles at each articulation joint are thus considered equal to zero, $\gamma_1 = \gamma_2 = \gamma_3 = 0$. The coordinates $\mathbf{X_{2B}}$ and $\mathbf{X_{3B}}$ define the longitudinal position of the joint **B** (hook-eye) with respect to the CG position of Units 2 and 3, respectively. The angles ϕ_1 and ϕ_2 describe the orientation of the arms of the A-dolly. The longitudinal coordinates of the dampers in this position are described by length a. Lateral coordinates of attachment points **L** and **N** on unit 3 and **K** and **M** on unit 2 are described by symmetric distances b and c, respectively. The length of arms **BL** and **BN** of the A-dolly and their orientation (ϕ_1 and ϕ_2) can be expressed as:

$$\phi_1 = \phi_2 = arctan\,(b/a)$$
$$BL = BN = \sqrt{a^2 + b^2} \qquad \textbf{(2.1)}$$

From Figure 2.4, it can be seen that the two dampers possess equal lengths (**KL** and **MN**), when the A–train double is traveling on a straight path. The two lengths, however, depend on parameters ***a***, ***b***, and ***c***. $\mathbf{C_{KL}}$ and $\mathbf{C_{MN}}$ describe the viscous damping coefficient due to dampers, as shown in Figure 2.4. The damping forces and moments developed due to articulation dampers are also directly related to parameters ***a***, ***b*** and ***c***, and the damping coefficients. The dampers are oriented such that $c > \sqrt{a^2 + b^2}$, in order to realize appreciable magnitude of damping moments. It is also suggested that distance **BK** be greater than the distance **BL**, such that the damper inclination angles β_1 and β_2 (Figure 2.5) are always less that $\pi/2$ radians (90°), when the two units experience any relative rotation about articulation joint **B,** either clockwise or counter-clockwise.

Figure 2.5 illustrates the orientation of the dampers between units 2 and 3, when the combination is subject to a turning maneuver. It can be seen that unit 3 rotates relative to unit 2 about the joint **B** at an angle γ_2. The lengths of dampers 1 and 2, denoted as **D1** and **D2**, respectively, vary considerably during the turning maneuvers. Depending upon the rate of change of **D1** and **D2**, a force will be developed across each damper, whose magnitude will depend upon their damping coefficients. The geometry of the two units, illustrated in Figure 2.5, permits the evaluations for changes in orientation and lengths of the dampers. The inclination angles between the lateral axis of unit 2 and the A-dolly arms, α_1 and α_2, can be derived from geometry and articulation angle γ_2 in the following manner:

$$\alpha_1 = \arctan(a/b) + \gamma_2$$
$$\alpha_2 = \arctan(a/b) - \gamma_2 \qquad \textbf{(2.2)}$$

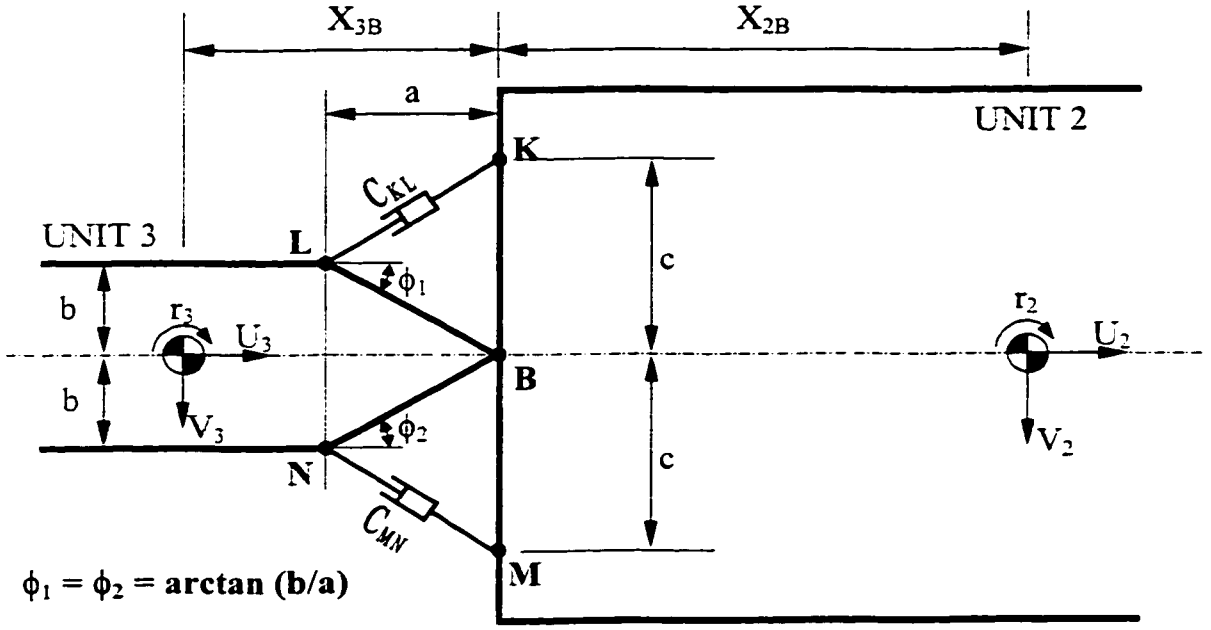

Figure 2.4: Kinematic representation of articulation dampers between units 2 and 3 of A-train double when the LCV is traveling along a straight path.

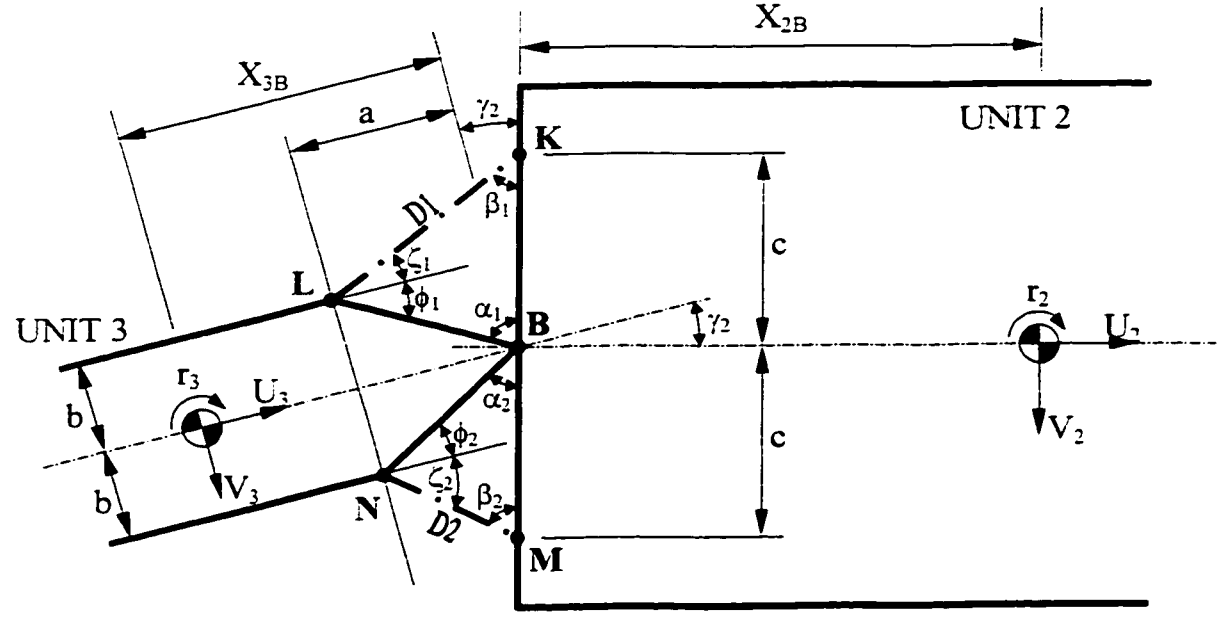

Figure 2.5: Kinematic representation of articulation dampers between units 2 and 3 of A-train double when the LCV is negotiating a curve.

The variations in lengths of dampers **D1** and **D2** are then evaluated as functions of α_1 and α_2, by applying the law of cosines to the triangles **BKL** and **BMN**. The instantaneous lengths are derived as:

$$D1 = KL = \sqrt{BL^2 + BK^2 - 2 \cdot BL \cdot BK \cdot \cos \alpha_1}$$
$$D2 = MN = \sqrt{BN^2 + BM^2 - 2 \cdot BN \cdot BM \cdot \cos \alpha_2} \qquad \textbf{(2.3)}$$

The forces developed by dampers act on units 2 and 3 along the axis of the dampers. It is thus essential to describe the instantaneous orientation of the two dampers. The application of law of sines to triangles **BKL** and **BMN** yields following expressions for β_1, β_2, ζ_1 and ζ_2, which completely describe the instantaneous orientation of the dampers:

$$\beta_1 = \arcsin\left(\frac{BL}{KL} \cdot \sin \alpha_1\right); \qquad \beta_2 = \arcsin\left(\frac{BN}{MN} \cdot \sin \alpha_2\right)$$
$$\zeta_1 = \pi - (\alpha_1 + \beta_1 + \phi_1); \quad \text{and} \quad \zeta_2 = \pi - (\alpha_2 + \beta_2 + \phi_2) \qquad \textbf{(2.4)}$$

Case II: Articulation Damping between Units 2 and 4

Figure 2.6 depicts the orientation of the articulation dampers installed between units 2 and 4, when the A–train double is traveling on a straight path. The kinematics associated with this new configuration is relatively more complex when compared with the kinematics presented in Case I. It can be seen that not only the articulation joint **B**

influences the kinematics of this configuration, but also the articulation joint **C** plays an important role. The position of each damper is assumed to be symmetric about the longitudinal axis passing through the CGs of the units of the A–train double. Consequently, the longitudinal axis passes through the articulation joints **B** and **C**, when the combination traverses a straight path. The mounting end of dampers 1 and 2 are identified as **K** and **M**, on unit 2, and **L** and **N**, located on unit 4, respectively. Point **B** represents the articulation joint that is common to units 2 and 3, and point **C** represents the articulation joint that is common to units 3 and 4. The lateral distances between the damper mounts and articulation joints, **BK**, **BM**, **BC**, **CL**, and **CN**, always remain constant. Owing to the symmetric locations of dampers, the lateral distances, **BK** and **BM**, also defined as ***c***, are equal. Parameters ***a*** and ***b*** describe the longitudinal and lateral position, respectively, of the dampers mounts on unit 4 with respect to the joint **C**.

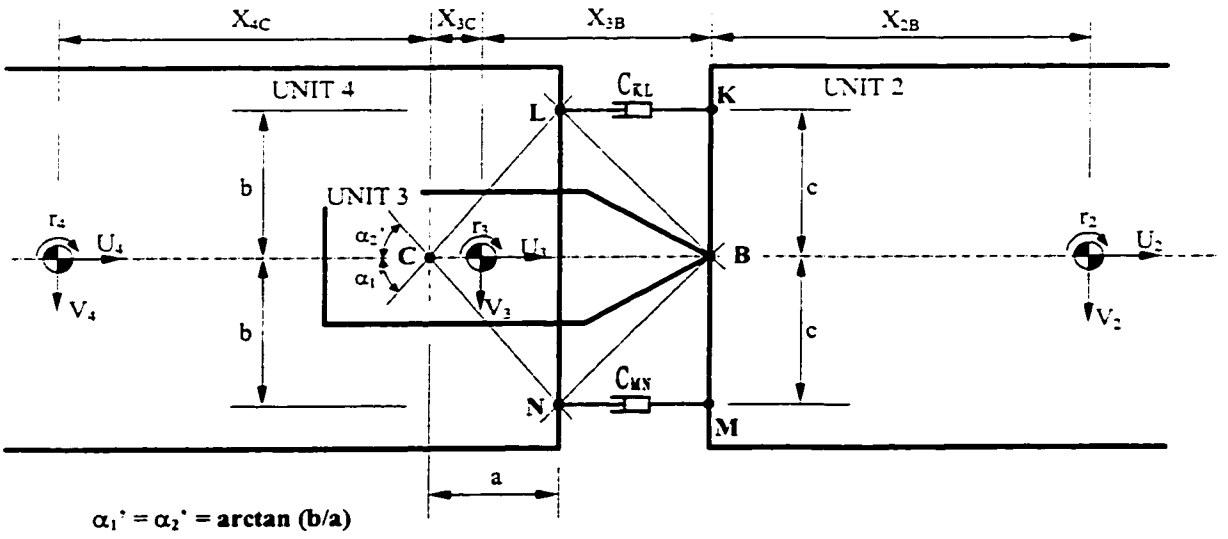

Figure 2.6: Kinematic representation of articulation dampers between units 2 and 4 of an A–train double when the LCV is traveling a straight path.

From Figure 2.6, the orientation of the damper mounts, α_1' and α_2', with respect to **C** and distances **BC**, **CL**, and **CN** can be derived as:

$$\alpha_1' = \alpha_2' = arctan\,(b/a) \tag{2.5}$$

$$BC = X_{3B} + X_{3C} \tag{2.6}$$

$$CL = CN = \sqrt{a^2 + b^2} \tag{2.7}$$

where X_{3B} and X_{3C} are the longitudinal coordinated of the mass center of the A-dolly (unit 3) relative to joints **B** and **C**, respectively. It should be noted that a parallel arrangement of dampers, yield **KL** = **MN**, and $b = c$. The distances c and b, however, will differ when dampers are mounted at certain inclination. The damper lengths **KL** and **MN** will also differ under a directional maneuver due to relative yaw rotations of units 2 and 4.

When the A–train double is subject to a turning maneuver, an articulation angle, γ_2, is developed due to relative yaw rotations of units 2 and 3. In a similar manner, an articulation angle γ_3 is realized due to yaw rotation of units 3 and 4 about the joint **C**. The instantaneous lengths of dampers 1 and 2, denoted by **D1** and **D2**, respectively, vary with variations in the articulation angles, as shown in Figure 2.7. The instantaneous damper lengths **D1** and **D2** can be computed from the geometry illustrated in Figure 2.7. The damping forces and moments imposed on the coupled units directly depend upon the time rates of change of **D1** and **D2**, damping coefficients, $\mathbf{C_{KL}}$ and $\mathbf{C_{MN}}$, and the angles θ_1, θ_2, ζ_1, and ζ_2. A kinematic analysis is thus performed to derive **D1**, **D2**, and the instantaneous damper orientations.

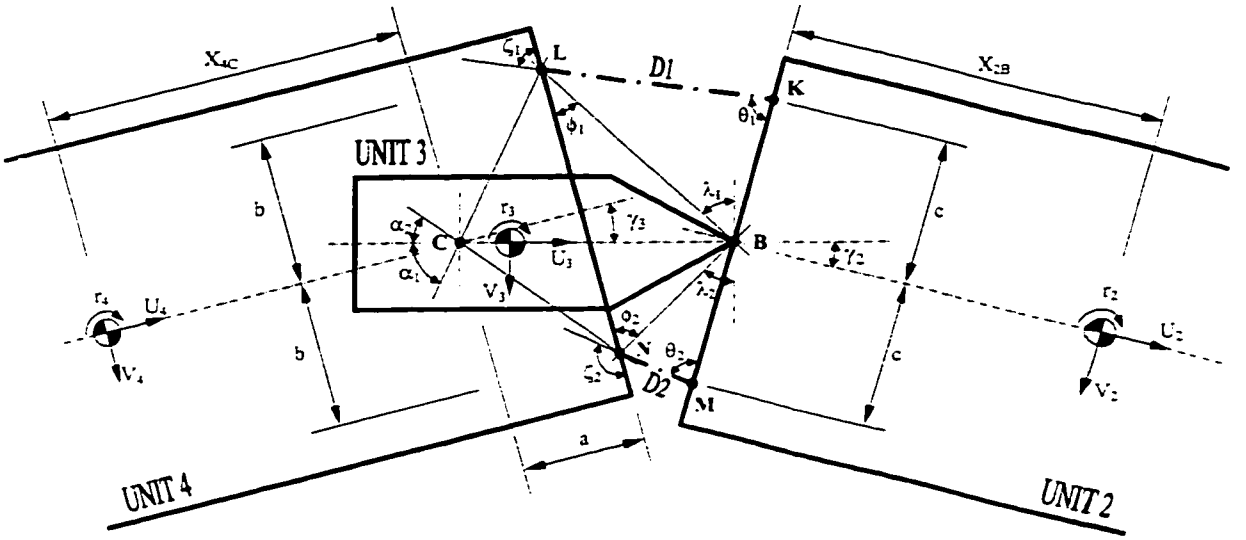

Figure 2.7: Kinematic representation of articulation dampers between units 2 and 4 of A–train double when the LCV is negotiating a curve.

The instantaneous orientations of damper mounts **L** and **N** on unit 4 with respect to the articulation joint **C** are related to the articulation angle γ_3, in the following manner:

$$\alpha_1 = \alpha_1' + \gamma_3$$

$$\alpha_2 = \alpha_2' - \gamma_3 \qquad \textbf{(2.8)}$$

The location of these mounts with respect to joints **B** and **C**, **BL** and **BN**, are derived as:

$$BL = \sqrt{BC^2 + CL^2 - 2 \cdot BC \cdot CL \cdot \cos \alpha_1}$$

$$BN = \sqrt{BC^2 + CN^2 - 2 \cdot BC \cdot CN \cdot \cos \alpha_2}$$

$$\angle CBL = \arcsin\left(\frac{CL}{BL} \cdot \sin \alpha_1\right); \qquad \angle CBN = \arcsin\left(\frac{CN}{BN} \cdot \sin \alpha_2\right) \qquad \textbf{(2.9)}$$

$$\angle BLC = \pi - (\alpha_1 + \angle CBL) \quad ; \qquad \angle BNC = \pi - (\alpha_2 + \angle CBN)$$

$$\phi_1 = \angle BLC - (\pi/2 - \alpha_1') \quad ; \qquad \phi_2 = \angle BNC - (\pi/2 - \alpha_2')$$

The instantaneous damper lengths, **D1**, and **D2**, can be computed from distances **BL** and **BN**, through analysis of triangles **BKL** and **BMN**, which take into account the effect of articulation angle γ_2. The orientations of distances **BL** and **BN** with respect to the fixed axis system of unit 3, can be expressed as:

$$\lambda_1 = \pi/2 - \angle CBL \; ; \qquad and \qquad \lambda_2 = \pi/2 - \angle CBN \qquad \textbf{(2.10)}$$

The instantaneous orientation of distances **BL** and **BN** with respect to unit 2 can be described by the following angles:

$$\angle KBL = \lambda_1 + \gamma_2 \; ; \qquad and \qquad \angle MBN = \lambda_2 - \gamma_2$$

$$\angle BLK = \arcsin\left(\frac{BK}{D1} \cdot \sin(\angle KBL)\right); \quad and \quad \angle BNM = \arcsin\left(\frac{BM}{D2} \cdot \sin(\angle MBN)\right)$$

(2.11)

The damper lengths are then derived from the triangle **BKL** and **BMN**, and above angles, as:

$$D1 = KL = \sqrt{BK^2 + BL^2 - 2 \cdot BK \cdot BL \cdot \cos\left(\angle KBL\right)}$$
$$D2 = MN = \sqrt{BM^2 + BN^2 - 2 \cdot BM \cdot BN \cdot \cos\left(\angle MBN\right)} \qquad \textbf{(2.12)}$$

The instantaneous orientation of the dampers, indicated by angles θ_1, θ_2, ζ_1, and ζ_2, indicated in Figure 2.7, are then derived as:

$$\theta_1 = \pi - \left(\lambda_1 + \gamma_2 + \angle BLK\right); \qquad \theta_2 = \pi - \left(\lambda_2 - \gamma_2 + \angle BNM\right)$$
$$\zeta_1 = \angle BLK + \phi_1; \qquad \text{and} \qquad \zeta_2 = \angle BNM + \phi_2 \qquad \textbf{(2.13)}$$

2.3.2 Damping Forces

The damping forces imposed on the coupled units are derived from the forces developed at each damper mounts, and depend upon the longitudinal and lateral component of velocities at the damper mounts, and upon the damping coefficients.

Case I: Articulation Damping between Units 2 and 3

The longitudinal and lateral components of velocities developed at the damper mounts (**K**, **L**, **M**, and **N**) can be related to the response vectors of the coupled units and

the angles described in Equations (2.4). From the geometry, illustrated in Figure 2.8, the instantaneous resultant velocities at the mounts along the dampers axes are derived as:

$$
\begin{aligned}
V_K &= (U + r_2 \cdot c) \cdot \sin \beta_1 - (V_2 - r_2 \cdot X_{2B}) \cdot \cos \beta_1 \\
V_L &= (U + r_3 \cdot b) \cdot \cos \zeta_1 - (V_3 + r_3 \cdot (X_{3B} - a)) \cdot \sin \zeta_1 \\
V_M &= (U - r_2 \cdot c) \cdot \sin \beta_2 + (V_2 - r_2 \cdot X_{2B}) \cdot \cos \beta_2 \\
V_N &= (U - r_3 \cdot b) \cdot \cos \zeta_2 + (V_3 + r_3 \cdot (X_{3B} - a)) \cdot \sin \zeta_2
\end{aligned}
\qquad \textbf{(2.14)}
$$

where $\mathbf{V}_\ell$ is the resultant velocity at the mount ℓ (ℓ = **K**, **L**, **M**, **N**) along the axis of the damper considered.

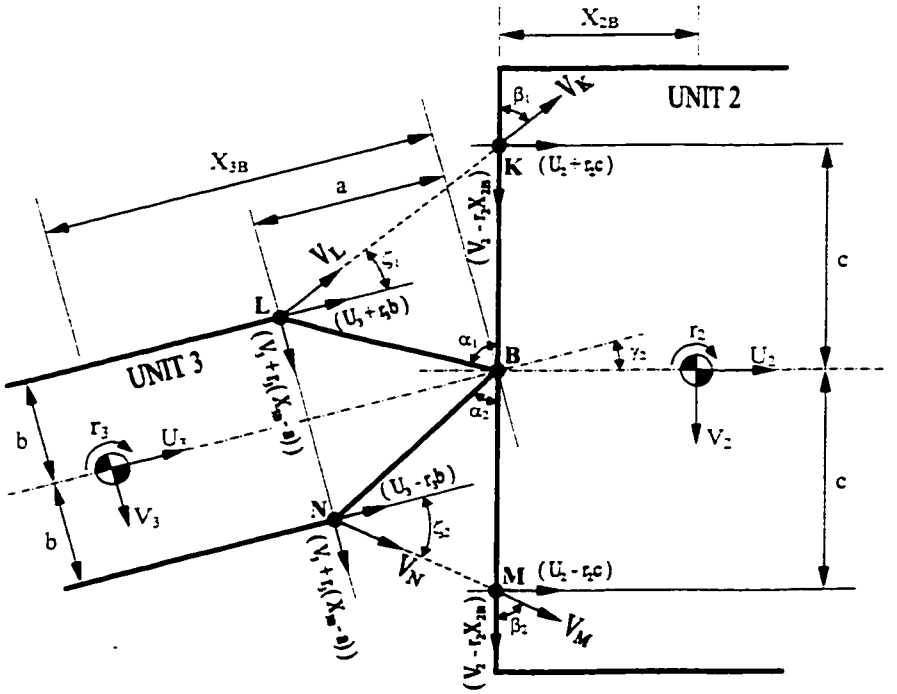

Figure 2.8: Resultant velocities at damper mounts K, L, M, and N (Case I).

The damping forces developed by articulation dampers, along their respective axis, are related to the relative velocities across the dampers, which are derived from:

$$V_{KL} = V_K - V_L \; ; \qquad and \qquad V_{MN} = V_M - V_N \tag{2.15}$$

where $\mathbf{V_{KL}}$ and $\mathbf{V_{MN}}$ are relative velocities across dampers 1 and 2, respectively. Assuming viscous damping, the damping forces developed by the two dampers can be computed from:

$$F_{KL} = C_{KL} \cdot V_{KL} \; ; \qquad and \qquad F_{MN} = C_{MN} \cdot V_{MN} \tag{2.16}$$

where $\mathbf{C_{KL}}$ and $\mathbf{C_{MN}}$ are the viscous damping coefficients of damper 1 and 2, respectively, and $\mathbf{F_{KL}}$ and $\mathbf{F_{MN}}$ are the respective damping forces developed along the dampers axis, which are shown as resultant mount forces $\mathbf{F_K} = \mathbf{F_L}$, and $\mathbf{F_M} = \mathbf{F_N}$ acting on the coupled units 2 and 3 in Figure 2.9. The longitudinal and lateral components of damping forces acting on the coupled units 2 and 3 can be derived from the articulation geometry shown in the figure, and expressed as:

$$\begin{aligned} F_{KX} &= F_{KL} \cdot \sin \beta_1 & F_{KY} &= F_{KL} \cdot \cos \beta_1 \\ F_{LX} &= F_{KL} \cdot \cos \zeta_1 & F_{LY} &= F_{KL} \cdot \sin \zeta_1 \\ F_{MX} &= F_{MN} \cdot \sin \beta_2 & F_{MY} &= F_{MN} \cdot \cos \beta_2 \\ F_{NX} &= F_{MN} \cdot \cos \zeta_2 & F_{NY} &= F_{MN} \cdot \sin \zeta_2 \end{aligned} \tag{2.17}$$

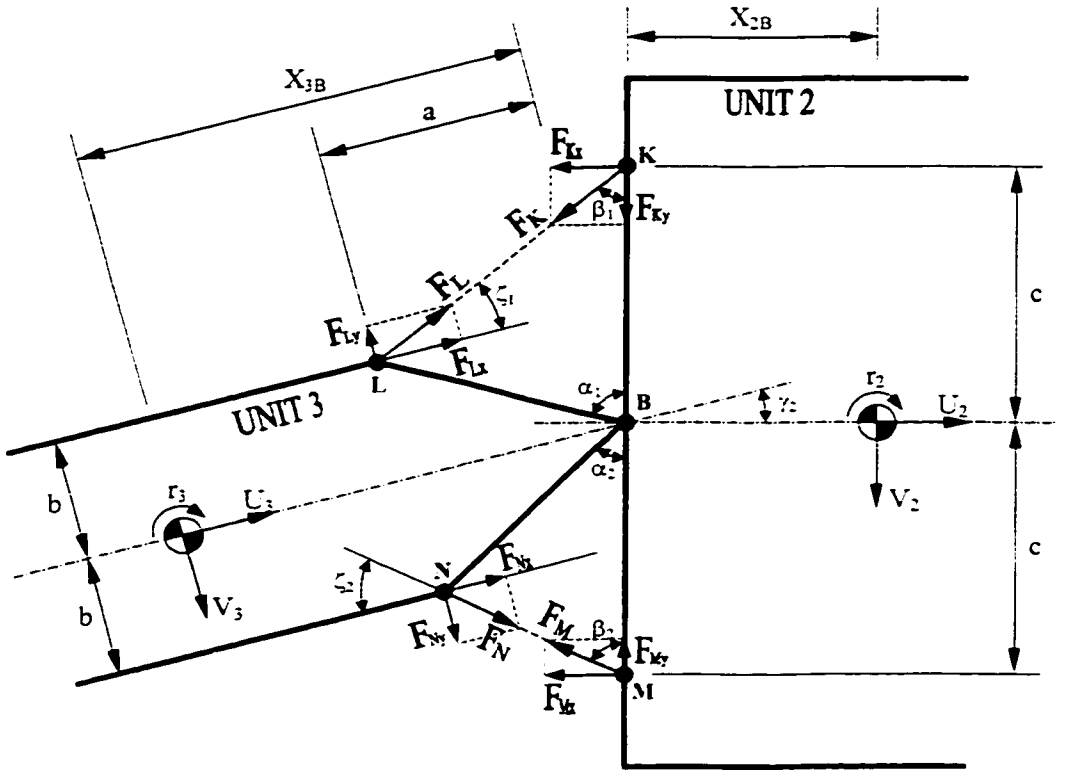

Figure 2.9: Damping forces acting at mounts K, L, M, and N (Case I).

Case II: Articulation Damping between Units 2 and 4

The resultant velocities developed at the damper mounts are related to the damper geometry, response velocities of the coupled units, and the angles described in Equations (2.13). From the geometry shown in Figure 2.10, the resultant velocities developed at the damper mounts are expressed as:

$$V_K = (U + r_3 \cdot c)\cdot \sin\theta_1 - (V_3 - r_3 \cdot X_{3B})\cdot \cos\theta_1$$

$$V_L = (U + r_4 \cdot b)\cdot \sin\zeta_1 + (V_4 + r_4 \cdot (X_{4C} + a))\cdot \cos\zeta_1 \qquad \textbf{(2.18)}$$

$$V_M = (U - r_3 \cdot c)\cdot \cos\left(\theta_2 - \frac{\pi}{2}\right) - (V_3 - r_3 \cdot X_{3B})\cdot \sin\left(\theta_2 - \frac{\pi}{2}\right)$$

$$V_N = (U - r_4 \cdot b)\cdot \cos\left(\zeta_2 - \frac{\pi}{2}\right) + (V_4 + r_4 \cdot (X_{4C} + a))\cdot \sin\left(\zeta_2 - \frac{\pi}{2}\right)$$

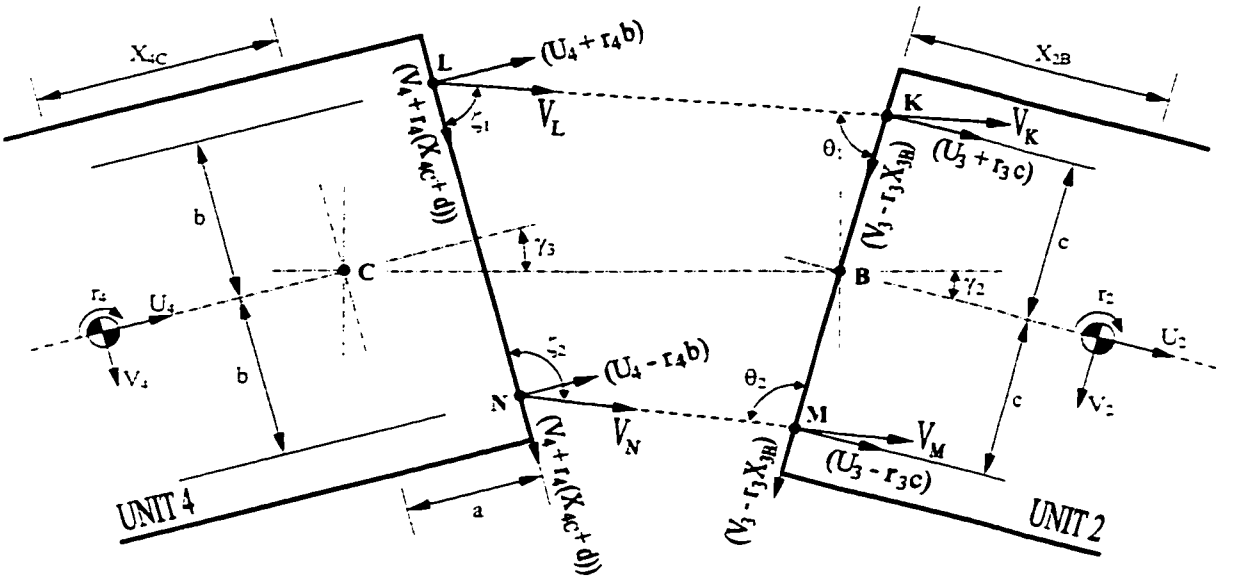

Figure 2.10: Resultant velocities at damper mounts K, L, M, and N (Case II).

The damping forces developed by the articulation dampers are related to relative velocities across the dampers, as described in Equations (2.15) and (2.16). The component of damping forces acting along the body-fixed axes of the coupled units, derived from the geometry shown in Figure 2.11, are expressed as:

$$F_{KX} = F_{KL} \cdot \sin\theta_1 \qquad F_{KY} = F_{KL} \cdot \cos\theta_1$$

$$F_{LX} = F_{KL} \cdot \sin\zeta_1 \qquad F_{LY} = F_{KL} \cdot \cos\zeta_1 \tag{2.19}$$

$$F_{MX} = F_{MN} \cdot \cos\left(\theta_2 - \frac{\pi}{2}\right) \qquad F_{MY} = F_{MN} \cdot \sin\left(\theta_2 - \frac{\pi}{2}\right)$$

$$F_{NX} = F_{MN} \cdot \cos\left(\zeta_2 - \frac{\pi}{2}\right) \qquad F_{NY} = F_{MN} \cdot \sin\left(\zeta_2 - \frac{\pi}{2}\right)$$

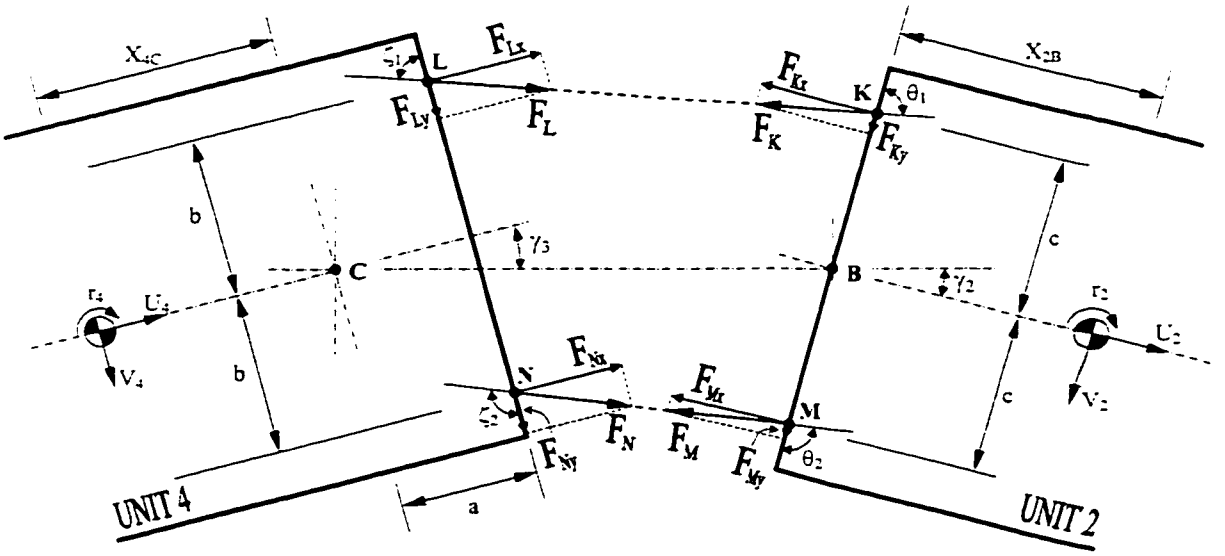

Figure 2.11: Damping forces acting at damper mounts K, L, M, and N (Case II).

2.4 Connecting Joints and Constraint Conditions

An A-train double consists of three different types of connecting joints: (1) the fifth wheels connecting units 1 and 2, and units 3 and 4; (2) the kingpins; and (3) the pintle hook connecting units 2 and 3. These joints are relatively rigid with respect to longitudinal, lateral and vertical translations but more complaint with respect to rotations,

and also involve certain kinematic conditions that must be satisfied. A fifth wheel coupling permits relative pitch and yaw rotations of both the leading unit and the following unit, while it resists relative roll motion due to its high roll stiffness. A pintle hook permits the roll, yaw, and pitch rotations of the following unit with respect to the leading unit. The lateral, longitudinal, and vertical displacements of the two connected units thus must be equal at the joint. A kingpin joint permits the yaw rotation of the two connected units, and thus yields identical lateral and longitudinal displacements of the two connected units at the joint. In the yaw-plane dynamics, considered in this dissertation, the relative rotations along the pitch and roll coordinates and vertical displacements can be neglected. The resulting velocities and forces at each joint are derived from the kinematic relations and appropriate considerations of the constraints, as presented in following subsection.

2.4.1 Constraint Velocities and Forces

The four units of the A–train double are free to yaw relative to each other at the articulation points **A**, **B**, and **C**, whereas the units that share articulation points are constraint to move together along the lateral and longitudinal directions. Similarly, each damper is free to rotate about a vertical axis passing through its end points, viz., **K**, **L**, **M**, and **N**. Equal and opposite constraint forces act on each of the units that have a common articulation joint, which is defined as the point shared by two consecutive units. These points are identified as **A**, **B**, and **C** in Figure 2.1. Figure 2.12 illustrates both forces and velocities at the three articulation joints. The joint forces are illustrated in terms of their X

and Y components along the body-fixed axis system of the leading unit, $\mathbf{F}_{kX}$ and $\mathbf{F}_{kY}$ (k = **A, B, C**), as shown in Figure 2.1. $\mathbf{F}_{iX}$ and $\mathbf{F}_{iY}$ (i = 2, 3, 4) represent the component of the constraint forces acting along the body-fixed axis system of the following unit. The components of constraint forces acting on each following unit can be expressed in terms of components of forces acting on the leading units. From Figure 2.12, the relationship between the constraint forces can be derived as:

$$F_{2X} = F_{AX} \cdot \cos\gamma_1 - F_{AY} \cdot \sin\gamma_1 \; ; \quad and \quad F_{2Y} = F_{AX} \cdot \sin\gamma_1 + F_{AY} \cdot \cos\gamma_1$$

$$F_{3X} = F_{BX} \cdot \cos\gamma_2 - F_{BY} \cdot \sin\gamma_2 \; ; \quad and \quad F_{3Y} = F_{BX} \cdot \sin\gamma_2 + F_{BY} \cdot \cos\gamma_2 \qquad \textbf{(2.20)}$$

$$F_{4X} = F_{CX} \cdot \cos\gamma_3 - F_{CY} \cdot \sin\gamma_3 \; ; \quad and \quad F_{4Y} = F_{CX} \cdot \sin\gamma_3 + F_{CY} \cdot \cos\gamma_3$$

The assumption of constant forward speed and small articulation angles yields, U = $U_1 = U_2 = U_3 = U_4$. In view of the longitudinal and lateral motion constraints imposed by different articulation joints, the lateral velocities of the coupled units along their respective body-fixed axis system, can be expressed in the following manner:

$$V_2 = V_1 + U \cdot \gamma_1 - X_{1A} \cdot r_1 - X_{2A} \cdot r_2$$

$$V_3 = V_2 + U \cdot \gamma_2 - X_{2B} \cdot r_2 - X_{3B} \cdot r_3 \qquad \textbf{(2.21)}$$

$$V_4 = V_3 + U \cdot \gamma_3 - X_{3C} \cdot r_3 - X_{4C} \cdot r_4$$

where $\mathbf{X}_{ik}$ (i = 1, 2, 3, and k = **A, B, C**) describe the longitudinal distance between the CG of unit i and the joint k.

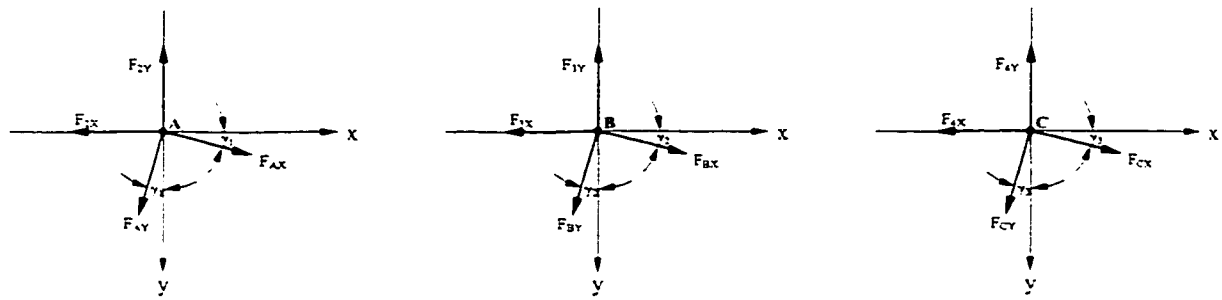

(a)

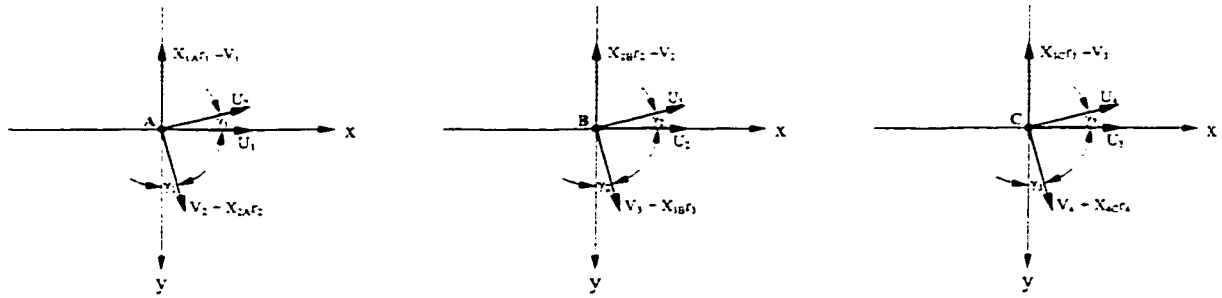

(b)

Figure 2.12: Constraint forces (a), and velocities (b) at articulation joints A, B, and C.

The time differentiation of Equations (2.21) yields relationships between the rates of change of lateral velocities of different units:

$$\dot{V}_2 = \dot{V}_1 + U \cdot \dot{\gamma}_1 - X_{1A} \cdot \dot{r}_1 - X_{2A} \cdot \dot{r}_2$$

$$\dot{V}_3 = \dot{V}_2 + U \cdot \dot{\gamma}_2 - X_{2B} \cdot \dot{r}_2 - X_{3B} \cdot \dot{r}_3 \qquad \textbf{(2.22)}$$

$$\dot{V}_4 = \dot{V}_3 + U \cdot \dot{\gamma}_3 - X_{3C} \cdot \dot{r}_3 - X_{4C} \cdot \dot{r}_4$$

where $\dot{r}_i$ are the yaw accelerations and $\dot{\gamma}_i$ are the articulation rates, which describe the relative yaw velocities of the coupled units, given by:

$$\dot{\gamma}_1 = r_1 - r_2 \; ; \qquad \dot{\gamma}_2 = r_2 - r_3 \; ; \qquad \textit{and} \qquad \dot{\gamma}_3 = r_3 - r_4 \qquad \textbf{(2.23)}$$

2.5 Tire Forces and Moments

In highway vehicles, all the primary control and disturbance forces that are applied to the vehicle, with the exception of aerodynamic and gravitational forces, are generated at the tire-road interface. A thorough understanding of the resulting forces and moments developed at the contact patch is extremely vital to study the ride quality, and handling behavior of ground vehicles. Although the driver attempts to control the vehicle direction and tractive and breaking forces through steering, throttle, gears, and the braking system, the resulting vehicle motion is attributed to lateral and longitudinal forces, developed at the tire-road interface. The lateral forces developed at the tire-road interface are responsible for cornering or steering of the vehicle. The tires further generate moments during cornering, which are attributed to the self–aligning properties of tires, and longitudinal slip of dual tire sets.

2.5.1 Slip Angles

The cornering forces and aligning moments at the tire-road interface depend strongly on the side-slip angle and vertical load acting on the tire, as shown in Figure 2.13. Typically, the cornering force increase nearly linearly with side-slip angle, α, until it reaches approximately 3 degrees. The cornering force varies nonlinearly with α, when $\alpha > 3$ degrees, and further increases with normal load F_z. The cornering force also depends upon the vehicle's operating parameters, such as forward speed, lateral speed, yaw rate, and steering angle, and tire's physical properties, such as lateral elasticity,

control the side-slip angle, in a highly nonlinear manner. The side-slip angle at a tire-road interface is developed due to lateral and forward velocity at the tire, which are derived from vehicle response variables.

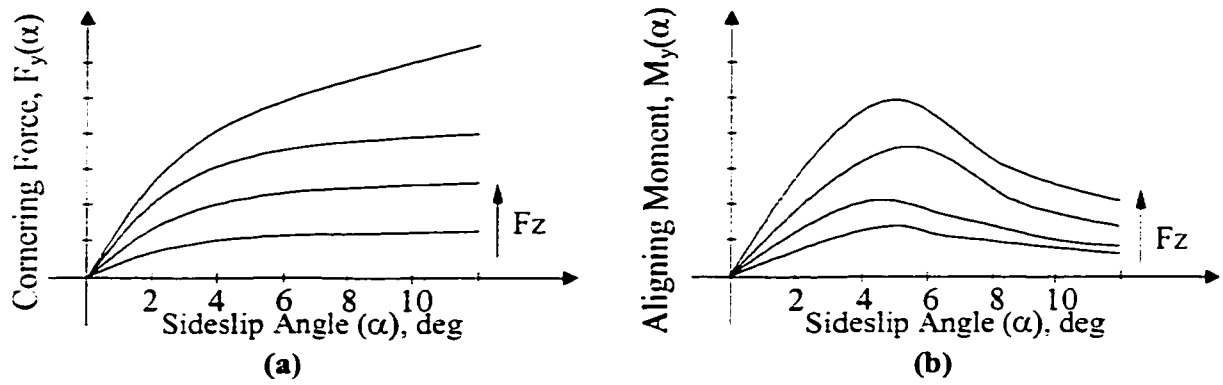

Figure 2.13: Influence of side-slip angles and normal load on cornering force (a), and self-aligning moment (b).

Figure 2.14 (a) illustrates the side-slip angle developed at the front-axle tire of unit 1, while Figure 2.14 (b) presents the side-slip angle developed at the rear axle tire. Assuming small angles, *arctan* (α) $\cong \alpha$, the side-slip angles for the front and each of the rear tires are defined as:

$$\alpha_{11} = \frac{V_1 + X_{11} \cdot r_1}{U_1} - \delta_f \tag{2.24}$$

$$\alpha_{ij} = \frac{V_i - X_{ij} \cdot r_i}{U_i}; \quad for \begin{cases} i = 1; & j = 2,3 \\ i = 2,3,4; & j = 1,2,3 \end{cases}$$

where α_{11} is the side-slip angle of the front-axle tires and α_{ij} are the side-slip angles of tires on the axle j (j = 1, 2, 3) of unit i (i = 1, 2, 3, 4). $\mathbf{X}_{ij}$ is the longitudinal distance of axle j from the CG of unit i, and δ_f is the steer angle of front axle tires, which is assumed to be identical for both tires. U_i, V_i, and r_i are the longitudinal, lateral and yaw velocities of unit i. The side-slip angles developed at the tires of remaining units are related to the velocity vector of the respective unit, in a similar manner.

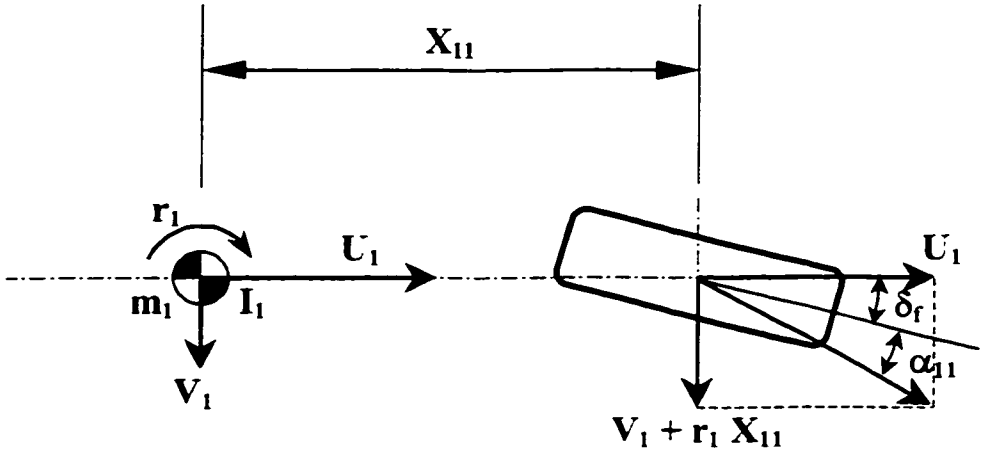

Figure 2.14 (a): Side-slip angles developed at a front axle tire.

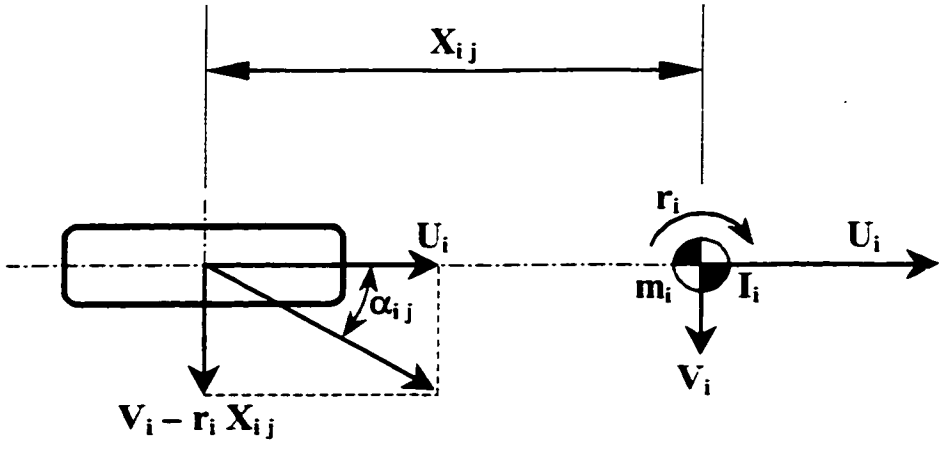

Figure 2.14 (b): Side-slip angles developed at a rear axle tire.

2.5.2 Tire Forces and Moments: Magic Formula

A pneumatic tire is a complex dynamic system, which possess mass/inertia and highly nonlinear compliance. Its static and dynamic response characteristics thus depend upon the tire properties and input conditions. A vast number of tire models have been developed to predict forces and moments generated at the tire-road interface [41, 42]. These tire models address a wide range of subjects related to tire mechanics, such as structural properties, and forces and moments, as applied for the study of ride and handling behavior of the vehicle. The study of directional dynamics of vehicles, in general, employs tire models that can predict interface forces. Such models can be classified into two general categories on the basis of the methodology [41]:

- Empirical models, which predict forces from measured data using either regression or functional relationships.
- Physical models, which attempt to model the forces through analysis of tire mechanics.

The empirical models make best use of the available measured data to predict tire forces and aligning moments under a range of operating conditions. Three different methods have been used thus far, namely, interpolation, simple functional approximation and complex functional approximation [41]. The models based upon interpolation and simple functional relations are known to be simple, which are considered applicable over a limited range of operating conditions. The models based upon complex functional approximations have been applied for wide range of operating conditions. In this study, a

model that belongs to complex functional approximation methods is used to describe the cornering forces and self-aligning moments developed by the tires. This model is known as the "Magic Formula" and provides a set of mathematical functions to describe the lateral forces, self-aligning moment and longitudinal forces developed by the tires as a function of the longitudinal and side-slip conditions, and vertical load [40].

Although this model is capable of estimating lateral forces and self-aligning moment under simultaneous existence of longitudinal and lateral slip conditions (cornering and breaking) only side-slip condition is considered in view of constant forward speed assumption associated with the yaw-plane model. The general form of the "Magic Formula" under pure side-slip or cornering conditions is given by [40]:

$$y(x) = D \cdot \sin\left[C \cdot \arctan\left\{B \cdot x - E \cdot \left(B \cdot x - \arctan\left(B \cdot x\right)\right)\right\}\right]$$

and **(2.25)**

$$Y(X) = y(x) + S_v$$
$$x = X + S_h$$

where the input variable x describes the side-slip angle, α_{ij}. The dependent variable $Y(X)$ describes either the lateral force, F_{ij}, or self-aligning moment due to pneumatic trail of the tire, $(M_{ij})_{PT}$. The coefficients B, C, D, and E are computed from measured data. S_h and S_v represent the offsets in the input and output variables that might arise from the measured data. Figure 2.15 illustrates the relationship between independent and dependent variables, derived from Equation (2.25). From Figure 2.15, the coefficient D is

computed from the peak value, y_{max}, in the x-y axes system. The coefficient D is thus known as the *peak factor*, given by:

$$D = y_{max} \tag{2.26}$$

The product BCD corresponds to the slope at the origin, given by:

$$BCD = d\left.\frac{y(x)}{dx}\right|_{\substack{x=0 \\ y=0}} \tag{2.27}$$

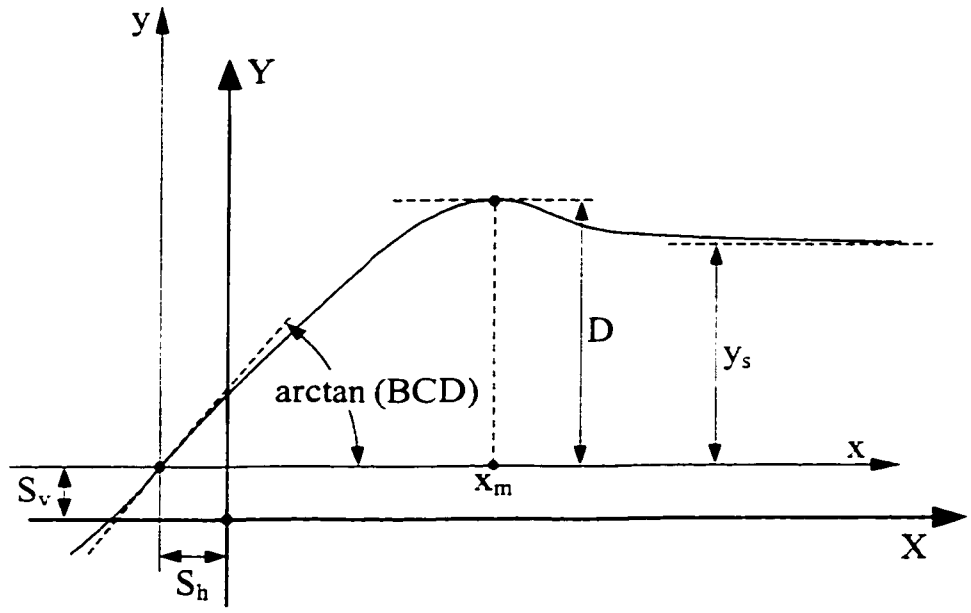

Figure 2.15: Typical tire characteristic.

In Figure 2.15, X_m relates to side-slip value at which the peak output, y_{max} is attained. y_s represents the asymptotic value of the output variable in the x-y axis system at

large values of side-slip angles, which satisfies Equation (2.26), when a peak value is not apparent. The coefficient ***C***, known as the *shape factor*, is computed as:

$$C = \frac{2}{\pi} \cdot arcsin\left(\frac{y_s}{D}\right) \tag{2.28}$$

The shape factor, ***C***, determines the shape of the resulting curve by controlling the limits of the range of the argument of the sine function. The coefficient ***B***, identified as the *stiffness factor*, can be computed from Equations (2.26) to (2.28), such that:

$$B = \frac{dy/dx\big|_{x=0}}{C \cdot D} \tag{2.29}$$

The coefficient ***E*** in Equation (2.25) is referred to as the *curvature factor*, and it controls the curvature near the peak value of the output variable [40]. This coefficient is computed from:

$$E = \frac{B \cdot X_m - tan\left(\frac{\pi}{2 \cdot C}\right)}{B \cdot X_m - arctan\left(B \cdot X_m\right)} \tag{2.30}$$

In this analysis, the coefficients ***B***, ***C***, ***D***, and ***E*** are computed from a given measured data, which serve as initial values for the Magic Formula described in Equation (2.25). The curve fitting routines, such as least square regression procedure, are then applied to derive optimal values of the coefficients to achieve minimal deviation from the

measured data. The Magic Formula has been extensively used in numerous reported studies on vehicle dynamics [42, 43] and is known to provide a reasonably good estimate of the forces and moments under a wide range of operating conditions. It should be noted, however, that a particular set of optimal Magic Formula coefficients, applied into Equation (2.25), defines a particular tire cornering properties for a given vertical load condition. Different sets of optimal Magic Formula coefficients, defining specific cornering properties of the tire, are thus required to be computed for each vertical load. A more complex form of the Magic Formula, which depends on up to 20 coefficients and is capable of predicting the tire cornering properties as a function of both side-slip and camber angles and vertical loads, is available. [40]. The version of the Magic Formula and its coefficients, described from Equations (2.25) to (2.30) are, however, acceptable for the purposes of this work, and thus applied for predicting the tire cornering properties.

LATERAL TIRE FORCES

The directional response of a vehicle subject to steering maneuvers at constant forward speed is primarily influenced by the cornering properties of tires. The cornering force, F_{ij}, is strongly related to the side-slip angle, α_{ij}, and the vertical load, $\mathbf{Fz}_{ij}$ [44]. The strong nonlinear dependency of the lateral force on the vertical or normal load and side-slip angle can be clearly observed from the measured data obtained for a Goodyear G286 11R24.5 at an inflation pressure of 13.5 kPa (93psi), which is summarized in Table 2.1 [45] and plotted in Figure 2.16. In freight vehicles, the axle loads and thus the tire loads may vary considerably depending upon the loading conditions. The lateral force

developed at the tire–road interface can thus vary considerably under varying load conditions.

For a given tire load, the measured data is analyzed to derive initial values of coefficients, ***B***, ***C***, ***D***, and ***E*** to be used in the Magic Formula, using Equations (2.26) to (2.30). Equation (2.25) is then solved and an error function, between the computed output function ***Y(x)*** and measured data, is computed. An optimization is performed to minimize the error function by selecting optimal values of the coefficients. The coefficients from the analysis and validity of the Magic Formula are presented in Chapter 3.

Table 2.1: Measured lateral force as a function of side-slip angle and vertical load for a Goodyear G286 11R24.5 tire at an inflation pressure of 13.5 kPa (93 psi) [45].

LATERAL FORCE (per tire), N					
Slip Angle, degrees	**VERTICAL LOAD, N**				
	0	**8940**	**20060**	**31110**	**41750**
0	0	0	0	0	0
1	0	1317	2862	3550	3724
2	0	2435	5393	6865	7328
4	0	4258	9376	12462	13798
8	0	6829	14352	19598	22427
12	0	8717	17178	23136	27042

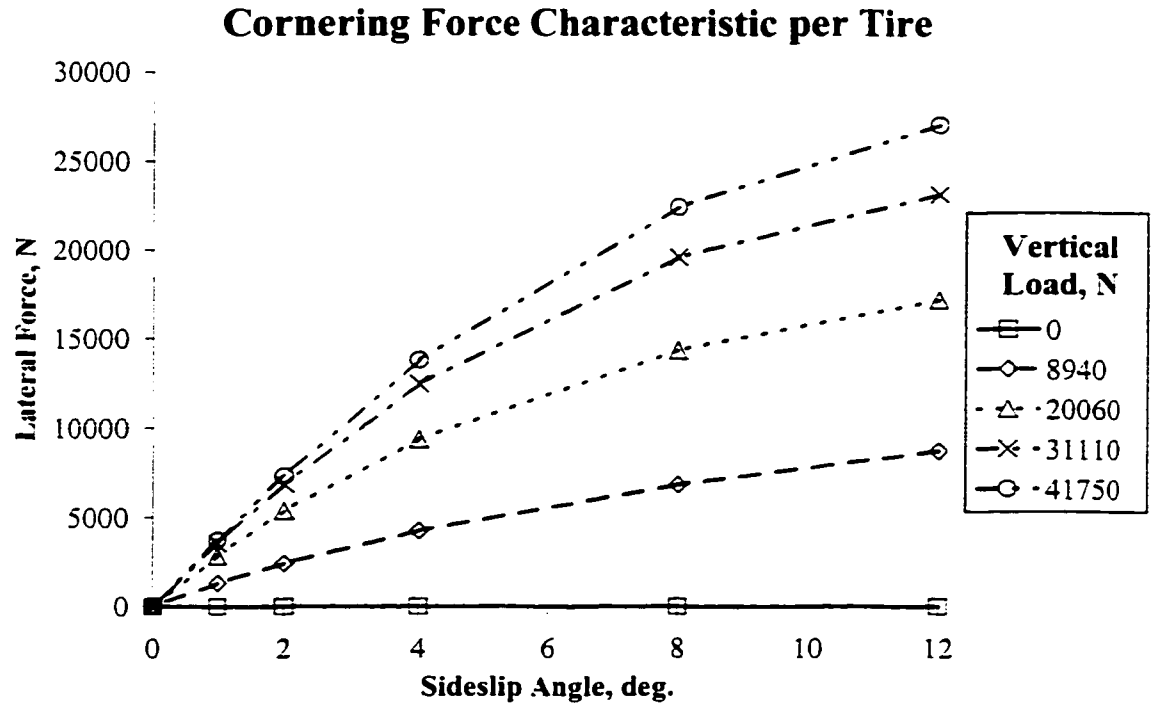

Figure 2.16: Measured lateral force characteristic of a Goodyear G286 11R24.5 tire at an inflation pressure of 13.5 kPa (93 psi) [45].

ALIGNING MOMENTS

The total aligning moment, M_{ij}, developed at the tire-road interface consist of two components, namely, an aligning moment due to the dual tire effect, $(M_{ij})_{DT}$, and an aligning moment due to the pneumatic-trail effect, $(M_{ij})_{PT}$. The former is created by a set of dual tires as a result of the longitudinal slip developed between the tires in a dual tire set constrained to roll at the same angular velocity on a curved path. The aligning moment developed by the dual tire set due to this effect is derived as [46]:

$$\left(M_{ij}\right)_{DT} = -\left(\frac{C_{Sij} \cdot (y_{DT})^2}{U_i}\right) \cdot r_i \qquad \textbf{(2.31)}$$

where C_{Sij} is the longitudinal stiffness of the tire on axle j of unit i, and y_{DT} is one–half of the lateral space between a dual tire set. U_i, and r_i are the forward speed, and the yaw rate, respectively, of the unit i, to which the axle is attached.

The aligning moment, M_{ij}, due to pneumatic trial, as in the case of the tire-cornering characteristic, is a strongly nonlinear function of side-slip angle and normal load. Table 2.2 shows the measured self-aligning torque for a Goodyear G286 11R24.5 tire at four different vertical loads and five different side-slip angles at an inflation pressure of 13.5 kPa (93psi) [45]. Figure 2.17 illustrates the variation in self-aligning moment with side-slip angle and normal load, which clearly illustrates the nonlinear behavior.

As in the case of lateral force, aligning moment due to pneumatic trail is obtained from the Magic Formula relationship, Equation (2.25). The coefficients B, C, D, and E are computed using the measured date and Equations (2.26) to (2.30). The total aligning moment developed at the tire-road interface, M_{ij}, is then obtained by combining the components due to dual tire spacing, $(M_{ij})_{DT}$, and due to pneumatic trail, $(M_{ij})_{PT}$:

$$M_{ij} = (M_{ij})_{DT} + (M_{ij})_{PT} \qquad \textbf{(2.32)}$$

Table 2.2: **Self-aligning torque due to slip angle and vertical load for a Goodyear G286 11R24.5 tire at an inflation pressure of 13.5 kPa (93 psi) [45].**

SELF-ALIGNING TORQUE, N-m					
Slip Angle, degrees	VERTICAL LOAD, N				
	0	8940	20060	31110	41750
0	0	0	0	0	0
1	0	32.72	117.12	211.41	299.35
2	0	53.82	201.66	377.4	549.7
4	0	69.31	281.21	562.65	872.15
8	0	70.84	281.68	577.09	959
12	0	73.83	260.2	492.89	788

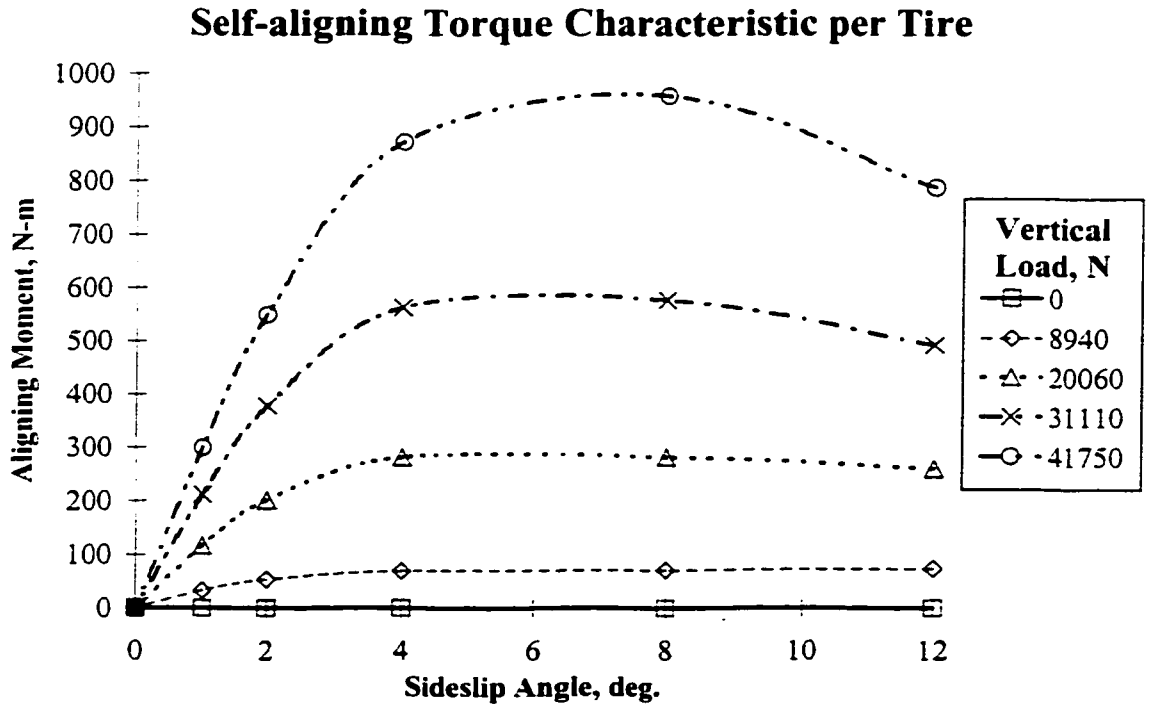

Figure 2.17: Measured self-alignment torque characteristic of a Goodyear G286 11R24.5 tire at an inflation pressure of 13.5 kPa (93 psi) [45].

2.6 Equations of Motion

Using the assumptions described in section 2.2.1, a nonlinear model for the planar yaw motion of the A–train double combination is developed, as shown in Figure 2.1. The yaw-plane model allows up to three axles for units 1, 2, and 4 and up to two axles for unit 3. The yaw-plane dynamic model is developed through systematic integration of nonlinear tire forces and moments, constraint velocities and forces, and damping forces. The governing equation of motion for the vehicle combination are derived to describe the lateral and yaw motions of each unit, while the forward speed is assumed constant. The equations of motion derived for two cases of articulation damping configurations are described in the following subsections.

2.6.1 Articulation Damping between Units 2 and 3 (Case I)

Unit 1:

$$m_1 \cdot \left(\dot{V}_1 + U \cdot r_1\right) = \sum_{j=1}^{3} F_{1j} + F_{AY}$$

$$I_1 \cdot \dot{r}_1 = X_{11} \cdot F_{11} - \sum_{j=2}^{3} \left(X_{1j} \cdot F_{1j}\right) - X_{1A} \cdot F_{AY} + \sum_{j=1}^{3} M_{1j} \qquad \textbf{(2.33)}$$

Unit 2:

$$m_2 \cdot \left(\dot{V}_2 + U \cdot r_2\right) = -F_{2Y} + \sum_{j=1}^{3} F_{2j} + F_{BY} + F_{KY} - F_{MY}$$

$$I_2 \cdot \dot{r}_2 = -X_{2A} \cdot F_{2Y} - \sum_{j=1}^{3} \left(X_{2j} \cdot F_{2j}\right) - X_{2B} \cdot F_{BY} + \sum_{j=1}^{3} M_{2j} - X_{2B} \cdot F_{KY} + X_{2B} \cdot F_{MY} - c \cdot F_{KX} + c \cdot F_{MX} \quad \textbf{(2.34)}$$

Unit 3:

$$m_3 \cdot \left(\dot{V}_3 + U \cdot r_3\right) = -F_{3Y} + \sum_{j=1}^{2} F_{3j} + F_{CY} - F_{LY} + F_{NY}$$

$$I_3 \cdot \dot{r}_3 = -X_{3B} \cdot F_{3Y} - \sum_{j=1}^{2} \left(X_{3j} \cdot F_{3j}\right) - X_{3C} \cdot F_{CY} + \sum_{j=1}^{2} M_{3j} - \left(X_{3B} - a\right) \cdot F_{LY} + \left(X_{3B} - a\right) \cdot F_{NY} + b \cdot F_{LX} - b \cdot F_{NX} \quad \textbf{(2.35)}$$

Unit 4:

$$m_4 \cdot \left(\dot{V}_4 + U \cdot r_4\right) = -F_{4Y} + \sum_{j=1}^{3} F_{4j}$$

$$I_4 \cdot \dot{r}_4 = -X_{4C} \cdot F_{4Y} - \sum_{j=1}^{3} \left(X_{4j} \cdot F_{4j}\right) + \sum_{j=1}^{3} M_{4j} \quad \textbf{(2.36)}$$

where m_i, and I_i are the mass and yaw mass moment of inertia of unit i (i = 1, 2, 3, 4). $\dot{V}_i$, $\dot{r}_i$, and r_i are the lateral acceleration, yaw acceleration, and yaw velocity, respectively, of unit i (i = 1, 2, 3, 4), with respect to the body-fixed system of each unit, as shown in Figure 2.1. **U** is the forward speed of the vehicle combination. $\mathbf{X}_{ij}$ are the longitudinal

distances between axle j of unit i (j = 1,2,3 for i = 1,2,4; and j = 1,2 for i = 3). $\mathbf{X}_{1A}$ and $\mathbf{X}_{2A}$ are the longitudinal distances between the CG of units 1 and 2 and articulation **A**. $\mathbf{X}_{2B}$ and $\mathbf{X}_{3B}$ are the longitudinal distances between the CG of units 2 and 3 and articulation **B**. $\mathbf{X}_{3C}$ and $\mathbf{X}_{4C}$ are the longitudinal distances between the CG of units 3 and 4 and articulation **C**. F_{ij} are the lateral forces developed by tires on axle j of unit i, which are derived using the Magic Formula expressed in Equations (2.25) to (2.30). M_{ij} are the total aligning moments developed by tires on axle j of unit i, as expressed in Equation (2.32). $\mathbf{F}_{AY}$, $\mathbf{F}_{BY}$, and $\mathbf{F}_{CY}$ are components of constraints forces acting on the leading units along their body-fixed y-axis due to coupling joints **A**, **B** and **C**, respectively, as shown in Figures 2.1 and 2.12. $\mathbf{F}_{2Y}$, $\mathbf{F}_{3Y}$ and $\mathbf{F}_{4Y}$ represent the constraint forces acting at articulation joints **A**, **B** and **C**, respectively, of following units along their body-fixed y-axis, as shown in Figures 2.1 and 2.12, and expressed in Equations (2.20). $\mathbf{F}_{\ell X}$ and $\mathbf{F}_{\ell Y}$ are longitudinal and lateral components of damping forces acting on the coupled units at mount ℓ (ℓ = **K**, **L**, **M** and **N**), as expressed in Equations (2.17). a, b and c are geometric parameters, which define the location of damper mounts between units 2 and 3, as shown in Figure 2.2.

2.6.2 Articulation Damping between Units 2 and 4 (Case II)

Unit 1:

$$m_1 \cdot \left(\dot{V}_1 + U \cdot r_1\right) = \sum_{j=1}^{3} F_{1j} + F_{AY}$$

$$I_1 \cdot \dot{r}_1 = X_{11} \cdot F_{11} - \sum_{j=2}^{3}\left(X_{1j} \cdot F_{1j}\right) - X_{1A} \cdot F_{AY} + \sum_{j=1}^{3} M_{1j} \qquad \textbf{(2.37)}$$

Unit 2:

$$m_2 \cdot \left(\dot{V}_2 + U \cdot r_2\right) = -F_{2Y} + \sum_{j=1}^{3} F_{2j} + F_{BY} + F_{KY} + F_{MY}$$

$$I_2 \cdot \dot{r}_2 = -X_{2A} \cdot F_{2Y} - \sum_{j=1}^{3}\left(X_{2j} \cdot F_{2j}\right) - X_{2B} \cdot F_{BY} + \sum_{j=1}^{3} M_{2j} - X_{2B} \cdot F_{KY} + X_{2B} \cdot F_{MY} - c \cdot F_{KX} + c \cdot F_{MX} \quad \textbf{(2.38)}$$

Unit 3:

$$m_3 \cdot \left(\dot{V}_3 + U \cdot r_3\right) = -F_{3Y} + \sum_{j=1}^{2} F_{3j} + F_{CY}$$

$$I_3 \cdot \dot{r}_3 = -X_{3B} \cdot F_{3Y} - \sum_{j=1}^{2}\left(X_{3j} \cdot F_{3j}\right) - X_{3C} \cdot F_{CY} + \sum_{j=1}^{2} M_{3j} \quad \textbf{(2.39)}$$

Unit 4:

$$m_4 \cdot \left(\dot{V}_4 + U \cdot r_4\right) = -F_{4Y} + \sum_{j=1}^{3} F_{4j} + F_{LY} + F_{NY}$$

$$I_4 \cdot \dot{r}_4 = -X_{4C} \cdot F_{4Y} - \sum_{j=1}^{3}\left(X_{4j} \cdot F_{4j}\right) + \sum_{j=1}^{3} M_{4j} + \left(X_{4C} + a\right) \cdot F_{LY} + \left(X_{4C} + a\right) \cdot F_{NY} + b \cdot F_{LX} + b \cdot F_{NX} \quad \textbf{(2.40)}$$

where m_i, and I_i are the mass and yaw mass moment of inertia of unit i (i = 1, 2, 3, 4). $\dot{V}_i$, $\dot{r}_i$, and r_i are the lateral acceleration, yaw acceleration, and yaw velocity, respectively, of unit i (i = 1, 2, 3, 4), with respect to the body-fixed system of each unit, as shown in Figure 2.1. **U** is the forward speed of the vehicle combination. $\mathbf{X}_{ij}$ are the longitudinal

distances between axle j of unit i (j = 1,2,3 for i = 1,2,4; and j = 1,2 for i = 3). $\mathbf{X}_{1A}$ and $\mathbf{X}_{2A}$ are the longitudinal distances between the CG of units 1 and 2 and articulation **A**. $\mathbf{X}_{2B}$ and $\mathbf{X}_{3B}$ are the longitudinal distances between the CG of units 2 and 3 and articulation **B**. $\mathbf{X}_{3C}$ and $\mathbf{X}_{4C}$ are the longitudinal distances between the CG of units 3 and 4 and articulation **C**. F_{ij} are the lateral forces developed by tires on axle j of unit i, which are derived using the Magic Formula expressed in Equations (2.25) to (2.30). M_{ij} are the total aligning moments developed by tires on axle j of unit i, as expressed in Equation (2.32). $\mathbf{F}_{AY}$, $\mathbf{F}_{BY}$, and $\mathbf{F}_{CY}$ are components of constraints forces acting on the leading units along their body-fixed y-axis due to coupling joints **A**, **B** and **C**, respectively, as shown in Figures 2.1 and 2.12. $\mathbf{F}_{2Y}$, $\mathbf{F}_{3Y}$ and $\mathbf{F}_{4Y}$ represent the constraint forces acting at articulation joints **A**, **B** and **C**, respectively, of following units along their body-fixed y-axis, as shown in Figures 2.1 and 2.12, and expressed in Equations (2.20). $\mathbf{F}_{\ell X}$ and $\mathbf{F}_{\ell Y}$ are longitudinal and lateral components of damping forces acting on the coupled units at mount ℓ (ℓ = **K**, **L**, **M** and **N**), as expressed in Equations (2.19). a, b and c are geometric parameters, which define the location of damper mounts between units 2 and 4, as shown in Figure 2.3.

Upon elimination of the constraints forces, using Equations (2.20), in Equations (2.33) to (2.36), for Case I, and in Equations (2.37) to (2.40), for Case II, substituting the rates of change of lateral velocities of units 2, 3 and 4 from Equations (2.22) and (2.23), and assuming constant forward speed (driving forces balanced by motion resistances), the yaw-plane dynamics of the vehicle, for each damped articulation case, can be represented

by a set of eight-first order differential equations of motion, describing in the matrix form as:

$$[A]\cdot\{\dot{x}\}=[B]\cdot\{x\}+\{MM\} \tag{2.41}$$

where $\{x\}$ is a vector of state-variables that consist of the eight dependent generalized coordinates, expressed as:

$$\{x\}=(V_1, r_1, r_2, r_3, r_4, \gamma_1, \gamma_2, \gamma_3)^T \tag{2.42}$$

The $[A]$ and $[B]$ are 8x8 matrices of vehicle's inertial properties and geometric parameters. The vector $\{MM\}$ contains the nonlinear tire forces and moments, and damping forces. The general structure of the matrices $[A]$ and $[B]$ and vector $\{MM\}$, together with their elements are described in Appendix I for Cases I and II.

2.7 Summary

A nonlinear yaw-plane analytical model of an A-train double combination incorporating damped articulations is developed to study the potential benefits in the response of the vehicle combination. Two concepts of damped articulations are suggested, namely, Case I, which incorporates damped articulation between units 2 and 3, and Case II, which incorporates damped articulations between units 2 and 4. A comprehensive kinematic analysis of the two configurations is performed, and its mathematical formulation, which reveals nonlinear geometric relationships, is

incorporated into the nonlinear yaw-plane model. Nonlinear tire forces and moments are formulated based on 'Magic Formula', whose coefficients can be optimized for given measured data of a tire. Finally, the yaw-plane equations of motion for a multi-unit A-train double is derived, incorporating the nonlinear tire forces and moments and damped articulations.

Chapter 3

Performance Measures and Methods of Analysis

3.1 General

Owing to relaxation of size and weight regulations on heavy vehicles, the freight transportation sector has adopted many variations in vehicle configurations and design parameters in order to improve the operating efficiency. The use of multi-trailer commercial vehicles or long combination vehicles (LCVs), such as doubles and triples, has thus been increasing throughout North America [26]. It has also been recognized that changes in vehicle weights and dimensional parameters, and configurations greatly affect the dynamic characteristics of the vehicle, which can limit the stability and handling capabilities of LCVs [29, 30, 31]. Many safety concerns have thus been raised due to lower stability and control limits of LCV's. An array of performance measures has thus been proposed to assess the stability, control, handling, and maneuverability of existing and new designs of LCVs [30]. In this chapter, the performance measures of an A-train double combination with articulation dampers are assessed and discussed in view of the present investigation. The assessment methodology together with necessary steering

excitations are described for each performance measure. A driver-vehicle model is proposed to analyze the vehicle behavior in closed-loop path-following maneuvers.

3.2 Performance Measures

During the application of a steering input and the achievement of the steady-state motion of the A-train, all the units of the combination undergo a transient state. The handling and directional control qualities of the combination are related to its steady-state and transient response characteristics. The steady-state and transient directional response characteristics of a vehicle combination may be evaluated under different steering maneuvers, namely, open loop and closed-loop maneuvers. In an open loop steering maneuver, a known time-history of steer angle of the front wheels is applied to the vehicle model. In a closed-loop maneuver, the directional input to the vehicle model is applied is terms of coordinates of the path while the required wheel steer angles are computed using a driver-vehicle model.

The directional control and handling performance characteristics of freight vehicles are frequently evaluated in terms of a set of performance measures related to lateral, yaw and roll response behavior of the combination [21, 30]. These performance measures are evaluated under a specified steering maneuver. The potential performance benefits of proposed articulation mechanisms can be effectively evaluated using these performance measures. A set of six performance measures are thus defined to assess the performance potentials of articulation damping concepts, which are related to both steady-state and transient lateral and yaw dynamic responses of the A-train double

combination. These selected performance measures include Transient Response Time, Understeer Coefficient (Ku), Steady-state High-speed Offtracking (HOF), Yaw Damping Ratio (YDR), Rearward Amplification (RWA) Ratio, and Transient high-speed Offtracking (TOF). The significance of these performance measures, in view of handling and control performance and the associated analysis methodologies, are discussed in the following subsections.

3.2.1 Transient Response Time

The transient response time performance measure of a combination is defined as the time required by each unit of the vehicle combination to reach 90% of its steady-state lateral acceleration when it undergoes the 'ramp' part of a ramp-step directional maneuver, as shown in Figure 3.1, which is performed in an open loop fashion. The measure thus relates to the vehicle's ability to damp out the lateral oscillations under a steer input. El-Gindy and Woodrooffe [47] have proposed that the transient response time ranging from 0.3s to 1.7s is considered acceptable. The proposed range, however, depends upon various factor related to driver and external disturbances which may be encountered during actual field measurements.

The transient response time performance of the A-train double combination is evaluated through solution of the set of differential equations, derived in chapter 2, under a ramp-step steer input. The recommended steer-input, which consists of two parts: a ramp input followed by a step portion, as shown in Figure 3.1, is applied to the front-

wheels. This proposed maneuver is used to evaluate both the transient and steady-state response of the A–train double, which is performed under following conditions:

i) Vehicle's forward speed, U, is constant and equal to 100km/h.

ii) The steering rate during the ramp portion is 5deg/s, which represents the maximum steering rate a driver can typically apply [47], and the maximum steering input at the wheels of the first axle of unit 1 is limited to 1 degree.

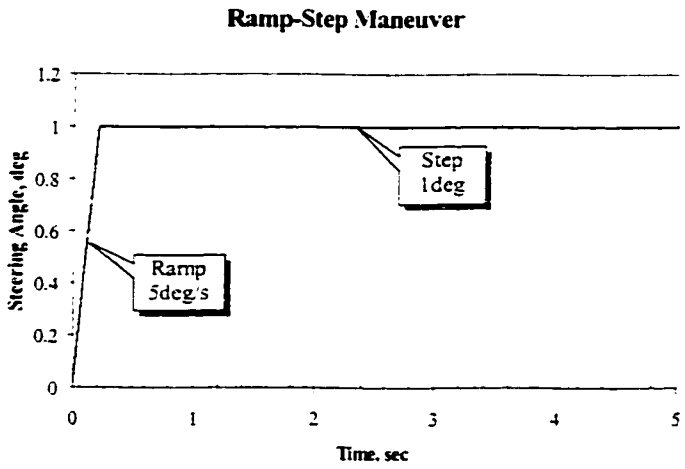

Figure 3.1: Ramp-step maneuver.

3.2.2 Understeer Coefficient (Ku)

The steady-state handling property of a ground vehicle is frequently described by its understeer coefficient (Ku), which is a complex function of tire cornering stiffness, vehicle weight distribution and geometry [44]. The handling performance of the A-train double is thus evaluated in terms of understeer coefficients of the combination when a response is attained under the ramp-step maneuver. The understeer coefficient of each

unit of the A-train double combination is derived from the equation governing the steady-state handling characteristic [44]. Depending upon the value of the understeer coefficient, the steady-state handling characteristics may be classified into three categories: neutral steer, understeer, and oversteer [44]. For the particular case of a tractor-semitrailer combination, it has been established that the combination is directionally stable when both units are understeer. An oversteer tractor may yield directional instability irrespective of the semitrailer's understeer coefficient [44].

In this study, the equations of motion for the yaw-plane dynamics of the A-train double combination are solved under the ramp-step steer input to derive steady-state values of lateral accelerations and articulation angles. The understeer coefficients of different units of the A-train double are then computed from the following relations, derived from steady-state handling analysis [44]:

Unit 1:

$$Ku_1 = -\left[\frac{3.6 \cdot WB_1 \cdot r_1/U - \delta_f}{a_{y1}}\right] \cdot g \qquad \textbf{(3.1)}$$

Unit i (i = 2, 3, 4):

$$Ku_i = -\left[\frac{3.6 \cdot WB_i \cdot r_i/U - \gamma_{(i-1)}}{a_{yi}}\right] \cdot g \qquad \textbf{(3.2)}$$

where

Ku_i = Understeer coefficient of unit i in degrees

WB_i = Wheelbase of unit i in m

r_i = Steady-state yaw rate of unit i with respect to its CG in deg./s

U = Forward speed of the A-train double in km/h

δ_f = Front wheel steer angle in degrees

$\gamma_{(i-1)}$ = Articulation angle (1, 2, 3) of coupled units in degrees

g = Acceleration due to gravity

a_{yi} = Steady-state lateral acceleration of unit i in m/s^2

The wheelbases of different units of the A-train double combination are defined as follows:

$$WB_1 = X_{11} + \left(\frac{X_{12} + X_{13}}{2}\right); \qquad WB_2 = X_{2A} + \left(\frac{X_{22} + X_{23}}{2}\right)$$

$$WB_3 = X_{3B} + X_{32}\ ; \qquad \text{and} \qquad WB_4 = X_{4C} + X_{43} \tag{3.3}$$

where X_{11}, X_{12}, X_{13}, X_{22}, X_{23}, X_{32}, X_{43}, X_{2A}, X_{3B}, and X_{4C} are identified in the yaw-plane model of the vehicle combination, shown in Figure 2.1.

A unit is considered to possess understeering characteristics when $Ku_i > 0$. Alternatively, the unit is considered as oversteer when $Ku_i < 0$. In the limiting case of $Ku_i = 0$, the unit is identified as neutral steer. In the event, any unit of the A-train double exhibits an oversteer response in steady-state, the particular unit is considered to possess a critical forward speed, beyond which the combination may exhibit a directionally unstable response. The critical speed can be computed directly from the understeer coefficient in the following manner:

$$U_{cr} = \sqrt{\frac{g \cdot WB \cdot 180}{-Ku \cdot \pi}} \times 3.6 \qquad (3.4)$$

where U_{cr} is the critical speed of the unit with oversteer characteristics in km/h, and Ku is the understeer coefficient of the unit in degrees.

It should be noted that the combination with an oversteer unit remains directionally stable for vehicle speed $U < U_{cr}$.

To evaluate the handling performance of the A-train when any of the unit is oversteer, a pass/fail criterion is applied by comparing the Ku (derived from steady-state response under defined ramp-step input) with the critical understeer coefficient, Ku_{cr}. The vehicle is considered to pass the criterion when $Ku > Ku_{cr}$, where Ku_{cr} is derived in the following manner [30, 44]:

$$(Ku_{cr})_i = -\frac{WB_i \cdot g}{U^2} \cdot \frac{648}{\pi} \qquad \text{for unit i (i = 1, 2, 3, 4)} \qquad (3.5)$$

3.2.3 Steady–state High–speed Offtracking (HOF)

Steady–state high–speed offtracking (HOF) is the steady-state lateral deviation between the path followed by the front axle of the first unit and the path followed by the rearmost axle of the last vehicle unit during the 'step' part of a ramp-step maneuver. The HOF provides a measure of vehicle's tendency to deviate laterally during a cornering maneuver and the path swept by the combination.

The HOF is computed from the steady-state response attained under the last portion of the ramp-step maneuver, as shown in Figure 3.1, while the forward speed of the vehicle is held constant at 100km/h [47]. The HOF of the combination is derived from the geometry of the combination, and a detailed derivation is presented in Appendix II. A suggested threshold value for this performance measures is 0.46m [30]. This value, however, is reported as an arbitrary value selected to illustrate the condition in which a minimal clearance of 0.15m remains between the last axle of the rearmost unit and the outside of a 3.6m wide conventional traffic lane, for a tractor with 2.44 overall-track-width.

3.2.4 Yaw Damping Ratio (YDR)

The yaw damping ratio (YDR) performance measure relates to rate of decay of the lateral acceleration oscillations of the rearmost unit of an articulated vehicle subject to a half-sine steer maneuver, also referred to as a pulse. Figure 3.2 illustrates the half-sine steer maneuver, which is applied at the front wheels in an open loop manner. Although this performance measure is rarely used in tractor-semitrailer combinations, it has been discussed and recognized by several research groups that this performance measure is important since it characterizes the directional damping ratio of the rearmost trailer of an articulated vehicle, such as doubles and triples [30]. Light damping in the yaw mode causes swaying of the trailer and could lead to a highway accident.

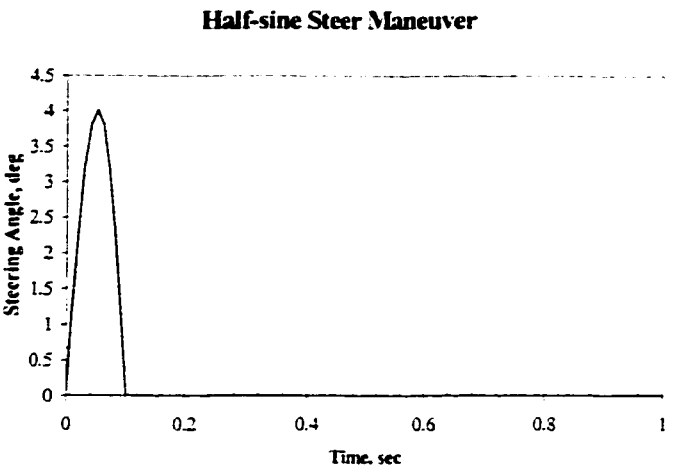

Figure 3.2: Half-sine (Pulse) maneuver.

The YDR of the A-train double combination is evaluated through solution of differential equations of motion describing the yaw plane dynamics under a half-sine steering input of 4°-amplitude in a time interval of 0.1s, as shown in Figure 3.2. The forward speed of the vehicle is held constant at 100km/h. The transient lateral acceleration response characteristics of the rearmost unit (unit 4) are evaluated and analyzed to derive the rate of decay of its free oscillations. Logarithmic decrement method [48] is applied to derive the rate of decay and the amount of yaw damping present in the system. The method is thus applied to derive the rate of decay in yaw rate oscillations of the unit 4. A larger yaw damping yields rapid decay of oscillations in yaw rate and lateral acceleration response and thus improves yaw and lateral dynamic performance of the A-train double. The logarithmic decrement, δ, is computed from amplitudes of two consecutive peaks of the freely oscillating either yaw rate or lateral acceleration response of unit 4 [48]:

$$\delta = ln\left(\frac{x_1}{x_2}\right) \tag{3.6}$$

where x_1 and x_2 are amplitudes of the two consecutive oscillations. The yaw damping ratio is then computed by:

$$YDR = \frac{\delta}{\sqrt{\delta^2 + (2\pi)^2}} \tag{3.7}$$

The recommended threshold value of YDR at a forward speed of 100km/h is 0.15 [30].

3.2.5 Rearward Amplification (RWA) Ratio

The rearward amplification (RWA) ratio of a combination describes its tendency to amplify its lateral motion from the lead unit to the rearmost unit. Different units of a LCVs exhibit varying amplitudes of yaw and lateral oscillations under a steering input, as shown in Figure 3.3. A LCV is also known to exhibit this tendency to amplify the oscillations as they progress from the lead unit to the rearmost unit [16, 30]. This behavior is mostly attributed to the constraints posed by the articulation mechanism coupling the trailer (unit 2) and the A-dolly (unit 3).

RWA ratio is a frequency-dependent measure, which is defined as the relationship between the maximum movement of the first and the last vehicle units under a specified

maneuver. It is usually given in terms of lateral acceleration or yaw rate gain, as illustrated in Figure 3.3, and is used to assess the dynamic stability of the vehicle.

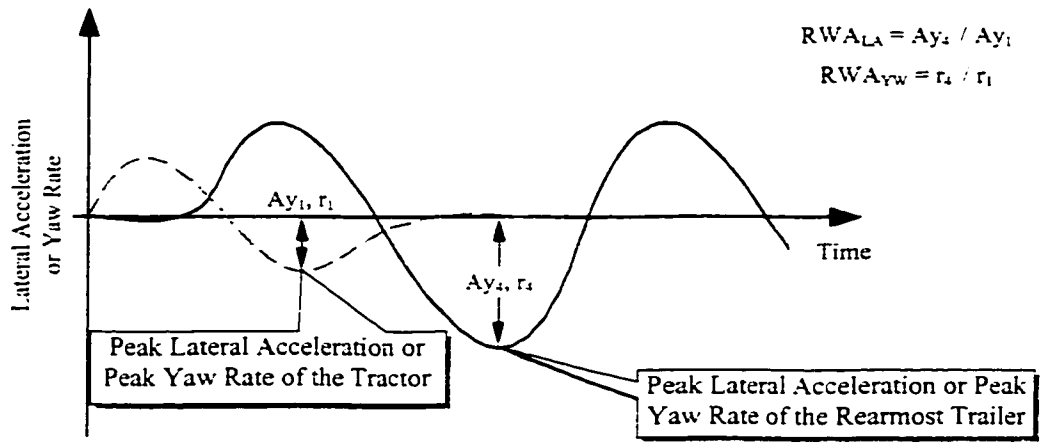

Figure 3.3: Illustration of rearward amplification.

The RWA of a LCV is evaluated under a rapid high-speed path-change maneuver, which is performed in a closed-loop manner by using the path-follower driver-vehicle model discussed in section 3.4. The forward speed of the vehicle is assumed to be constant at 100km/h. The path-change maneuver is selected such that the lateral acceleration at the CG of the first unit approaches approximately 0.15g (1.47m/s^2) within the time constraints of 3.0 seconds. Figure 3.4 describes the coordinates of the path followed during a single path-change maneuver, which is conducted in closed-loop manner during the simulation. RWA of lateral acceleration, RWA_{LA}, is defined as the ratio of the peak lateral acceleration at the CG of the rearmost unit (unit 4), $\mathbf{A_{y4}}\,|_{\mathbf{peak}}$, to the peak lateral acceleration at the CG of the tractor (unit 1), $\mathbf{A_{y1}}\,|_{\mathbf{peak}}$, as shown in Figure 3.3, and it is expressed by:

$$RWA_{LA} = \frac{A_{Y4}|_{peak}}{A_{Y1}|_{peak}} \qquad \textbf{(3.8a)}$$

Similarly, RWA of yaw rate, RWA_{YW}, characterizes the amplification or attenuation of the yaw directional response of the A-train in terms of the ratio of peak yaw rate at the CG of the rearmost unit (unit 4), $\mathbf{r_4}\,|_{\mathbf{peak}}$, to the peak yaw rate at the CG of the tractor (unit 1), $\mathbf{r_1}\,|_{\mathbf{peak}}$, as shown in Figure 3.3, and it is expressed by:

$$RWA_{YW} = \frac{r_4|_{peak}}{r_1|_{peak}} \qquad \textbf{(3.8b)}$$

The recommended threshold value for RWA_{LA} and RWA_{YW} is 2.2 or less [30].

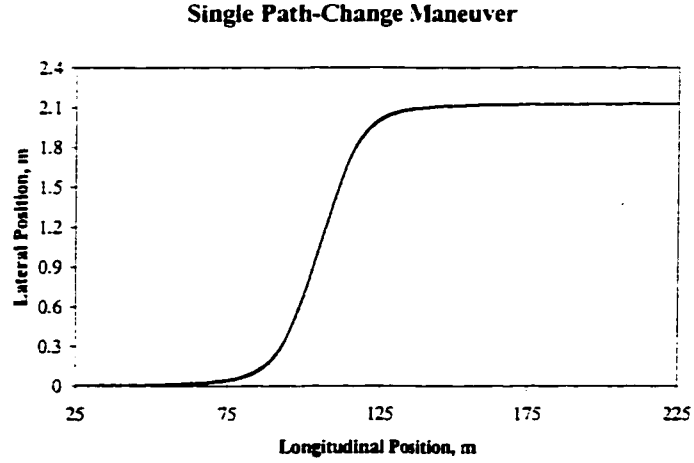

Figure 3.4: Single path-change maneuver.

3.2.6 Transient High–speed Offtracking (TOF)

Transient high-speed offtracking (TOF) of a LCV is defined as the maximum lateral overshoot of the path followed by last axle of the rearmost unit with respect to the path followed by the first axle of the unit 1. The TOF is evaluated under a high-speed path-change maneuver performed at a constant forward speed of 100km/h [30]. The performance threshold value for TOF has been recommended as 0.8m [30].

The recommended values for the selected performances measures are summarized in Table 3.1.

Table 3.1: Suggested values for the selected performance measures [16, 30, 47].

Performance Measures	Threshold Value or Range
Transient Response Time, s	from 0.30 to 1.70
Ku, deg.	$> Ku_{cr}$
HOF, m	≤ 0.46
YDR	≥ 0.15
RWA	≤ 2.20
TOF, m	≤ 0.80

3.3 Closed-loop Steering Maneuvers

The analysis of the performance measures, such as RWA and TOF, necessitates the analysis of vehicle model under path-change maneuvers to be performed in a closed-loop manner. A closed-loop steering input involves the description of coordinates of the

path to be followed by the vehicle, driver's perception of the path, path errors, and driver's reaction. The driver's perception and reaction behaviors thus need to be considered in conjunction with the nonlinear yaw-plane model of the vehicle. In this study, two different maneuvers are considered to evaluate the dynamic performance of the candidate vehicle, namely, single path-change [27, 30] and double path-change maneuvers [27]. The latter is usually referred to as evasive or obstacle avoidance maneuver. These maneuvers had invariably implemented in full-scale tests and performance analysis [15, 49]. The closed-loop path-follower driver-vehicle model is formulated to derive the front wheel steer angles required to minimize the lateral deviation between the desired trajectory and the trajectory followed by the CG of the leading unit (unit 1).

The trajectory of the desired path can be described either by a look-up table [22, 27] or by appropriate polynomial functions [50]. The look-up table approach involves description of coordinates of a large number of points on the path and interpolations to derive intermediate points, while polynomial or describing functions define the path coordinates in a continuous manner. A high-degree polynomial function, however, may be required to describe the paths followed by single and double path-change maneuvers. For instance, an eight-order polynomial function has been proposed to describe the path coordinates for a single path-change maneuver [50].

In this dissertation, a regression function similar to the Magic Formula presented in section 2.5.2, is formulated to describe the coordinated of both single and double path-change maneuvers. The methodology associated with identification of various

coefficients of Equation (2.25) for both path-change maneuvers is described in the follows subsections.

3.3.1 Single Path-Change Maneuver

The desired path to be followed by the vehicle during a single path-change maneuver may be represented by a combination of linear segments, as shown in Figure 3.5. Let **SP1** be the total lateral displacement of the vehicle, and **SP4** be the total forward displacement. Let **SP2** and **SP3** be longitudinal displacements of the vehicle realized prior to and during the primary path-change task, as shown in Figure 3.5. The total lateral displacement in a lane-change maneuver is often limited to 3.6m, which differs considerably from the 2.13m path-change recommended maneuver [30]. A path-change maneuver required to assess the vehicle performance in terms of RWA and TOF thus involves a total lateral displacement of only 2.13m. The value of **SP1** in this study is thus limited to 2.13m. **SP2** is defined as the longitudinal distance that the vehicle travels before it reaches 10% of the total lateral displacement. **SP2** is expressed in terms of the preview distance, which is a distance from the vehicle's CG to certain point connected on the vehicle (preview point), which follows the desired path.

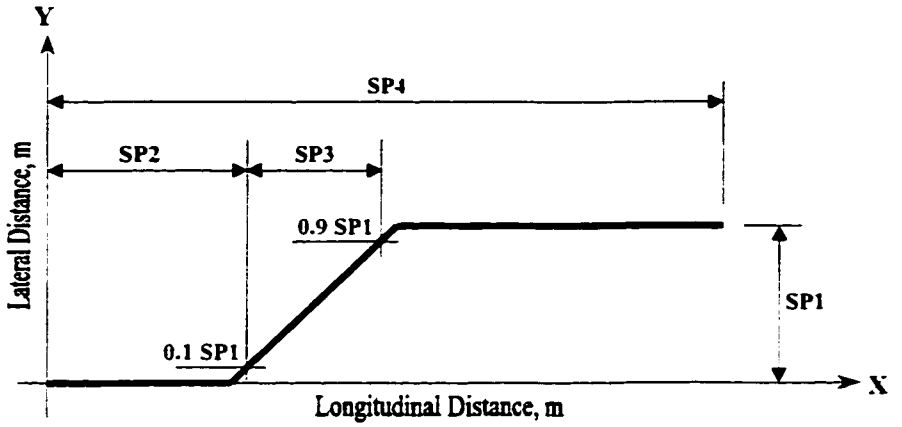

Figure 3.5: Piecewise linear approximation of the desired path during a single path-change maneuver.

In this study, the distance **SP2** is expressed as a function of the preview distance in the following manner:

$$SP2 = 3 \cdot Preview\_Distance + 30 \qquad (3.9)$$

Equation (3.9) is proposed based on trial and error such that when the driver-vehicle model 'look at' the desired path, at the beginning of the simulation, the corresponding lateral-position is at most 0.1% of the total lateral displacement, **SP1**.

SP3 is identified as the actual longitudinal distance that the vehicle travels during the single path-change, and is also described as the distance traveled by the vehicle as it traverses laterally from 10% to 90% of the total lateral displacement, **SP1**. The values ranging from 30m to 50m for **SP3** have been reported in the literature [27, 50]. **SP4**, which represents the total longitudinal distance traveled by the vehicle, is suggested to be equal to:

$$SP4 = SP2 + 8 \cdot SP3 \qquad \textbf{(3.10)}$$

Equation (3.10) is also obtained through trial and error such that the total time required for simulation of the single path-change maneuver is long enough to ensure that the A-train double reaches a steady-state condition after performing that maneuver. **SP4** may thus be different for a different vehicle configuration. The total time required for simulation of the single path-change maneuver can be computed from **SP4**, Equation (3.10), and the vehicle forward speed, in the following manner:

$$T_s = \frac{SP4}{U} * 3.6 \qquad \textbf{(3.11)}$$

where T_s is the total simulation time in seconds, and U is the vehicle forward speed in km/h.

The Magic Formula presented for predicting the tire cornering properties, as shown in Figure 3.6, can be revised to represent a single path-change maneuver, as shown in Figure 3.4. The required shape can thus be expressed by shifting the origin of the Magic Formula curve to appropriate longitudinal and lateral coordinates.

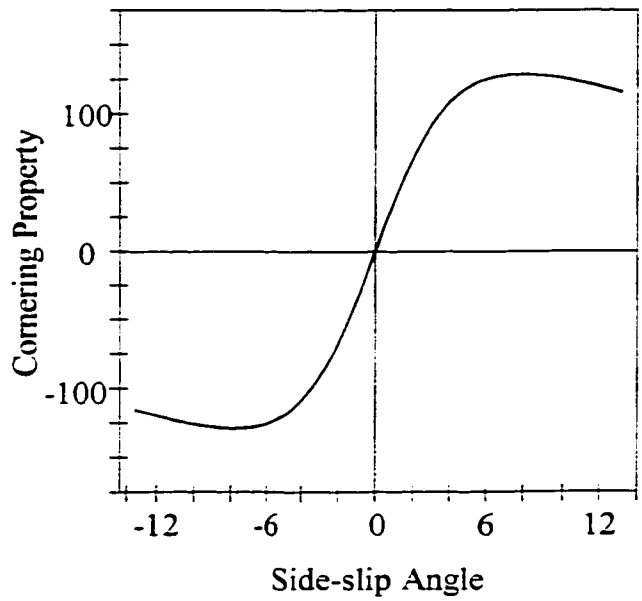

Figure 3.6: The Magic Formula tire model curve [40].

A single path-change maneuver in the form of a continuos function can thus be given by the revised Magic Formula. The expression is thus given by:

$$Y(x) = D \cdot [sin\{arctan\{B \cdot x - E \cdot (B \cdot x - arctan(B \cdot x))\}\} + 1 - Offset\_Y]$$

and **(3.12)**

$$x = X - S_h$$

where, **Y** is the lateral distance traveled by the vehicle and is expressed in meters, and it is function of the input variable **x**, which depends upon the actual longitudinal coordinate **X** and S_h. S_h corresponds to the horizontal shift of the origin required such that the new horizontal coordinate corresponds to the mid-point of the longitudinal distance that the vehicle travels during the single path-change, **SP3**, plus the previous longitudinal distance **SP2.** S_h is thus related to the longitudinal distances **SP2** and **SP3** by:

$$S_h = SP2 + \frac{SP3}{2} \tag{3.13}$$

Offset_Y is the amount of additional offset that is needed to shift vertically the single path-change curve so that the first point of the curve starts at **Y** = 0, and is given by:

$$Offset\_Y = \sin\left\{ \arctan\left\{B \cdot x - E \cdot \left(B \cdot x - \arctan\left(B \cdot x\right)\right)\right\}\right\} + 1 \Big|_{at\ X=0} \tag{3.14}$$

The product of coefficients ***B*** and ***D*** corresponds to the slope of the path-change curve in section **SP3**, as shown in Figure 3.5, and is thus expressed as:

$$B \cdot D = \frac{SP1}{SP3} \tag{3-15}$$

D corresponds to the distance the origin of curve, as shown in Figure 3.6, needs to be shifted vertically such that the new vertical coordinate of that 'origin' corresponds to the mid-point of the total lateral displacement, **SP1**. Similarly, coefficient ***E*** corresponds to the "curvature factor" defined in section 2.5.2, and it was found to be equal to −1.5, which allows **SP3** to correspond to the lateral distance starting and terminating at 10% and at 90%, respectively, of the total lateral displacement **SP1**. Coefficients ***B***, ***D*** and ***E*** were thus established as:

$$B = \frac{2}{SP3}; \qquad D = \frac{SP1}{2}; \qquad E = -1.5 \tag{3.16}$$

By using **SP1** = 2.13m, **SP3** = 30m, and **Preview_Distance** = 20m and applying Equations (3.9) through (3.16), the computed single path-change maneuver shown in Figure 3.4 was obtained.

3.3.2 Double Path-Change Maneuver

The coordinates of the desired path during a double path-change maneuver may be represented in piecewise linear approximation as shown in Figure 3.7. The longitudinal and lateral distance parameters are identified by **SP1**, **SP2**, **SP3**, and **SP4**, as shown in the figure.

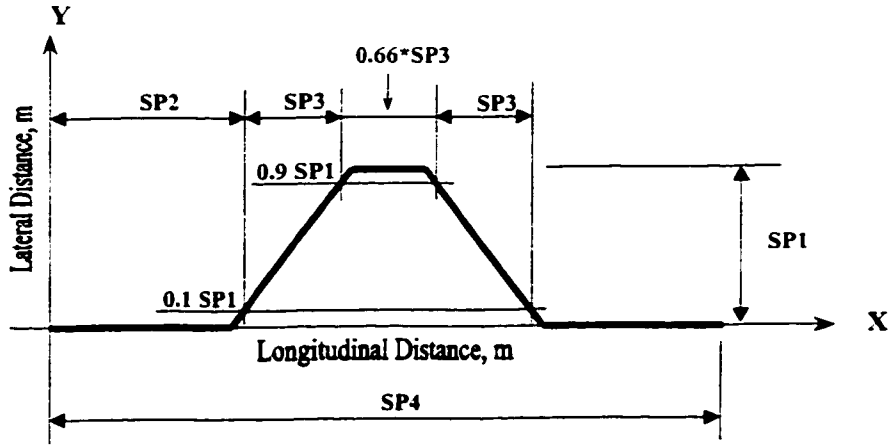

Figure 3.7: Piecewise linear approximation of the desired path during a double path-change maneuver.

SP1 represents the total lateral displacement of the vehicle; **SP2** defines the longitudinal distance traveled by the vehicle as it reaches the 10% of the total lateral displacement, and is expressed as a function of the preview distance as described by Equation (3.9). **SP3** describes the longitudinal distance traveled during first part of the double path-change maneuver, which represents lateral motion of the vehicle from 10% to 90% of the total lateral displacement. **SP3** also represents the longitudinal distance traveled by the vehicle when it changes its lateral position from 90% to 10% of the total lateral displacement during second part of the maneuver. **SP4** represents the total longitudinal distance traveled by the vehicle, and it is suggested, to be equal to:

$$SP4 = SP2 \quad + \quad 13 \cdot SP3 \tag{3.17}$$

Equation (3.17) is obtained through trial and error such that the total time required for simulation of the double path-change maneuver is long enough to ensure that the A-train double reaches a steady-state condition after performing that maneuver. **SP4** may thus be different for a different vehicle. The total time required for simulation of the double path-change maneuver can be computed from **SP4** as a function of the vehicle forward speed, and is defined by Equation (3.11).

The double path-change maneuver continuos function is derived from first derivative of Equation (3.12), from which the term consisting of the derivative of the argument of *arctan* is discarded. The double path-change maneuver function can thus be described by:

$$Y(x) = SP1 \cdot \left[\frac{\cos\{\arctan\{B \cdot x - E \cdot (B \cdot x - \arctan(B \cdot x))\}\}}{1 + [B \cdot x - E \cdot (B \cdot x - \arctan(B \cdot x))]^2} - Offset\_Y \right]$$

and **(3.18)**

$$x = X - S_h$$

where, **Y** is the lateral distance traveled by the vehicle and is expressed in meters, and is function of the input variable **x**, which depends upon the actual longitudinal coordinate **X** and S_h. The terms S_h, **Offset_Y**, and coefficients B and E, from Equation (3.18), are expressed as:

$$S_h = SP2 + 1.33(SP3)$$

$$Offset\_Y = \left. \frac{\cos[\arctan\{B \cdot x - E \cdot (B \cdot x - \arctan(B \cdot x))\}]}{1 + [B \cdot x - E \cdot (B \cdot x - \arctan(B \cdot x))]^2} \right|_{at\ X = 0} \qquad \textbf{(3.19)}$$

$$B = \frac{2}{2.66 \cdot SP3}; \qquad E = -5$$

X and **Y(x)** are longitudinal and lateral distance traveled by the vehicle, respectively, in meters. S_h corresponds to a horizontal shift of the curve that allows the first point of the curve to start at **X** = 0. **Offset_Y** is the amount of vertical offset which is needed to shift vertically the curve so that the first point of the curve starts at **Y** = 0. A value of E = –5 allows **SP3** to be in the specified range from 10% to 90% of the total lateral displacement. By using **SP1** = 2.13m, **SP3** = 30m, and **Preview_Distance** = 20m and applying Equations (3.9), (3.11), and Equations (3.17) through (3.19), the double

path-change maneuver, shown in Figure 3.8, is obtained. It has to be pointed out that Equation (3.17) is only valid in the range, $\mathbf{0 \leq X \leq 2}S_h$, and that $\mathbf{Y(x) = 0}$ for $\mathbf{X > 2}S_h$.

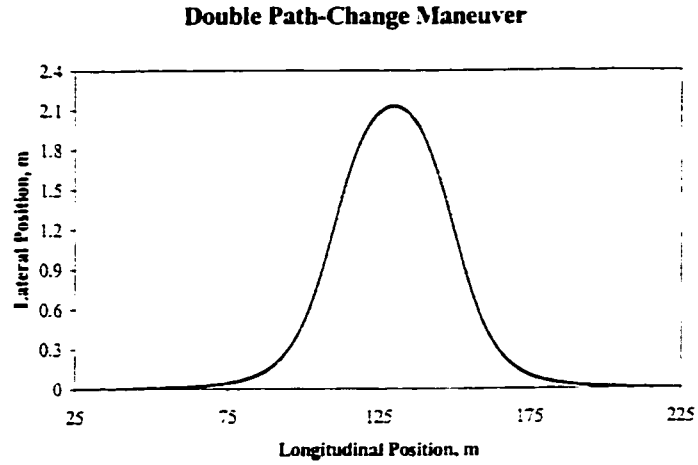

Figure 3.8: Double path-change maneuver.

3.4 Path-follower Driver-vehicle Model

The path-follower driver-vehicle model is developed to describe the closed-loop steering control of a vehicle along a prescribed path, which is based upon the preview and certain control abilities of the driver. A closed-loop path-follower model computes the front wheel steer angle, such that the CG of unit 1 follows the required path with minimal lateral deviation. A vast number of driver models have been reported in the literature, which are mostly developed for the directional control analysis of two-axle single unit vehicles [51, 52, 53]. These models are based upon preview, prediction, and compensation strategies, and involve driver behavior in terms of perception, prediction,

reaction, muscular dynamics and control abilities. In this study, a relatively simple driver-vehicle model is developed based upon the preview and prediction control.

Figure 3.9 illustrates the basic kinematics involved in such a model, and the goal is to find the steering control to cause the future vehicle's position (estimated or predicted path) to track the desired path. The driver is considered as an ideal controller capable of steering the vehicle, such that certain point on the vehicle (preview point), follows the desired path. The "preview" term is associated with models that are able to observe or predict the future desired path. The "predictive" term is used to describe the estimation process by which the model computes the future vehicle position in time.

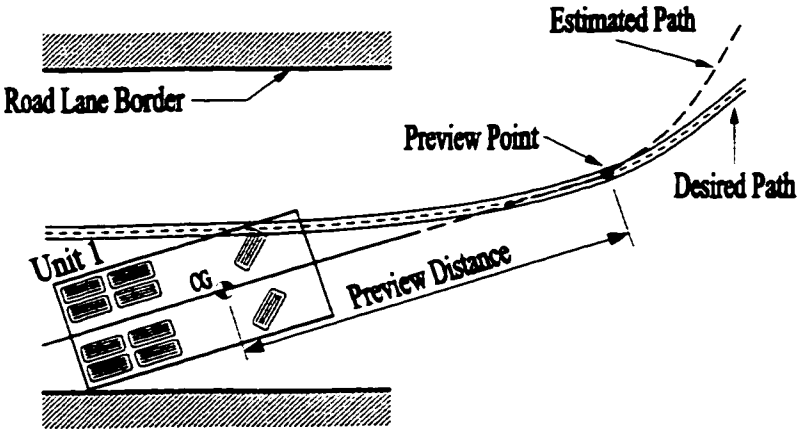

Figure 3.9: Typical path geometry used in predictive/preview driver-vehicle model formulation.

Figure 3.10 illustrates structure of a closed-loop predictive/preview driver-vehicle system.

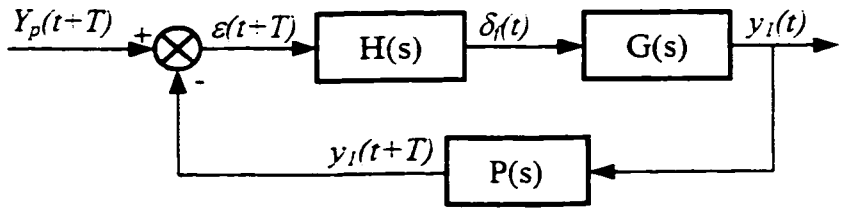

Figure 3.10: Structure of the closed-loop predicted/preview driver-vehicle model.

H(s) is the transfer or describing function of the driver, i.e., the controller. $\delta_f(t)$ is the steering control signal generated by the driver in order to track the desired path. The function **G(s)** describes the dynamics of the A-train double, derived from nonlinear equations of motion. $y_1(t)$ is the current absolute lateral position of unit 1 and function **P(s)** describes the preview control strategy used to estimate the future lateral position of unit 1, $y_1(t+T)$. $Y_p(t+T)$ is the desired lateral position at (t+T), and $\varepsilon(t+T)$ is an error function describing the estimated lateral deviation, which is the difference between the lateral coordinates of the desired and predicted paths.

The describing functions for the driver, **H(s)**, and the preview control, **P(s)**, are expressed as:

$$H(s) = Kp \cdot e^{-s\tau} \tag{3.20}$$

$$P(s) = 1 + s \cdot T + s^2 \cdot \frac{T^2}{2} \tag{3.21}$$

where τ is referred to as the transport lag, which is related to the time delay limitations displayed by the human operator during tracking tasks. The parameter Kp is a constant gain, and T is the preview interval, over which the model provides an estimate of the

lateral position of unit 1. In such a driver-vehicle model, parameters Kp, τ, and T are adjusted such that the desired steering and path tracking performance are obtained. The preview interval T is also expressed in terms of the preview distance and forward speed of the vehicle, U, such that:

$$T = 3.6 \cdot \frac{Preview\_Distance}{U} \tag{3.22}$$

The coupled driver-vehicle model, shown in Figure 3.10, together with Equations (3.20) and (3.21), yield following expressions for the front wheel steer angle and estimated lateral position of the vehicle:

$$\delta_f(t) = \varepsilon(t+T) \cdot H(s) = Kp \cdot \left[Y_p(t+T) - y_1(t+T)\right] \cdot e^{-s\tau} \tag{3.23}$$

$$y_1(t+T) = y_1(t) \cdot P(s) = y_1(t) \cdot \left[1 + s \cdot T + s^2 \cdot \frac{T^2}{2}\right] = y_1(t) + \dot{y}_1(t) \cdot T + \ddot{y}_1(t) \cdot \frac{T^2}{2} \tag{3.24}$$

The steering control law is thus defined as:

$$\delta_f(t) = Kp \cdot \left[Y_p(t+T) - y_1(t) - \dot{y}_1(t) \cdot T - \ddot{y}_1(t) \cdot \frac{T^2}{2}\right] \cdot e^{-s\tau} \tag{3.25}$$

where

$\delta_f(t)$ = Front steering angle, rad.

t = Current time, s

$Y_p(t+T)$ = Desired absolute lateral position, m

$y_1(t)$ = Current absolute lateral position of unit 1, m

$\dot{y}_1(t)$ = Current absolute lateral velocity of unit 1, m/s

$\ddot{y}_1(t)$ = Current absolute lateral acceleration of unit 1, m/s^2

T = Preview interval, s

Kp = Constant gain, rad./m

τ = Transport lag, s

s = Laplace operator

From Equation (2.41), it can be seen that the state vector $\{x\}$ does not explicitly contain the state-variable corresponding to the current absolute lateral position of unit 1. The nonlinear equations of motion describing the yaw-plane dynamic of the A-train double are thus revised to include, the actual absolute lateral position of unit 1, $y_1(t)$, and its corresponding heading angle, $\psi_1(t)$, in order to perform simulations under close-loop steering maneuvers. The absolute lateral position and orientation of unit 1 are derived from two additional first order differential equations:

$$\dot{y}_1 = V_1 + U \cdot \psi_1$$
$$\dot{\psi}_1 = r_1 \qquad \textbf{(3.26)}$$

The equations of motion in the matrix form are thus expressed as:

$$[A_a]\cdot\{\dot{x}_a\} = [B_a]\cdot\{x_a\} + \{MM_a\} \qquad \textbf{(3.27)}$$

where $\{x_a\}$ is the revised state-vector, given by:

$$\{x_a\} = (V_1, r_1, r_2, r_3, r_4, \gamma_1, \gamma_2, \gamma_3, y_1, \psi_1)^T \tag{3.28}$$

$[A_a]$ is a 10x10 matrix of the mass and inertial properties of each of the A–train double, and $[B_a]$ is a 10x10 matrix of vehicle parameters and the forward speed, U. The column vector $\{MM_a\}$ contains ten elements which are determined by vehicle parameters, such as nonlinear cornering forces, aligning moments, and damping forces and moments. $[A_a]$, $[B_a]$, $\{MM_a\}$, and $\{x_a\}$ can be expressed in terms of $[A]$, $[B]$, $\{MM\}$, and $\{x\}$, respectively. Therefore, by expanding the matrices and vectors of Equation (3.27), the following expression is obtained:

$$\left[\begin{array}{c:cc} & 0 & 0 \\ [A]_{8\times 8} & \vdots & \vdots \\ & 0 & 0 \\ \hdashline 0 \cdots 0 & 1 & 0 \\ 0 \cdots 0 & 0 & 1 \end{array}\right]_{10\times 10} \cdot \left\{\begin{array}{c} \{\dot{x}\}_{8\times 1} \\ \hdashline \dot{y}_1 \\ \dot{\psi}_1 \end{array}\right\}_{10\times 1} = \left[\begin{array}{c:cc} & 0 & 0 \\ [B]_{8\times 8} & \vdots & \vdots \\ & 0 & 0 \\ \hdashline 1\ 0 \cdots 0 & 0 & U \\ 0\ 1 \cdots 0 & 0 & 0 \end{array}\right]_{10\times 10} \cdot \left\{\begin{array}{c} \{x\}_{8\times 1} \\ \hdashline y_1 \\ \psi_1 \end{array}\right\}_{10\times 1} + \left\{\begin{array}{c} \{MM\}_{8\times 1} \\ \hdashline 0 \\ 0 \end{array}\right\}_{10\times 1}$$

The lateral and yaw dynamic behavior of the A-train double is analyzed under a single path-change closed-loop maneuver. Its performance is evaluated in terms of rearward amplification (RWA) and transient high-speed offtracking (TOF). The

parameters Kp, τ, and T are adjusted to achieve desired path tracking performance. Table 3.2 summarizes the parameters derived for the driver-vehicle model and path-change maneuvers corresponding to different forward speeds.

Table 3.2: The driver-vehicle model and path-change maneuver parameters as a function of forward vehicle speed.

	A-Train Double Loaded					
	Single path-change Maneuver			Double path-change Maneuver		
Forward Speed km/h	**70**	**100**	**120**	**70**	**100**	**120**
Preview_Distance, m	10.00	16.00	20.00	11.00	15.20	17.75
Kp, rad./m	0.14	0.14	0.125	0.14	0.14	0.14
τ, s	0.06	0.06	0.06	0.06	0.06	0.06
SP1, m	2.13	2.13	2.13	2.13	2.13	2.13
SP3, m	40	40	40	40	40	40

Figure 3.11 (a) illustrates the front wheel steer angle computed for the single path-change maneuver at a forward speed of 100km/h, and Figure 3.11 (b) illustrates both the desired and the actual path described by the CG of unit 1 of the A-train double for single path-change maneuver at a forward speed of 100km/h.

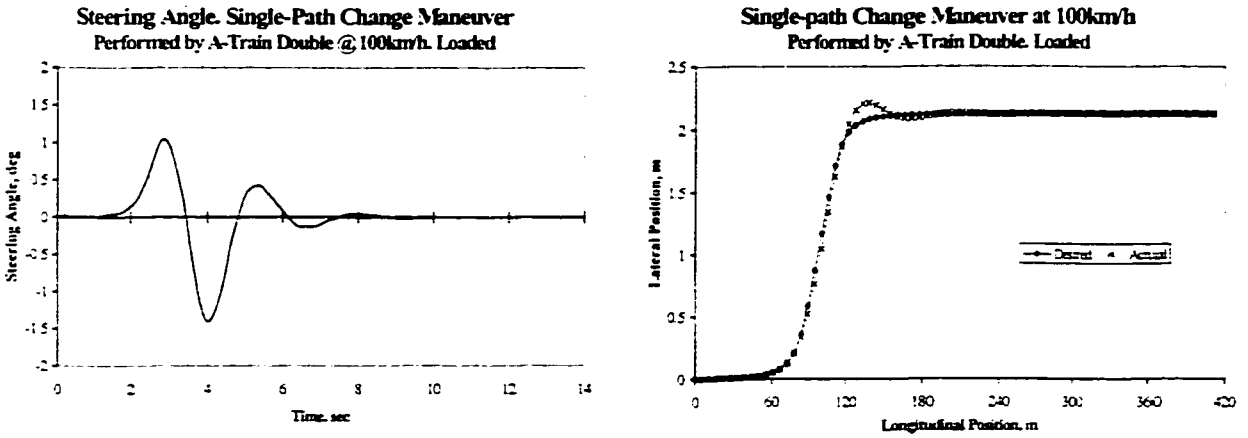

(a) (b)

Figure 3.11: (a) Front wheel steer angle; and (b) Path followed by unit 1 during a single path-change maneuver, derived from the driver-vehicle model.

The comparison reveals that the proposed path-follower model tracks the desired trajectory reasonably well with exception of the overshot and oscillations observed near the correction phase of the steering.

Utilizing the parameters of Table 3.2 for the double path-change closed-loop maneuver, the driver-vehicle model is used along with the nonlinear yaw-plane model to compute the steering angle needed. Figure 3.12 (a) illustrates the front wheel steer angle computed for a double path-change maneuver performed by the fully loaded A-train double at a forward speed of 100km/h. Figure 3.12 (b) illustrates both the desired and the actual path described by the CG of unit 1 of the A-train double for the same maneuver.

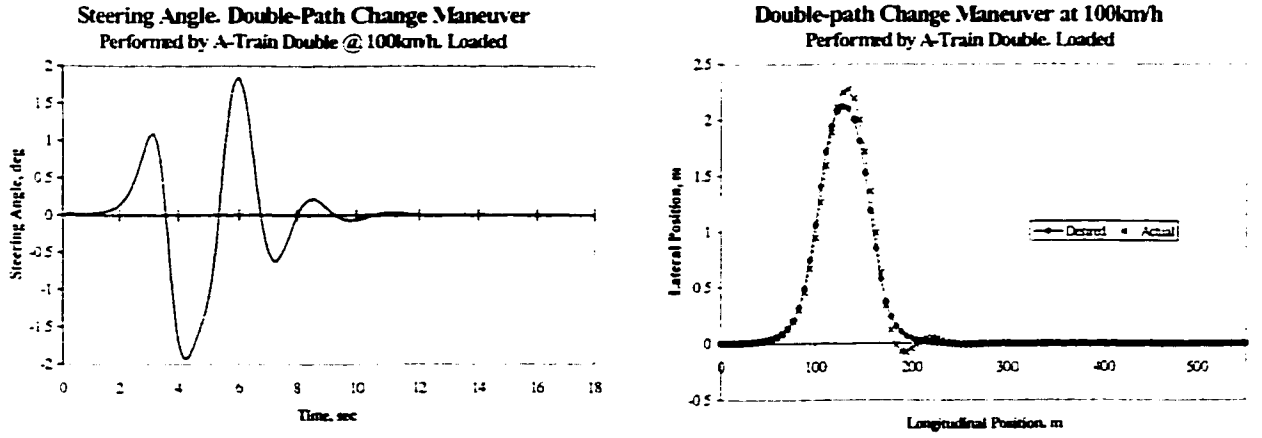

(a) (b)

Figure 3.12: (a) Front wheel steer angle and (b) Path followed by unit 1 during a double path-change maneuver, derived from the driver-vehicle model.

The comparison reveals that the proposed path-follower model tracks the desired trajectory reasonably well with exception of the overshot, the undershot, and oscillations observed near the correction phases of the steering.

3.5 Summary

Six performance measures are proposed to evaluate the dynamic behavior of the A-train double combination. Each of these performance measures is described and the methods for analyzing them are also presented. Both open loop and closed-loop directional maneuvers to assess the performance measures are described. A method to describe closed-loop maneuvers, namely, single and double path-change maneuvers, through continuos functions is proposed. This method consists in applying the Magic Formula concept, in which each term and coefficients of the Magic Formula are defined by different mathematical expressions, which use parameters obtained from the layout of

desired paths. The path-follower driver-vehicle model is explained and presented to carry out the closed-loop maneuver. The parameters of the driver-vehicle model, Kp, τ, and T, needed to perform the single path-change maneuver are computed and adjusted to achieve desired path tracking performance. It is shown that the models can effectively simulate the single and double path-change maneuvers.

Chapter 4

Feasibility Analysis of Damped Articulation Concepts

4.1 General

Enhancement of lateral dynamics performance of a tractor semitrailer combination has been attempted in many earlier studies by introducing some form of damping, either coulomb damping or viscous damping, at the articulation joint [6, 7, 8, 11, 27, 28]. Winkler [26] proposed the implementation of innovative dollies to enhance the dynamic performance of LCVs. The potential performance benefits of viscously damped articulation mechanisms to improve the directional stability of LCVs, however, have not been investigated. In this study, a feasibility analysis of the proposed concepts in damped articulation between the units of an A-train double combination is carried out in terms of potential performance gain or loss of performance measures values. The results of the feasibility analysis are used to select one suitable concept for further parametric sensitivity analyses to derive desirable geometric parameters.

4.2 Baseline Vehicle

The selected configuration for the LCV used in this study is a seven-axle A-train double combination vehicle, which consists of a three-axle tractor (unit 1), a two-axle semitrailer (unit 2), a single-axle A-dolly (unit 3), and a single-axle semitrailer (unit 4). The weights and dimensional parameters of the candidate vehicle together with the axle loads are shown in Table 4.1. The table also presents the parameters of the A-train under two loading conditions; namely, empty and fully loaded [54]. The tire load data presented in Table 4.2 along with the data presented in Tables 2.1 and 2.2 are used to compute the Magic Formula's coefficients to derive the lateral forces and self-aligning moments developed by each tire as a function of the side-slip angle and vertical load. Since the cornering properties of tires strongly depend upon the normal load, the normal load on each tire of the combination is evaluated from the axle loads. Table 4.2 summarizes the tire loads together with the longitudinal stiffness Cs_{ij} of the tire.

Table 4.1: Weights and dimensional parameters of the baseline A-train double [54].

Parameters of the baseline A-train double combination					
	Loading Condition	units			
		1	2	3	4
Mass, kg	Empty	7037	5448	1135	2951
	Loaded	7037	29283	1135	14755
Yaw Mass Moment of Inertia, kg-m^2	Empty	36055	106905	724	46969
	Loaded	36055	395937	724	124655
Wheelbase, m		3.66	10.97	2.03	6.40

Half-spacing of dual tire sets, y_{DT}, m	0.159m

Vertical load at axle j of unit i (Fz_{ij}, N)

	Empty	Loaded		Empty	Loaded		Empty	Loaded
Fz_{11}	41909.6	53444.8	Fz_{12}	23582.5	75713.5	Fz_{13}	23582.5	75713.5
Fz_{21}	0	0	Fz_{22}	16701.5	75713.5	Fz_{23}	16701.5	75713.5
Fz_{31}	0	0	Fz_{32}	21155.2	79053.8	Fz_{33}	----------	----------
Fz_{41}	0	0	Fz_{42}	0	0	Fz_{43}	18928.3	76827.0

Longitudinal distances between CG of unit i to axle j of the same unit (X_{ij}, m)

	Empty	Loaded		Empty	Loaded		Empty	Loaded
X_{11}	1.55	1.55	X_{12}	1.50	1.50	X_{13}	2.72	2.72
X_{21}	0	0	X_{22}	3.51	4.58	X_{23}	4.73	5.80
X_{31}	0	0	X_{32}	0	0	X_{33}	--------	---------
X_{41}	0	0	X_{42}	0	0	X_{43}	2.22	3.00

Longitudinal distances between CG of unit i to articulation joints A, B and C (X_{iA}, X_{iB}, and X_{iC}, m)

	Empty	Loaded		Empty	Loaded		Empty	Loaded
X_{1A}	1.75	1.75	X_{2B}	5.64	6.71	X_{3C}	0	0
X_{2A}	6.86	5.78	X_{3B}	2.03	2.03	X_{4C}	4.18	3.40

Overall widths at axle j of unit i (OW_{ij}, m)

OW_{11} = 2.44	OW_{12} = 2.44	OW_{13} = 2.44
OW_{22} = 2.44	OW_{23} = 2.44	OW_{32} = 2.44
OW_{43} = 2.44		

Table 4.2: Vertical load per tire under different loading conditions and longitudinal stiffness of the tire.

Tire vertical load at j axle of unit i (Fz'_{ij}, N)								
	Empty	**Loaded**		**Empty**	**Loaded**		**Empty**	**Loaded**
Fz'_{11}	20954.8	26722.4	Fz'_{12}	5895.63	18928.3	Fz'_{13}	5895.63	18928.3
Fz'_{21}	0	0	Fz'_{22}	4175.38	18928.3	Fz'_{23}	4175.38	18928.3
Fz'_{31}	0	0	Fz'_{32}	5288.81	19763.4	Fz'_{33}	0	0
Fz'_{41}	0	0	Fz'_{42}	0	0	Fz'_{43}	4732.09	19206.7

Tires longitudinal stiffness at axle j of unit i (C_{Sij}, N/unit slip)		
$C_{S11} = 0.000$	$C_{S12} = 151232$	$C_{S13} = 146784$
$C_{S21} = 0.000$	$C_{S22} = 146784$	$C_{S23} = 146784$
$C_{S31} = 0.000$	$C_{S32} = 146784$	----------
$C_{S41} = 0.000$	$C_{S42} = 0.000$	$C_{S43} = 146784$

4.2.1 Magic Formula Coefficients

Tire cornering forces and self-aligning moments are nonlinear functions that depend upon both tire side-slip angles and vertical load applied on the tire. These nonlinear functions, however, can be mathematically expressed by using the Magic Formula, Equation (2.25), described in section 2.5.2. It should be noted that tire loads of the candidate vehicle (Table 4.2) do not correspond with the tire loads used to characterize the measured lateral forces and self-aligning moments (Tables 2.1 and 2.2), for the Goodyear G286 11R24.5 tires. Linear interpolations are thus performed to obtain the lateral forces and self-aligning moments developed by the tires of the A-train double corresponding to the specified actual vertical loads. Tables 4.3 and 4.4 summarize the interpolated values of lateral force and self-aligning moments, respectively, as a function of the vertical load and side-slip angles. The tabulated values are used to obtain an initial estimate of the Magic Formula coefficients, ***B***, ***C***, ***D***, and ***E***, using Equations (2.26)

through (2.30). The estimated values of Magic Formula coefficients for lateral forces and self-aligning moments under different vertical load conditions are presented in Tables 4.5 and 4.6, respectively. An optimization problem is formulated and solved to derive optimal values of coefficients for lateral forces and self-aligning moments by minimizing the error between the curves described by Equation (2.25) and the measured data under various vertical load conditions. Non-linear least squared methodology is used in optimization where the initially estimated values of coefficients serve as the starting values. The optimized Magic Formula coefficients derived for the lateral force and self-aligning moments under different vertical loads are summarized in Tables 4.7 and 4.8, respectively.

Table 4.3: Interpolated values for the lateral force developed by the tire as a function of vertical load and side-slip angle.

Side-slip Angle, Degrees	LATERAL FORCE, N								
	Tire Vertical Load, N								
	4175.38	**4732.09**	**5288.81**	**5895.63**	**18928.3**	**19206.7**	**19763.4**	**20954.8**	**26722.4**
0	0	0	0	0	0	0	0	0	0
1	615.10	697.11	779.12	868.52	2704.8	2743.4	2820.8	2917.7	3276.8
2	1137.25	1288.89	1440.52	1605.80	5092.0	5166.1	5314.1	5512.2	6280.5
4	1988.68	2253.83	2518.99	2808.01	8855.1	8983.3	9239.5	9625.9	11236.6
8	3189.45	3614.70	4039.97	4503.50	13586.4	13774.7	14151.3	14776.8	17515.0
12	4071.23	4614.05	5156.89	5748.57	16316.9	16528.7	16952.3	17660.5	20770.3

Table 4.4: Interpolated values for self-alignment moment developed by the tire as a function of tire vertical load and side-slip angle.

Side-slip Angle, Degrees	LATERAL FORCE, N								
	Tire Vertical Load, N								
	4175.38	4732.09	5288.81	5895.63	18928.3	19206.7	19763.4	20954.8	26722.4
0	0	0	0	0	0	0	0	0	0
1	15.2817	17.3192	19.3568	21.5777	108.531	110.644	114.869	124.755	173.971
2	25.1364	28.4878	31.8394	35.4925	186.614	190.315	197.717	215.891	307.619
4	32.3709	36.6869	41.0031	45.7076	259.645	264.950	275.558	304.000	450.899
8	33.0855	37.4968	41.9082	46.7166	260.222	265.501	276.056	305.602	459.792
12	34.4819	39.0794	43.6771	48.6884	241.233	245.899	255.229	279.043	400.496

Table 4.5: Estimated values of Magic Formula coefficients for tire lateral force as a function of tire vertical load.

Magic Formula Coefficients	Tire Vertical Load, N								
	4175.38	4732.09	5288.81	5895.63	18928.3	19206.7	19763.4	20954.8	26722.4
B	8.6565	8.6565	8.6564	8.6565	9.4977	9.5098	9.5338	9.4659	9.0392
C	1	1	1	1	1	1	1	1	1
D	4071.2	4614.1	5156.9	57.486	16317	16529	16952	17661	20770
E	0	0	0	0	0	0	0	0	0

Table 4.6: Estimated values of initial Magic Formula coefficients for self-aligning moment as a function of tire vertical load.

Magic Formula Coefficients	Tire Vertical Load, N								
	4175.38	4732.09	5288.81	5895.63	18928.3	19206.7	19763.4	20954.8	26722.4
B	25.392	25.392	25.392	25.392	31.639	31.674	31.741	31.926	32.207
C	1	1	1	1	0.75529	0.75384	0.75113	0.73263	0.6731
D	34.482	39.079	43.677	48.688	260.22	265.5	276.06	305.6	459.79
E	0	0	0	0	2.0231	2.0162	2.0034	1.9329	1.7625

Table 4.7: Optimal values of Magic Formula coefficients for tire lateral force as a function of tire vertical load.

Magic Formula Coefficients	Tire Vertical Load, N								
	4175.38	**4732.09**	**5288.81**	**5895.63**	**18928.3**	**19206.7**	**19763.4**	**20954.8**	**26722.4**
B	5.1663	5.1631	5.1665	5.1591	6.1063	6.1173	6.1392	6.0088	5.2444
C	1.6062	1.6078	1.6068	1.6093	1.5271	1.5267	1.5259	1.5492	1.7024
D	4075.8	4617.3	5160.3	5751.8	16318	16530	16953	17661	20772
E	0.33828	0.33714	0.33538	0.33897	0.36213	0.36238	0.36285	0.36	0.3441

Table 4.8: Optimal values of Magic Formula coefficients for self-aligning moment as a function of tire vertical load.

Magic Formula Coefficients	Tire Vertical Load, N								
	4175.38	**4732.09**	**5288.81**	**5895.63**	**18928.3**	**19206.7**	**19763.4**	**20954.8**	**26722.4**
B	29.005	29.005	29.005	29.005	15.503	15.443	15.332	14.418	11.386
C	0.84142	0.84142	0.84142	0.84142	1.5343	1.5384	1.5461	1.6094	1.8744
D	35.858	40.639	45.42	50.631	268.29	273.82	284.89	315.99	477.39
E	-1.6839	-1.6839	-1.6839	-1.6839	-0.31364	-0.3071	-0.29524	-0.17277	0.14869

The optimal values of coefficients are applied to derive Magic Formula expressions for tire lateral forces and self-aligning moments developed by the tire as a function of side-slip angle and the vertical loads of the A-train double combination, which are summarized in Table 4.2. The Equation (2.25) is solved by letting $S_h = S_v = 0$ since the measured data does not exhibit horizontal and vertical offset. The equations for the range of the vertical load are expressed as follows:

$F_z = 4175.38N$

$$F(\alpha)\Big|_{F_z=4175.38N} = 4075.8 \cdot \sin\left[1.6062 \cdot \arctan\left\{5.1663 \cdot \alpha - 0.33828 \cdot \left(5.1663 \cdot \alpha - \arctan\left(5.1663 \cdot \alpha\right)\right)\right\}\right]$$

$$M(\alpha)\Big|_{F_z=4175.38N} = 35.858 \cdot \sin\left[0.84142 \cdot \arctan\left\{29.005 \cdot \alpha + 1.6839 \cdot \left(29.005 \cdot \alpha - \arctan\left(29.005 \cdot \alpha\right)\right)\right\}\right] \quad \textbf{(4.1)}$$

$F_z = 4732.09N$

$$F(\alpha)\Big|_{F_z=4732.09N} = 4617.3 \cdot \sin\left[1.6078 \cdot \arctan\left\{5.1631 \cdot \alpha - 0.33714 \cdot \left(5.1631 \cdot \alpha - \arctan\left(5.1631 \cdot \alpha\right)\right)\right\}\right]$$

$$M(\alpha)\Big|_{F_z=4732.09N} = 40.639 \cdot \sin\left[0.84142 \cdot \arctan\left\{29.005 \cdot \alpha + 1.6839 \cdot \left(29.005 \cdot \alpha - \arctan\left(29.005 \cdot \alpha\right)\right)\right\}\right] \quad \textbf{(4.2)}$$

$F_z = 5288.81N$

$$F(\alpha)\Big|_{F_z=5288.81N} = 5160.3 \cdot \sin\left[1.6068 \cdot \arctan\left\{5.1665 \cdot \alpha - 0.33538 \cdot \left(5.1665 \cdot \alpha - \arctan\left(5.1665 \cdot \alpha\right)\right)\right\}\right]$$

$$M(\alpha)\Big|_{F_z=5288.81N} = 45.42 \cdot \sin\left[0.84142 \cdot \arctan\left\{29.005 \cdot \alpha + 1.6839 \cdot \left(29.005 \cdot \alpha - \arctan\left(29.005 \cdot \alpha\right)\right)\right\}\right] \quad \textbf{(4.3)}$$

$F_z = 5895.63N$

$$F(\alpha)\Big|_{F_z=5895.63N} = 5751.8 \cdot \sin\left[1.6093 \cdot \arctan\left\{5.1591 \cdot \alpha - 0.33897 \cdot \left(5.1591 \cdot \alpha - \arctan\left(5.1591 \cdot \alpha\right)\right)\right\}\right]$$

$$M(\alpha)\Big|_{F_z=5895.63N} = 50.631 \cdot \sin\left[0.84142 \cdot \arctan\left\{29.005 \cdot \alpha + 1.6839 \cdot \left(29.005 \cdot \alpha - \arctan\left(29.005 \cdot \alpha\right)\right)\right\}\right] \quad \textbf{(4.4)}$$

$F_z = 18928.3N$

$$F(\alpha)\big|_{F_z=18928.3N} = 16318 \cdot \sin\left[1.5271 \cdot \arctan\left\{6.1063 \cdot \alpha - 0.36213 \cdot (6.1063 \cdot \alpha - \arctan(6.1063 \cdot \alpha))\right\}\right]$$

$$M(\alpha)\big|_{F_z=18928.3N} = 268.29 \cdot \sin\left[1.5343 \cdot \arctan\left\{15.503 \cdot \alpha + 0.31364 \cdot (15.503 \cdot \alpha - \arctan(15.503 \cdot \alpha))\right\}\right] \quad \textbf{(4.5)}$$

$F_z = 19206.7N$

$$F(\alpha)\big|_{F_z=19206.7N} = 16530 \cdot \sin\left[1.5267 \cdot \arctan\left\{6.1173 \cdot \alpha - 0.36238 \cdot (6.1173 \cdot \alpha - \arctan(6.1173 \cdot \alpha))\right\}\right]$$

$$M(\alpha)\big|_{F_z=19206.7N} = 273.82 \cdot \sin\left[1.5384 \cdot \arctan\left\{15.443 \cdot \alpha + 0.3071 \cdot (15.443 \cdot \alpha - \arctan(15.443 \cdot \alpha))\right\}\right] \quad \textbf{(4.6)}$$

$F_z = 19763.4N$

$$F(\alpha)\big|_{F_z=19763.4N} = 16953 \cdot \sin\left[1.5259 \cdot \arctan\left\{6.1392 \cdot \alpha - 0.36285 \cdot (6.1392 \cdot \alpha - \arctan(6.1392 \cdot \alpha))\right\}\right]$$

$$M(\alpha)\big|_{F_z=19763.4N} = 284.89 \cdot \sin\left[1.5461 \cdot \arctan\left\{15.332 \cdot \alpha + 0.29524 \cdot (15.332 \cdot \alpha - \arctan(15.332 \cdot \alpha))\right\}\right] \quad \textbf{(4.7)}$$

$F_z = 20954.8N$

$$F(\alpha)\big|_{F_z=20954.8N} = 17661 \cdot \sin\left[1.5492 \cdot \arctan\left\{6.0088 \cdot \alpha - 0.36 \cdot (6.0088 \cdot \alpha - \arctan(6.0088 \cdot \alpha))\right\}\right]$$

$$M(\alpha)\big|_{F_z=20954.8N} = 315.99 \cdot \sin\left[1.6094 \cdot \arctan\left\{14.418 \cdot \alpha + 0.17277 \cdot (14.418 \cdot \alpha - \arctan(14.418 \cdot \alpha))\right\}\right] \quad \textbf{(4.8)}$$

$\underline{F_Z = 26722.4N}$

$$F(\alpha)\Big|_{F_Z=26722.4N} = 20772 \cdot \sin\left[1.7024 \cdot \arctan\left\{5.2444 \cdot \alpha - 0.3441 \cdot (5.2444 \cdot \alpha - \arctan(5.2444 \cdot \alpha))\right\}\right]$$

$$M(\alpha)\Big|_{F_Z=26722.4N} = 477.39 \cdot \sin\left[1.8744 \cdot \arctan\left\{11.386 \cdot \alpha + 0.14869 \cdot (11.386 \cdot \alpha - \arctan(11.386 \cdot \alpha))\right\}\right] \quad \textbf{(4.9)}$$

where $F(\alpha)$ is the lateral force in N derived as a function of the side-slip angle, α, which is expressed in radians, and $M(\alpha)$ is the self-aligning moment in N-m, which is also a function of the side-slip angle, α.

Figures 4.1 (a) and 4.1 (b) illustrate the comparison of the tire lateral force and self-aligning moment derived from the Magic Formula with that of the measured data for two different vertical loads. The results clearly show the effectiveness of Magic Formula for accurately predict the cornering properties of tires.

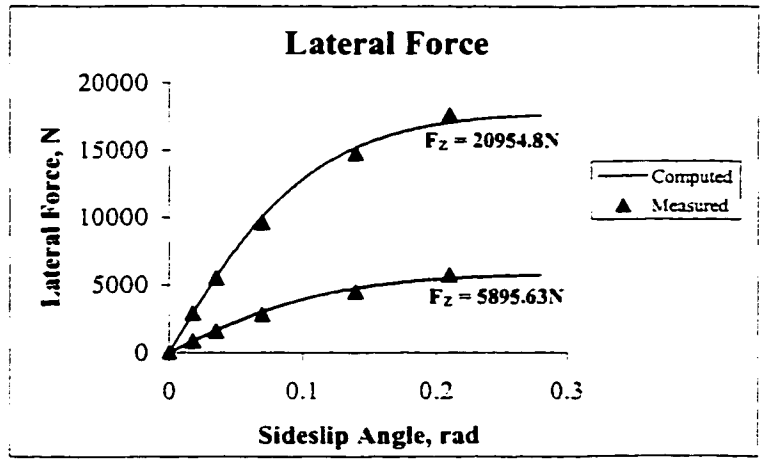

(a)

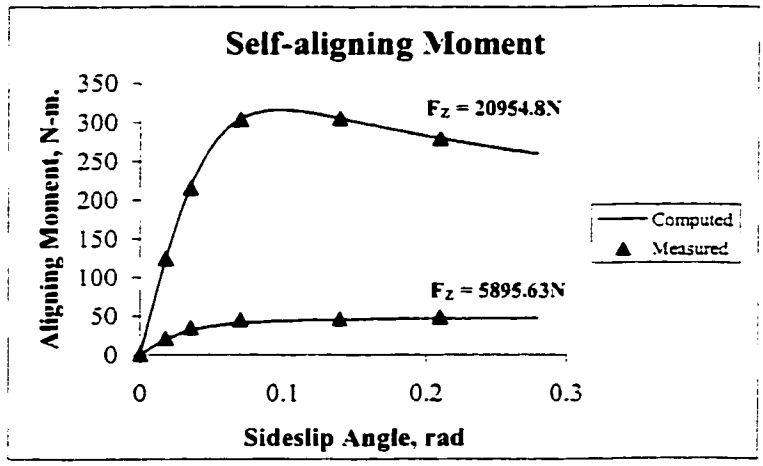

(b)

Figure 4.1: Comparison between measured data and curve fitting obtained by using the Magic Formula approach. (a) Lateral force (b) Self-aligning moment.

4.3 Feasibility Analysis

The feasibility of the proposed concepts in damped articulations is initially investigated to evaluate their relative potential performance benefits or limitations. The relative performance potentials are assessed in terms of the selected performance

measures, for baseline geometric parameters of both concepts. The analyses are performed for different values of damping coefficients, $\mathbf{C_{KL}}$ and $\mathbf{C_{MN}}$, which are expected to strongly influence the dynamic response of the A-train double. From the kinematic analysis of proposed concepts, it is also apparent that geometric nonlinearities of the damped articulations, which depend on parameters ***a***, ***b*** and ***c***, affect the response of the A-train double by imposing nonlinear forces and moments about articulation joints **B** or **C**. The parameter ***a***, ***b*** and ***c*** are thus fixed to baseline values for the preliminary feasibility analysis in order to evaluate the influence of the damping coefficient and the concepts on the response of the A-train. The feasibility analysis thus consists in identifying the effects of damped articulations, specifically damping coefficients, on the dynamic response of the A-train double in terms of the selected performance measures, described in chapter 3, for each of the suggested concepts. The A-train double is considered fully loaded and its forward speed (U) is held constant at 100km/h.

The geometric parameters ***a*** and ***b*** are selected as 0.8m and 0.38m, respectively, for the Case I as shown in Figure 2.2, while the parameter ***c*** is considered equal to 1.0m. Parameter ***a***, for Case II, is selected as 0.91m [54], as shown in Figure 2.3, while the parameters ***b*** and ***c*** are considered equal to 1.0m. The response of the A-train double is computed for various values of damping coefficients, namely, 10kN-s/m, 100kN-s/m and 1000kN-s/m. The response characteristics corresponding to 10kN-s/m damping may be considered close to that of the vehicle with undamped or conventional articulation. Furthermore, the feasibility of the concepts is analyzed in terms of response characteristics of the tractor and rearmost units (1 and 4).

Each selected performance measure is evaluated according to the procedures and steering maneuvers described in chapter 3. These performance measures permit the analysis of transient as well as steady-state directional response of the A-train double, through specific open loop directional maneuvers, for each of the selected damping coefficient values and also for each of the proposed concepts of damped articulations (Cases I and II). The dynamic response of the vehicle is also investigated under a single path-change maneuver, performed in a closed-loop maneuver, which incorporates the driver-vehicle model.

The simulation of the baseline A-train double combination is performed under each directional maneuver, by numerically solving the nonlinear differential equations of motion obtained from the yaw-plane model. Figures 4.2 and 4.3 illustrate the dynamic responses of units 1 and 4, respectively, in terms of lateral acceleration and yaw rate responses, for different values of damping coefficients and for each damping concept, while the A-train double is subject to a single path-change maneuver. The results are obtained by using the specified method for evaluation of rearward amplification (RWA) performance measure, described in section 3.2. Figures 4.4 and 4.5 depict the influence of damped articulations on the response characteristics of articulation angles, γ_2 and γ_3, and the side-slip angles developed at the tires on axles 3-2 and 4-3, α_{32} and α_{43}, respectively. Figure 4.6 illustrates the influence of different damping coefficients on the front wheel steer angle required to negotiate a single path-change maneuver and the path followed by the CG of unit1.

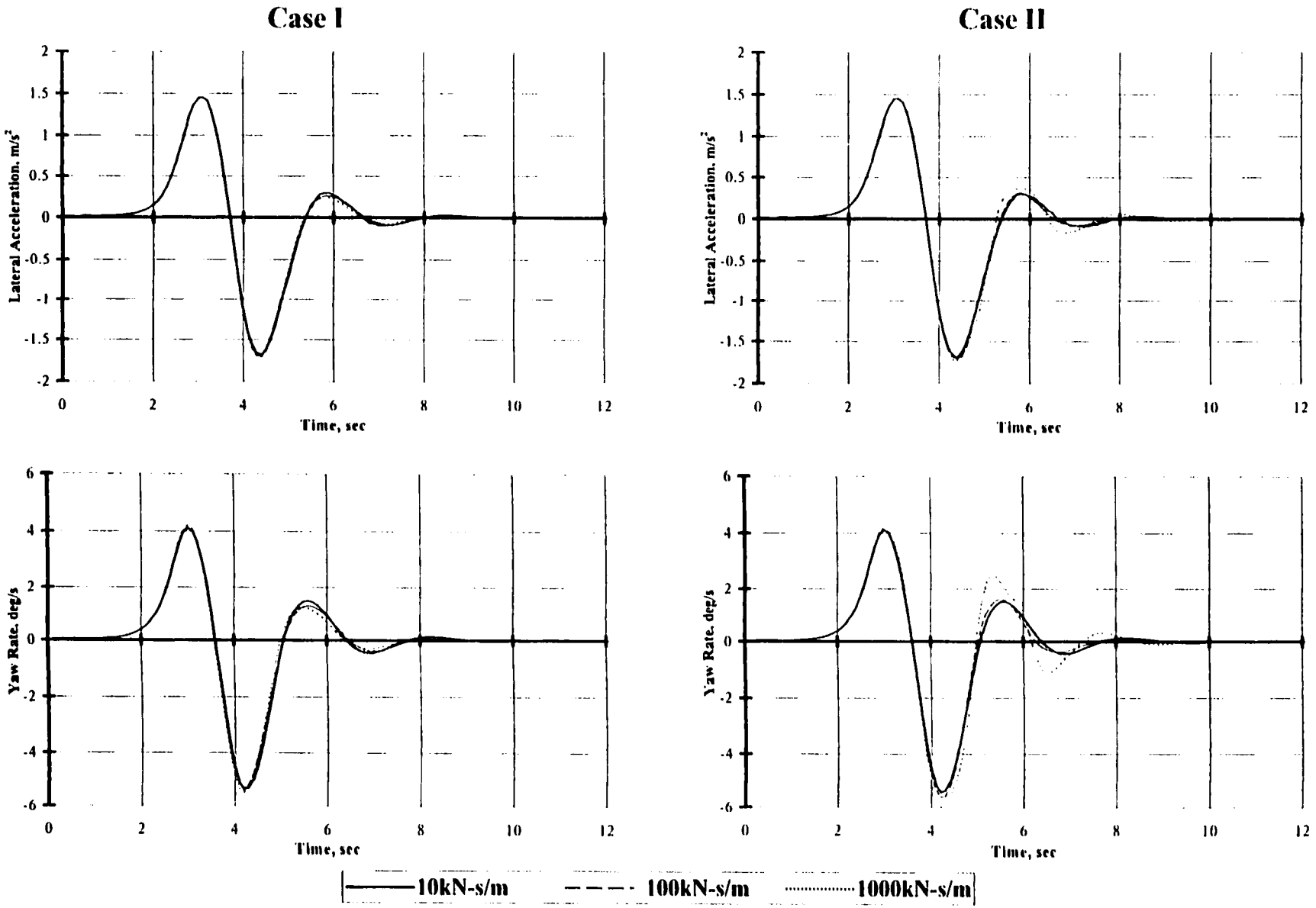

Figure 4.2: **Influence of damped articulation concepts and damping coefficient on the lateral acceleration and yaw rate response of unit 1 (U = 100km/h, loaded vehicle).**

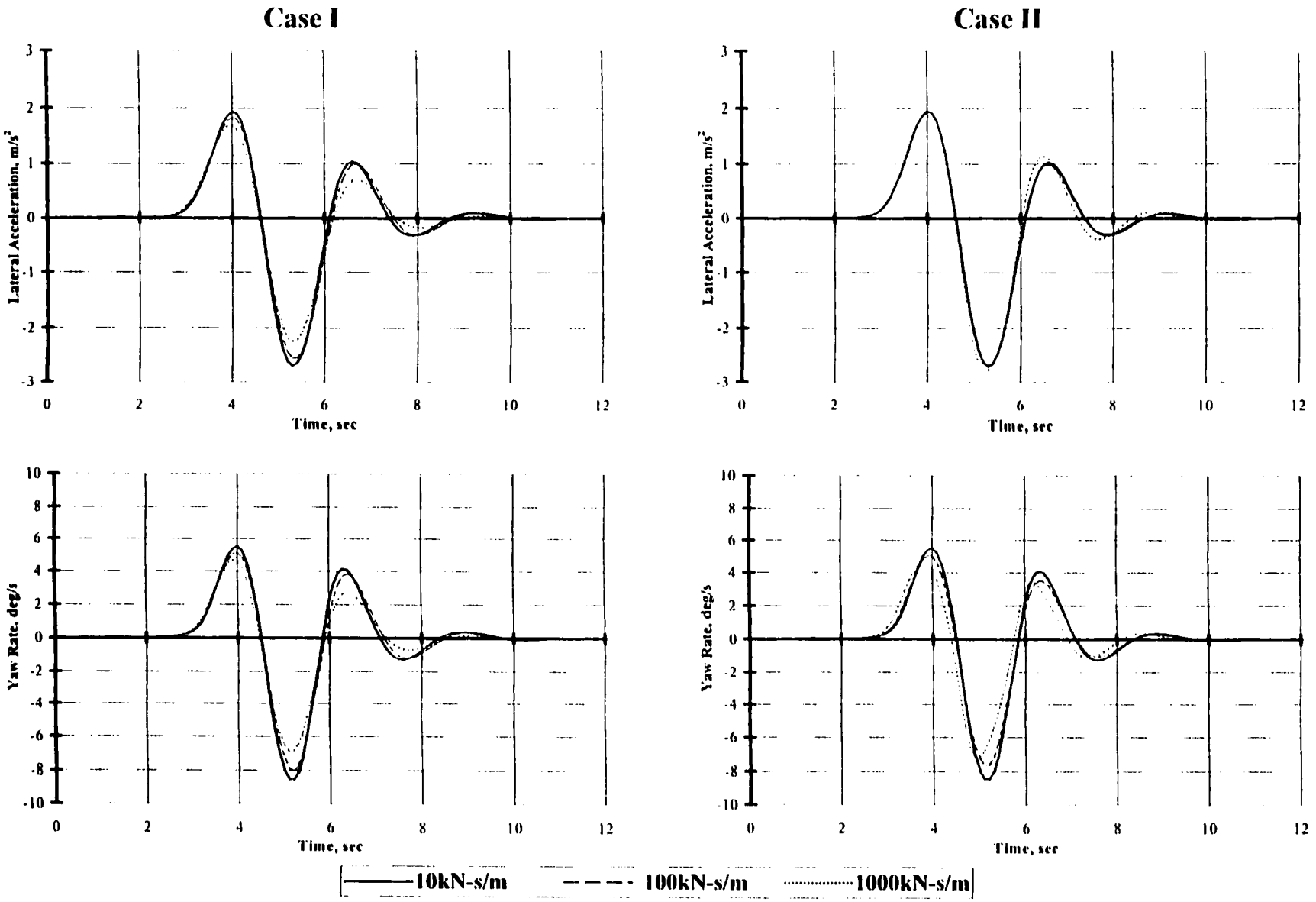

Figure 4.3: **Influence of damped articulation concepts and damping coefficient on the lateral acceleration and yaw rate response of unit 4 (U = 100km/h, loaded vehicle).**

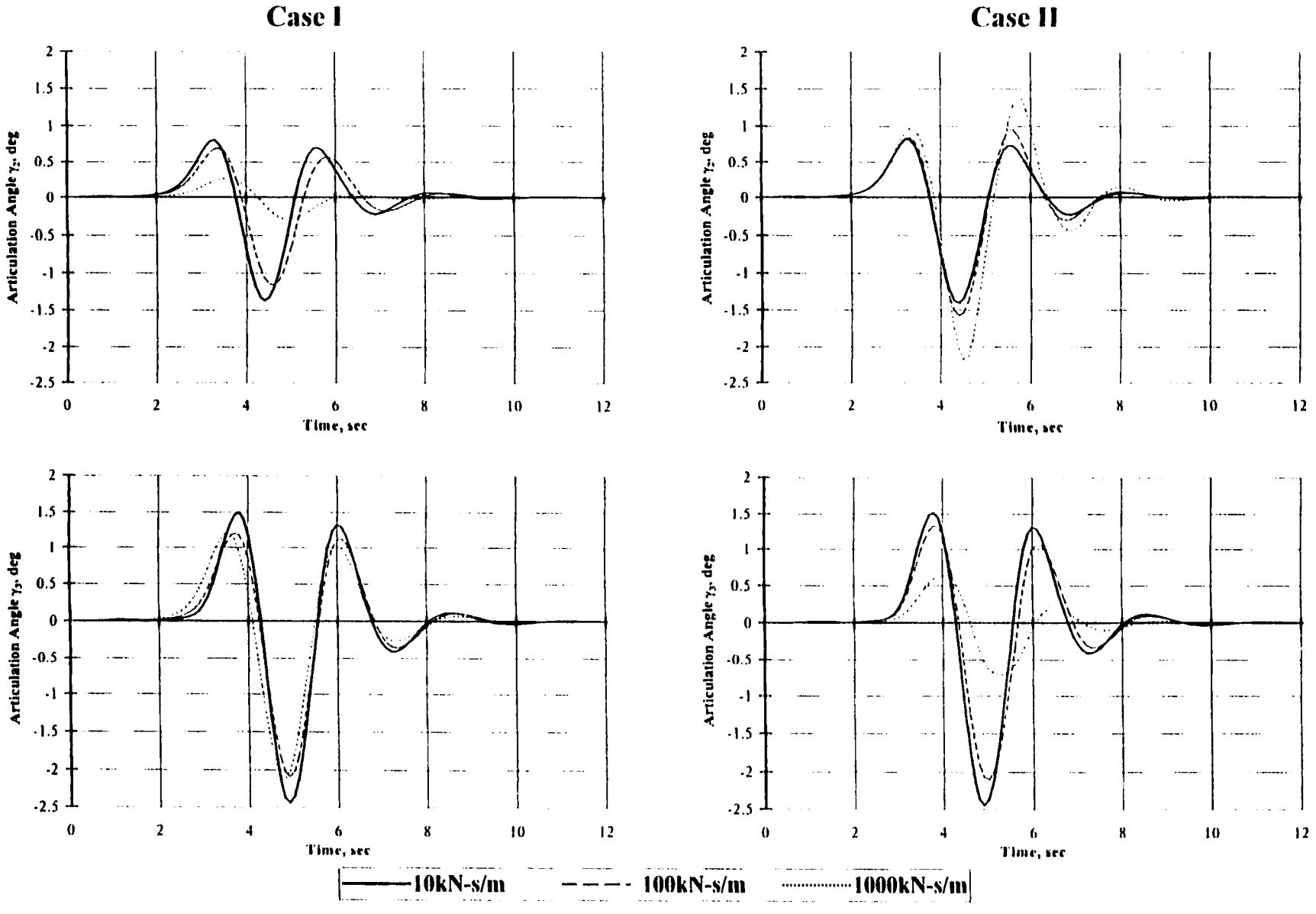

Figure 4.4: **Influence of damped articulation concepts and damping coefficient on the articulation angles γ_2 and γ_3 response (U = 100km/h, loaded vehicle).**

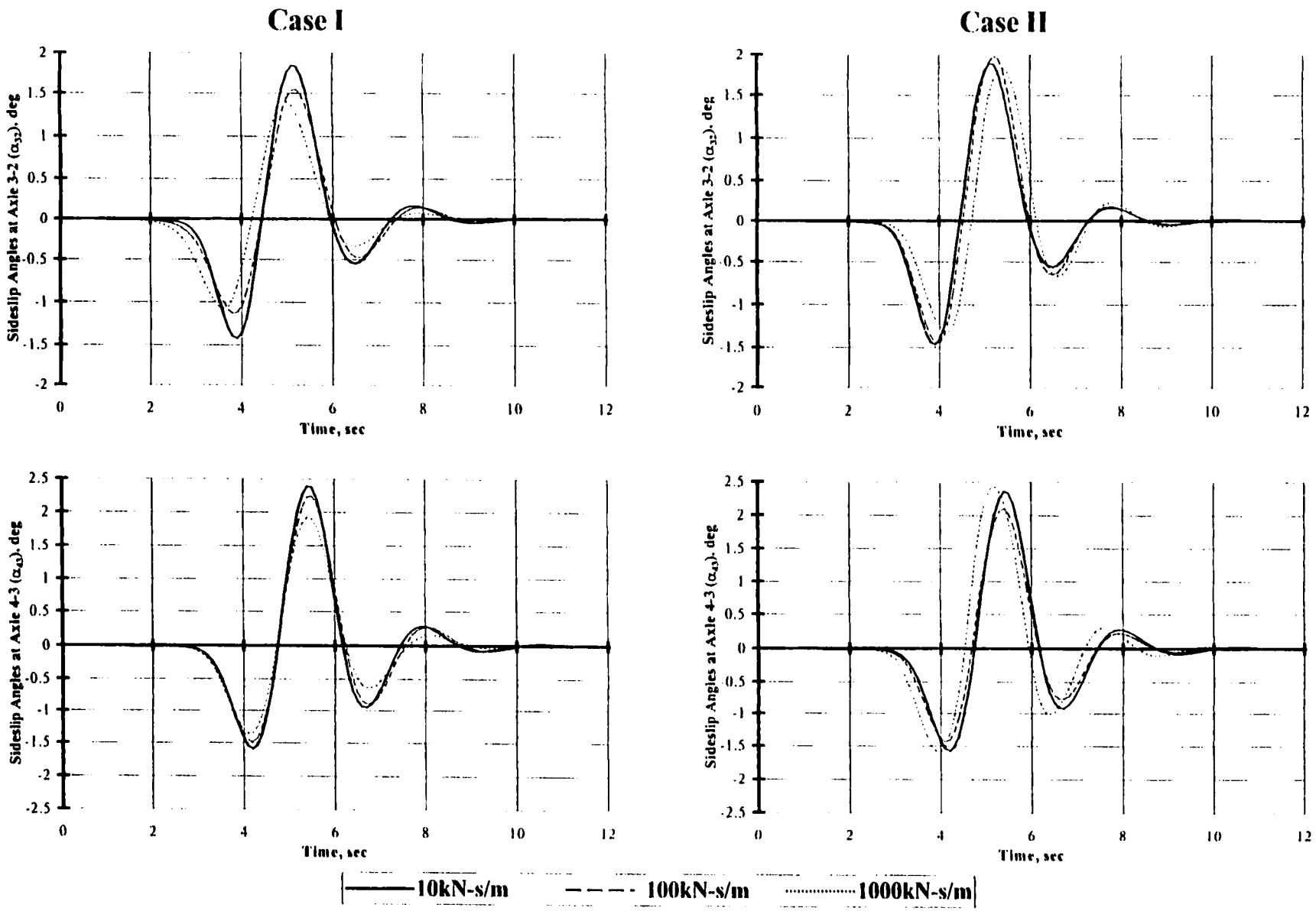

Figure 4.5: **Influence of damped articulation concepts and damping coefficient on the side-slip angles response at axles 3-2 and 4-3 (U = 100km/h, loaded vehicle).**

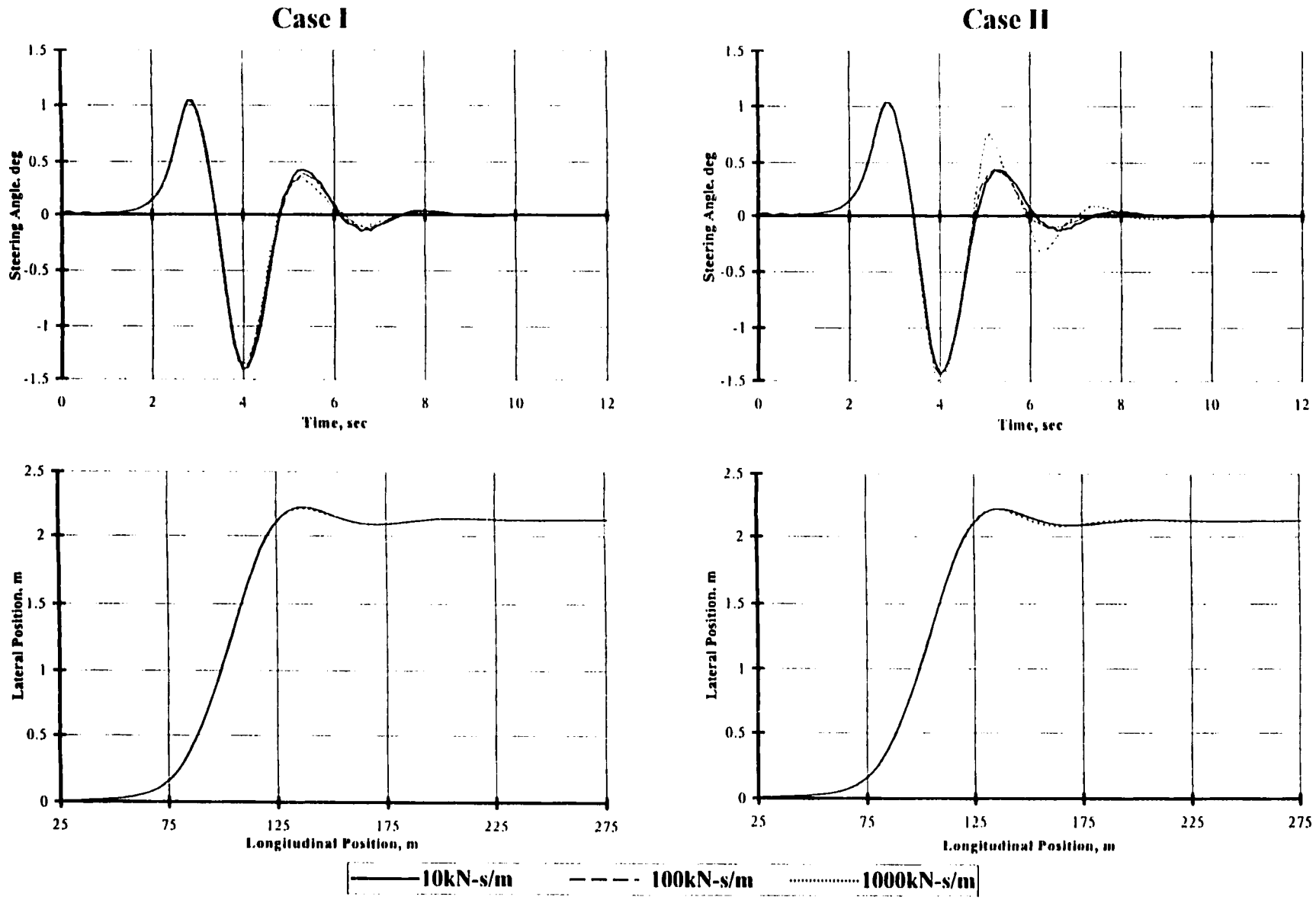

Figure 4.6: **Influence of damped articulation concepts and damping coefficient on the required steering angle and path followed by unit 1 (U = 100km/h, loaded vehicle).**

The results show that the proposed damped articulation concepts and variations in damping coefficients affect the dynamic response of the rearmost trailer (unit 4) significantly. The influence of damped articulations on the directional response of unit 1 is relatively insignificant, specifically for the Case I (dampers between units 2 and 3). The damped articulations between units 2 and 3 (Case I) yield slight reduction in lateral acceleration and yaw rate response of unit 1 (during corrective steering) with increase in damping, as shown in Figure 4.2. The Case II causes increased lateral acceleration and yaw rate response of unit 1, which is more pronounced with higher damping coefficients. In view of the higher lateral acceleration and yaw rate response of unit 1 of the combination with Case II of damped articulations, this case cannot be considered feasible.

The Case I damped articulation yields considerable reduction in the peak lateral acceleration and yaw rate response of unit 4, specifically with high damping (1000kN-s/m), as shown in Figure 4.3. The dampers in Case II, on the other hand, cause higher lateral acceleration, which may lead to higher rearward amplification. The yaw rate response of unit 4, however, decreases with increase in articulation damping coefficient. The articulation dampers in this case further cause significantly higher articulation angle between units 2 and 3 (γ_2), as shown in Figure 4.4, which may aggravate vehicle jackknife. The articulation angle γ_2 in Case I decreases with increase in articulation damping. The articulation angle between units 3 and 4 (γ_3), however, decreases with both damping concepts. This decrease is more pronounced with heavily damped articulation in Case II.

The damped articulation concept in Case I further yields slightly lower demand on the front wheel steer angle during the corrective phase required to perform the single path-change maneuver, which tends to decrease further with increase in damping, as shown in Figure 4.6. As shown for Case II, the required steer angle tends to increase, specifically under high damping. This case may thus pose increased steering effort from the driver.

The side-slip angles developed at tires of axles 3-2 (rear axle tires of unit 3, α_{32}) and 4-3 (rear axle tires of unit 4, α_{43}) also decrease with increase in damping coefficient for the Case I damped articulation, as shown in Figure 4.5. These results reveal lower cornering demand on tires, which may be attributed to reduced articulation angles. The Case II, on the other hand, reveals either slight reduction or increase in side-slip angles with variations in the damping coefficients. The results shown in Figure 4.5 further reveal that α_{32} in Case I and α_{43} in Case II tend to lead the side-slip angle response obtained under high damping. In Case II, α_{32}, on the other hand, lags that developed under high damping.

The peak (maximum and minimum) values of the articulation and side-slip angles obtained with Case I and Case II of damped articulation are summarized in Tables 4.9 and 4.10, respectively. The results show that the Case I of damped articulation yields considerable reductions in peak values, specifically with high articulation damping. The peak values of articulation angles γ_2 and γ_3 decrease by –72.24% and –19.33%, respectively, when damping coefficient is increased from 10kN-s/m to 1000kN-s/m. The corresponding reduction of γ_2 and γ_3 for $\mathbf{C_{KL}} = \mathbf{C_{MN}}$ = 100kN-s/m are obtained as –14.58% and –19.15%, respectively. For Case II, γ_3 tends to decrease with increase in

damping coefficient, while γ_2 increases considerably. An increase in damping coefficient from 10kN-s/m to 1000kN-s/m yields –71% and +69.9% change in peak values of γ_3 and γ_2, respectively. The corresponding changes for 100kN-s/m are attained as –13.85% and +16.55%, respectively for γ_3 and γ_2. An increase in damping coefficient in Case I also yields a decrease in peak values of α_{32} and α_{43}. The most significant reduction in the peak value of side-slip angles are attained for $\mathbf{C_{KL}} = \mathbf{C_{MN}}$ = 1000kN-s/m, which are computed as –24.4% and –19.44%, respectively for α_{32} and α_{43}. The corresponding reductions for $\mathbf{C_{KL}} = \mathbf{C_{MN}}$ = 100kN-s/m are–20.54% and –6.51%, respectively. The influence of integrating damped articulations between units 2 and 4 (Case II) does not reveal a clear trend in terms of α_{32} and α_{43}. The variations in α_{32} and α_{43} are attained as +4.56% and –11.16% for $\mathbf{C_{KL}} = \mathbf{C_{MN}}$ = 100kN-s/m, and –9.82% and +2.57% for $\mathbf{C_{KL}} = \mathbf{C_{MN}}$ = 1000kN-s/m, respectively.

Table 4.9: Influence of damped articulation on the peak values of articulation and side-slip angles (Case I).

		Damping Coefficient, kN-s/m (C_{KL}, C_{MN})					
		10		100		1000	
Articulation Angle, deg		γ_2	γ_3	γ_2	γ_3	γ_2	γ_3
Peak value	**Maximum**	0.8045	1.4927	0.6905	1.2068	0.2706	1.2041
	Minimum	-1.3665	-2.4359	-1.1673	-2.0877	-0.2837	-2.1074
Side-slip Angle, deg		α_{32}	α_{43}	α_{32}	α_{43}	α_{32}	α_{43}
Peak value	**Maximum**	1.8493	2.3970	1.5484	2.2507	1.4020	1.9310
	Minimum	-1.4237	-1.5923	-1.1313	-1.4886	-1.0763	-1.3675

Table 4.10: **Influence of damped articulation on the peak values of articulation and side-slip angles (Case II).**

		Damping Coefficient, kN-s/m (C_{KL}, C_{MN})					
		10		100		1000	
Articulation Angles, deg		γ_2	γ_3	γ_2	γ_3	γ_2	γ_3
Peak value	**Maximum**	0.8223	1.5197	0.9584	1.3347	1.3970	0.6412
	Minimum	-1.4063	-2.4416	-1.5807	-2.1035	-2.1793	-0.7083
Side-slip Angles, deg		α_{32}	α_{43}	α_{32}	α_{43}	α_{32}	α_{43}
Peak value	**Maximum**	1.8965	2.3641	1.9830	2.1003	1.8341	2.4248
	Minimum	-1.4667	-1.5805	-1.4492	-1.4432	-1.3226	-1.5883

From the results shown in Figures 4.2 to 4.6, it may be concluded that the damped articulations between units 2 and 3 (Case I) offers certain performance potential benefits to achieve enhanced directional performance of the A-train double. The damped articulations between units 2 and 4 (Case II), however, may lead to relatively poor directional performance. The performance potentials of the two concepts are further evaluated in terms of the performance measures and discussed in the following section.

4.4 Feasibility Analysis Based upon Performance Measures

The dynamic performance of the A-train double with different damped articulation configurations is assessed in terms of six selected performance measures, described in section 3.2. The transient response time, understeer coefficient (Ku), steady-state high-speed offtracking (HOF), and yaw damping ratio (YDR) performance

measures are evaluated under open loop steering maneuvers. The rearward amplification (RWA) and transient high-speed offtracking (TOF) performance measures are evaluated under a closed-loop maneuver, namely, single path-change maneuver. The recommended criteria to evaluate each of the selected performance measures have been summarized in Table 3.1. A numerical solution of the nonlinear yaw-plane model is performed using different open loop directional maneuvers. The directional response characteristics of the tractor (unit 1) and the rearmost trailer (unit 4) of the A-train double are obtained for each of the proposed damped configurations (Case I and Case II) corresponding to different values of the damping coefficients. The results of the study are discussed below.

4.4.1 Articulation Dampers between Units 2 and 3 (Case I)

The response characteristics of the combination units are evaluated to derive the performance measures values using the methodology described in section 3.2. The computed values of the performance measures, evaluated under open loop directional maneuvers, are summarized in Table 4.11, when articulation dampers are integrated between units 2 and 3 (Case I). The table also includes the critical understeer coefficients, Ku_{cr}, for units 1 and 4, and the critical velocities for the units that may exhibit oversteer characteristics. The Table 4.12 summarizes the computed values for each of the performance measure evaluated under the closed-loop directional maneuvers. The Table 4.12 also summarizes the computed peak values of lateral acceleration and yaw rate response for units 1 and 4 during the same maneuver.

Table 4.11: Performance measure values computed from open loop directional maneuvers for units 1 and 4 (Case I).

Performance Measures		Damping Coefficient, kN-s/m ($C_{KL} = C_{MN}$)					
		10		100		1000	
		Unit 1	Unit 4	Unit 1	Unit 4	Unit 1	Unit 4
Transient Response Time, sec		1.3550	1.6790	1.3460	1.7100	1.2190	1.7500
Ku, deg		1.9228	-0.0660	1.9226	-0.0665	1.9212	-0.0673
	Ku_{cr}, deg	-2.6661	-4.6620	-2.6661	-4.6620	-2.6661	-4.6620
	U_{cr}, km/h		840.3485		837.4013		832.6035
HOF, m			0.0919		0.0920		0.0934
YDR	Lateral Acceleration		0.4092		0.4432		0.6006
	Yaw Rate		0.4319		0.4425		0.5182

Table 4.12: Performance measure values computed from closed-loop directional maneuver for units 1 and 4 (Case I).

Performance Measures		Damping Coefficient, kN-s/m ($C_{KL} = C_{MN}$)					
		10		100		1000	
		Unit 1	Unit 4	Unit 1	Unit 4	Unit 1	Unit 4
RWA	Lateral Acceleration		1.5859		1.5125		1.2998
	Yaw Rate		1.5939		1.5100		1.2647
TOF, m			0.4366		0.4284		0.3969
Peak Lateral Accel., m/s^2		1.7061	2.7057	1.6999	2.5709	1.7241	2.2410
Peak Yaw Rate, deg/s		5.3938	8.5973	5.3182	8.0304	5.4707	6.9186

A comparison of the computed performance measures, reported in Tables 4.11 and 4.12, with the suggested threshold values, reported in Table 3.1, suggest that the computed values for Ku, HOF, YDR, RWA, and TOF performance measures are within the specified threshold values, irrespective of the damping coefficient values. Transient

response time performance measure, however, is slightly higher than the maximum allowable value of 1.7, reported in Table 3.1, for unit 4 for damping coefficient ≥ 100kN-s/m. The results show that the transient response time of unit 1 decreases by –10.04% and increases by +4.23% for unit 4, when the damping coefficient is changed from 10kN-s/m to 1000kN-s/m. The corresponding variations in Ku reveal similar trend with a decrease of –0.08% and increase of –1.97%, respectively for units 1 and 4. The corresponding changes of Ku for units 1 and 4 when $C_{KL} = C_{MN}$ = 100kN-s/m are attained as –0.01% and +0.76%, respectively. It can be noted from Table 4.11 that unit 1 shows understeer characteristics (Ku > 0), whereas unit 4 shows an oversteer behavior (Ku < 0), irrespective of the damping coefficient values. The critical velocity for unit 4, however, is quite large (above 832km/h) and Ku values for unit 4 are well above its critical values. The critical velocity of unit 4 is slightly affected when damping coefficients are changed from 10kN-s/m to 1000kN-s/m. The change is in the order of –0.92% and the corresponding variation in HOF is obtained as +0.11%, when damping coefficient are varied from 10kN-s/m to 100kN-s/m, and +1.63% when damping coefficients are varied from 10kN-s/m to 1000kN-s/m.

The yaw damping ratio (YDR) of unit 4 in terms of both the lateral acceleration and the yaw rate increases considerably when the damping coefficients are increased. The most significant changes in YDR of unit 4 are attained for $C_{KL} = C_{MN}$ = 1000kN-s/m, which are computed as +46.77% and +19.98%, for lateral acceleration and yaw rate response, respectively. The corresponding changes of YDR in terms of both lateral acceleration and yaw rate for unit 4 when $C_{KL} = C_{MN}$ = 100kN-s/m are attained as +8.31% and +2.45%, respectively. The RWA response of the A-train double in terms of

both lateral acceleration (RWA_{LA}) and yaw rate (RWA_{YW}) decrease considerably under high damping, as illustrated in Table 4.12. The transient high-speed offtracking (TOF) of the combination also decreases with increase in damping coefficient. The most significant reductions of these performance measures are obtained when the heavier damping coefficient is applied. RWA_{LA} and RWA_{YW} are reduced by –18.04% and –20.65%, respectively, when the damping coefficient changes from 10kN-s/m to 1000kN-s/m. TOF is reduced by –9.09% under the same damping conditions. The reductions of RWA_{LA}, RWA_{YW} and TOF when $\mathbf{C_{KL}} = \mathbf{C_{MN}}$ = 100kN-s/m are attained as –4.63%, –5.26% and –1.88%, respectively. The results further show that the peak values of lateral acceleration and yaw rate response of unit 1 vary only slightly when damped articulations are incorporated between units 2 and 3. Important reductions, however, are observed for unit 4. The variation in peak lateral acceleration response of unit 1 with $\mathbf{C_{KL}} = \mathbf{C_{MN}}$ = 100kN-s/m and $\mathbf{C_{KL}} = \mathbf{C_{MN}}$ = 1000kN-s/m are obtained as –0.36% and +1.06%, respectively. The corresponding variations in peak yaw rate response of unit 1 are obtained as –1.4% and +1.43%, respectively. The peak lateral acceleration and peak yaw rate response of unit 4 reduce by –4.98% and –6.59%, respectively, for $\mathbf{C_{KL}} = \mathbf{C_{MN}}$ = 100kN-s/m, by –17.17% and –19.53%, respectively for $\mathbf{C_{KL}} = \mathbf{C_{MN}}$ = 1000kN-s/m.

4.4.2 Articulation Dampers between Units 2 and 4 (Case II)

Tables 4.13 and 4.14 summarize the computed values of the dynamic performance measures for units 1 and 4 of the A-train double configuration, when damped articulations are integrated between units 2 and 4 (Case II). The tables also

present the critical understeer coefficients, critical velocities, and the peak values of lateral accelerations and yaw rates of units 1 and 4.

Table 4.13: Performance measure values computed from open loop directional maneuvers for units 1 and 4 (Case II).

Performance Measures		Damping Coefficient, kN-s/m ($C_{KL} = C_{MN}$)					
		10		100		1000	
		Unit 1	Unit 4	Unit 1	Unit 4	Unit 1	Unit 4
Transient Response Time, sec		1.3350	1.6800	1.2590	1.6900	1.1780	1.6890
Ku, deg		1.9228	-0.0719	1.9229	-0.1250	1.9229	-0.5834
Ku_{cr}, deg		-2.6661	-4.6620	-2.6661	-4.6620	-2.6661	-4.6620
U_{cr}, km/h			805.0123		610.6916		282.6895
HOF, m			0.0919		0.0920		0.0940
YDR	Lateral Acceleration		0.4180		0.5102		-----
	Yaw Rate		0.4375		0.5025		0.7280

Table 4.14: Performance measure values computed from closed-loop directional maneuver for units 1 and 4 (Case II).

Performance Measures		Damping Coefficient, kN-s/m ($C_{KL} = C_{MN}$)					
		10		100		1000	
		Unit 1	Unit 4	Unit 1	Unit 4	Unit 1	Unit 4
RWA	Lateral Acceleration		1.5926		1.5530		1.5930
	Yaw Rate		1.5642		1.3611		1.2063
TOF, m			0.4344		0.4251		0.4191
Peak Lateral Accel., m/s^2		1.7040	2.7138	1.7369	2.6975	1.7521	2.7911
Peak Yaw Rate, deg/s		5.4505	8.5256	5.6553	7.6977	6.0010	7.2389

The results in Tables 4.13 and 4.14 show that the values of the selected performance measures remain within the suggested threshold values, irrespective of the damping coefficients used. The influence of damped articulations between units 2 and 4 is more pronounced on the transient response time of unit 1 than that of unit 4. When the damping coefficients are increased from 10 to 100kN-s/m, the transient response times reduce by –5.69% and increase by +0.6%, respectively for units 1 and 4. A further increase in viscous damping coefficient, $C_{KL} = C_{MN}$ = 1000kN-s/m, yields further reduction in the transient response time of unit 1 (–11.76%) and a slight increase in that of unit 4 (+0.54%). The variations in damping coefficients yield only minimal influence on the understeer coefficient (Ku) for unit 1. The understeer coefficient (Ku), for unit 4, however, is strongly affected with increase in damping. The variations in damping coefficients from 10kN-s/m to 100kN-s/m produces an absolute change of Ku of up to 73%, while variations in damping coefficients from 10kN-s/m to 1000kN-s/m produces an absolute change of Ku of up to 711%. Since Ku is negative for unit 4, this unit exhibits significant oversteer behavior and the corresponding critical velocity reduces from 805km/h to 282.7km/h, when damping coefficients are varied from 10kN-s/m to 1000kN-s/m. The proposed concept in damped articulation also yields increase in the steady-state high-speed offtracking performance, which increases by +0.11% when damping coefficient changes from 10kN-s/m to 100kN-s/m, and +2.29% when damping coefficient changes from 10kN-s/m to 1000kN-s/m. The addition of dampers between units 2 and 4 yields significant change of YDR of unit 4 in terms of both the lateral acceleration and the yaw rate, specifically with higher damping coefficients. The most significant changes in YDR of unit 4 are attained for $C_{KL} = C_{MN}$ = 1000kN-s/m, for which the lateral

acceleration response of unit 4 is non-oscillatory, while the YDR based upon yaw increases by +66.40%. The corresponding changes in YDR of units 4 for $\mathbf{C_{KL}} = \mathbf{C_{MN}}$ = 100kN-s/m are attained as +22.06% and +14.86%, respectively, on the basis of lateral acceleration and yaw rate response.

This damping articulation concept yields insignificant variations in rearward amplification (RWA), defined on the basis of lateral acceleration response, while RWA based upon yaw rate response decreases with increase in articulation damping. The RWA_{LA} decreases by only –2.49%, when the damping coefficient is increased from 10kN-s/m to 100kN-s/m, and increases slightly (+0.03%) when the damping coefficient is increased to 1000kN-s/m. RWA_{YW} and TOF of unit 4, however, decrease with increase in the damping coefficients. The most significant reductions of these performance measures are obtained with the heavier damping coefficient ($\mathbf{C_{KL}} = \mathbf{C_{MN}}$ = 1000kN-s/m). The RWA_{YW} and TOF reduce by –22.88% and –3.52%, respectively, when the damping coefficient changes from 10kN-s/m to 1000kN-s/m. The peak lateral acceleration response of units 1 and 4 either increase or decrease slightly with increase in articulation damping. The variations in peak lateral acceleration of unit 4 corresponding to 100kN-s/m and 1000kN-s/m damping are obtained as –0.6% and +2.85%, respectively, whereas peak lateral acceleration of unit 1 are attained as +1.93% and +2.82%, respectively. The corresponding variations in peak yaw rate response of unit 4 are observed as –9.71% and –15.09%, for 100kN-s/m and 1000kN-s/m damping, respectively. The peak yaw rate response of unit 1, however, increases as the damping coefficient increases from +3.76 to +10.1%, for 100kN-s/m and 1000kN-s/m damping, respectively.

Although the directional performance of the A-train double with the proposed

damped articulations (Case I and Case II) is well within the suggested threshold values, the damped articulations between units 2 and 3 (Case I) yields considerable improvement in performance measures related to handling, rearward amplification, lateral acceleration and yaw rate response of the vehicle combination. The Case II of damped articulation, on the other hand, yields only slight improvement in some of the performance measures and slight deterioration in the others with exception of Ku, which is strongly affected by the damped articulations. The articulation damping between units 2 and 3 (Case I) is thus considered to be feasible, and further parametric studies are performed to derive desirable geometric parameters.

4.5 Summary

A set of weights and dimensional parameters of the candidate A-train double combination vehicle is presented and the Magic formula approach is applied to predict the tire cornering properties as a function of vertical load and side-slip angles. A feasibility analysis of the proposed concepts in damped articulations is performed to evaluate their relative potential performance benefits or limitations, which are assessed in terms of the recommended performance measures. From the results thus obtained, it is concluded that the damped articulation between units 2 and 3 (Case I) offers significant performance potential benefits to achieve enhanced directional performance of the A-train double. The damped articulations between units 2 and 4 (Case II), however, may lead to relatively poor directional performance. In the following chapter, a parametric study is performed to derive desirable geometric parameters for Case I.

Chapter 5

Parametric Study of the A–Train Double with Damped Articulation between Units 2 and 3

5.1 General

It is recognized that performance of A-trains, doubles or triples, exhibit poor dynamic behavior, specifically rearward amplification, under emergency maneuvers such as single or double path change maneuvers [26]. Two different concepts of viscously damped articulations mechanisms were proposed and analyzed in the previous chapter to enhance the dynamic performance of an A-train double combination. From the feasibility analysis, presented in chapter 4, it was concluded that the proposed concept, comprising damped articulations between units 2 and 3 (Case I), offers considerable potential performance benefits in terms of directional performance of the A-train double. The performance potentials of this damped articulation is also dependent upon the damping coefficient and a number of geometric parameters, ***a***, ***b*** and ***c***, illustrated in Figure 2.2. A comprehensive parametric study is thus performed to identify appropriate geometric and damping parameters for the concept considered more feasible (Case I). The potential

performance benefits of damped articulation with recommended values of geometric parameters (***a***, ***b*** and ***c***) and damping coefficients ($\mathbf{C_{KL}}$ and $\mathbf{C_{MN}}$) are evaluated in terms of the selected performance measures. These performance measures are compared with those obtained for a conventional (without damped articulations) A-train double. The relative potential performance gains of damped articulation are further evaluated under a more demanding maneuver, such as a double path-change maneuver.

5.2 Parametric Study

Damping coefficient parameter, $\mathbf{C_{KL}}$ and $\mathbf{C_{MN}}$, strongly influence the dynamic response of the A-train double when damped articulations are integrated between units 2 and 3. Furthermore, geometric parameters, ***a***, ***b*** and ***c***, shown in Figure 2.2, impose nonlinear forces and moments about articulation joint **B**. These geometric parameters may thus also affect the directional response of the A-train double combination. While the influence of damping coefficients on the directional performance of the A-train double with damped articulations is clearly demonstrated from the preliminary feasibility analysis, a comprehensive parametric study is needed to enhance an understanding of the contributions due to variations in geometric parameter. The results of the parametric study may also be used to select appropriate values for damping coefficients and the geometric parameters.

Parameter ***a*** and ***b*** define the locations of the damper mounts on the A-dolly (unit 3), while parameter ***c*** defines the location of the damper mounts on the first semitrailer (unit 2), as shown in Figure 2.2. The former parameters, however, are more related to the

design of the A-dolly. Since a specific design of A-dolly is used in this study, parameters a and b are thus held constant, such that a = 0.80m and b = 0.38m. The damper orientation, parameter c, can be theoretically varied from 0 m to 1.22m. The parametric study is thus performed to investigate the influence of variation in c together with damping coefficients, C_{KL} and C_{MN}. Identical values of damping coefficients due to right and left dampers are considered to ensure symmetry about the longitudinal axis. The influence of variations in these parameters is analyzed in terms of peak lateral acceleration, and peak yaw rate, rearward amplification (RWA), and peak side-slip and articulation angles, and transient high-speed offtracking (TOF) responses of the A-train double combination under a single path-change maneuver. The analyses are performed for a fully-loaded A-train double combination with a constant forward speed (U) of 100km/h.

The damper orientation parameter c, is varied in the 0.6m to 1.2m range with increments of 0.20m, while the damping coefficients, C_{KL} and C_{MN}, are varied from 1kN-s/m to 1024kN-s/m in 1-octave increments. Figures 5.1 and 5.2 illustrate the influence of variations in both the damping coefficients and the parameter c on the percentage (%) variations in the peak lateral acceleration and yaw rate response, respectively, of the four units of the A-train double, subject to a single path-change maneuver. The results show the % change in the response parameters attributed to changes in the parameters considered. The % change in the response parameters is evaluated with respect to the response parameters of a conventional A-train double without damped articulation, subject to identical loading and maneuver. These reference values of the response parameters are summarized in Table 5.1.

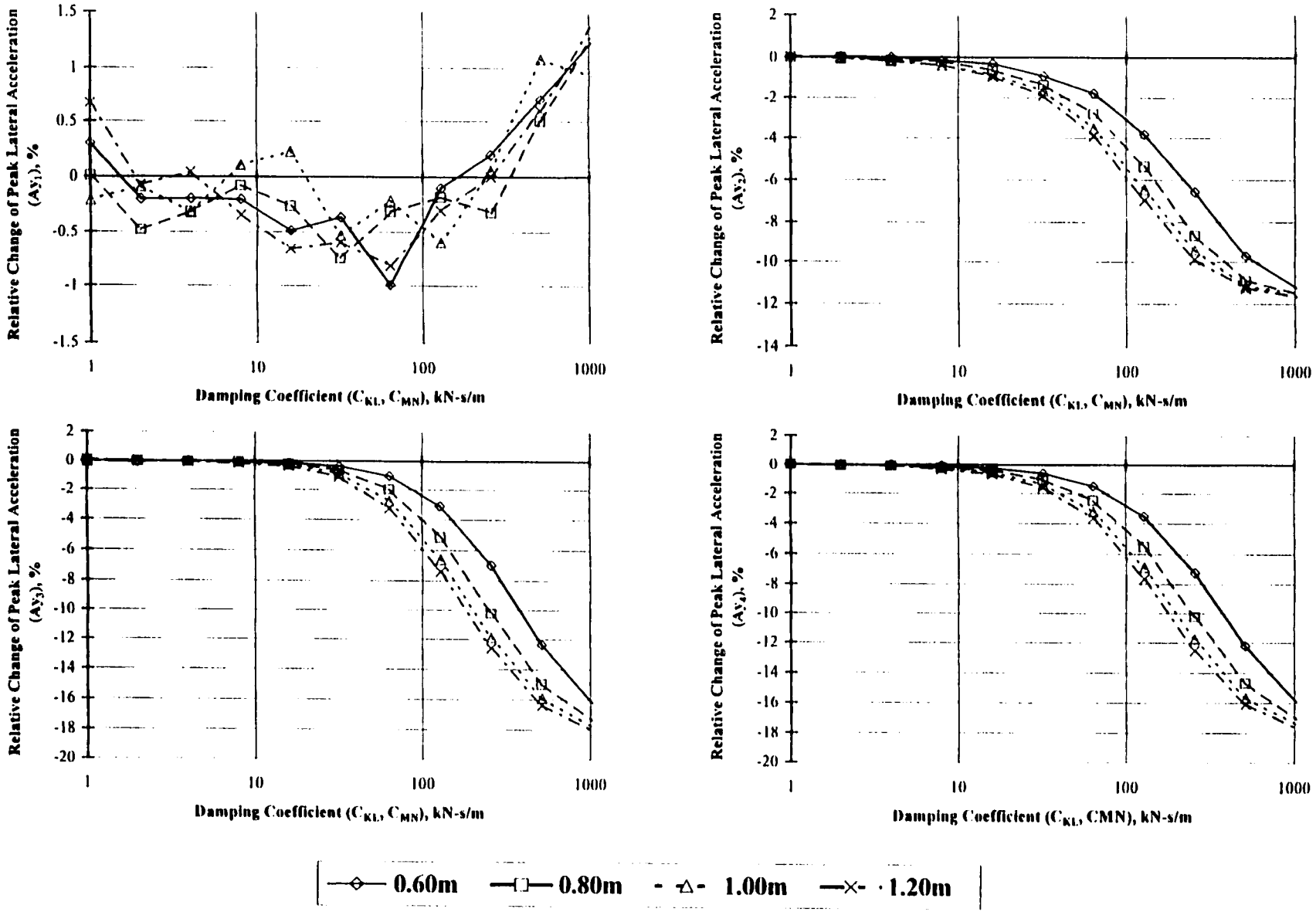

Figure 5.1: **Influence of variations in damping coefficients and parameter 'c' on the peak lateral acceleration response of the A-train double combination.**

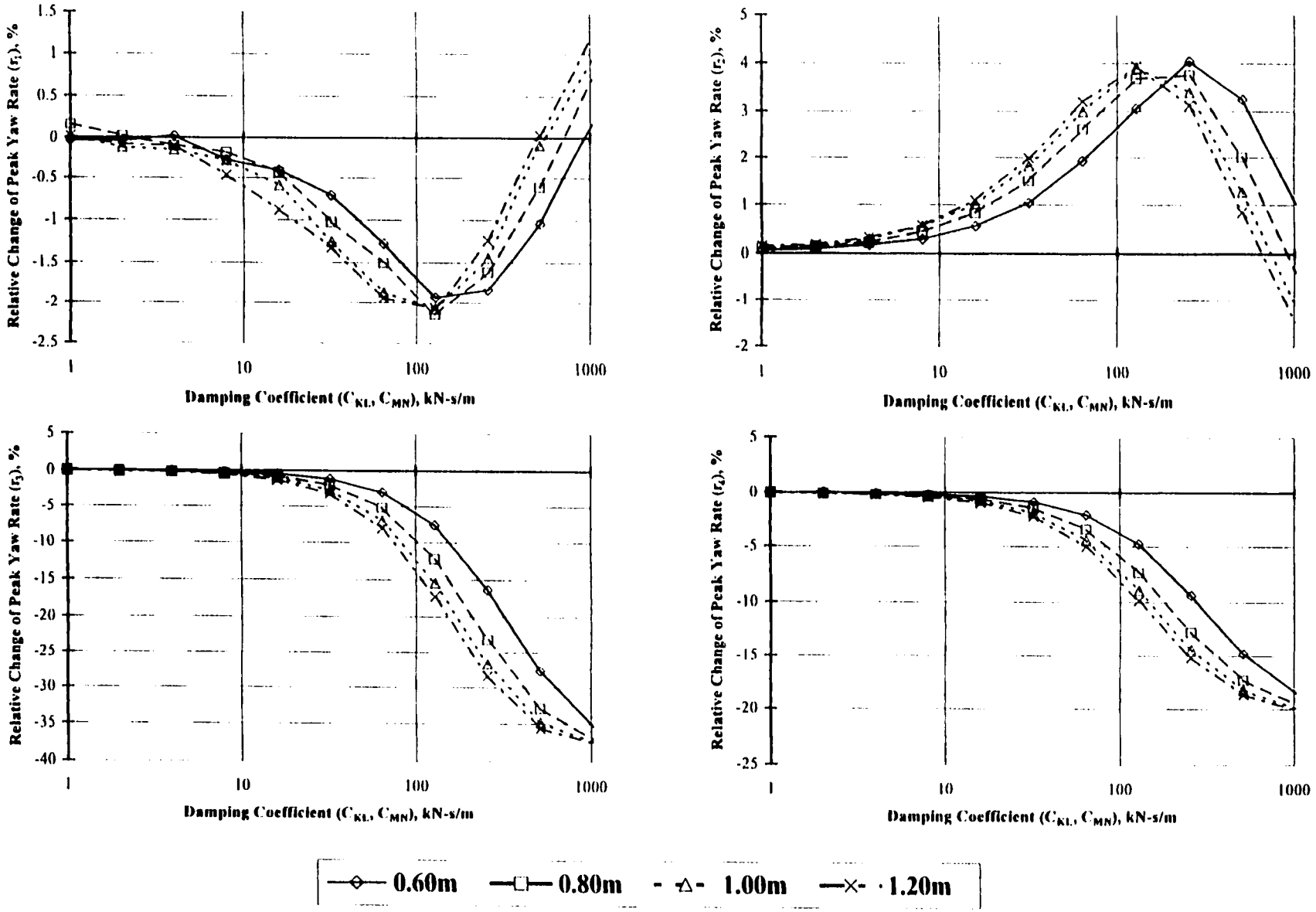

Figure 5.2: **Influence of variations in damping coefficients and parameter 'c' on the peak yaw rate response of the A-train double combination.**

Table 5.1: Reference values of the response parameters of the A-train double without damped articulation ($C_{KL} = C_{MN} = 0$), evaluated under a path-change maneuver.

		Unit 1	Unit 2	Unit 3	Unit 4
RWA	Lateral Acceleration		1.0057		1.5929
	Yaw Rate		0.8755		1.5942
TOF, m					0.4360
Peak Lateral Acceleration, m/s^2		1.7043	1.7139	2.5588	2.7148
Peak Yaw Rate, deg./s		5.4198	4.7452	7.1091	8.6403

Articulation Angle, deg.	γ_1	γ_2	γ_3
Peak values	1.9777	1.3805	2.4798

Side-slip Angle, deg.	α_{11}	α_{12}	α_{13}	α_{22}	α_{23}	α_{32}	α_{43}
Peak values	1.4035	1.1652	1.3274	1.2727	1.4591	1.8792	2.4074

Figure 5.3 depicts the influence of the damping coefficients and parameter c on the rearward amplification, in term of both the lateral acceleration and the yaw rate. The variations in RWA of both lateral acceleration (RWA_{LA}) and yaw rate (RWA_{YW}) are presented in terms of amplification attained for units 1 and 2 ($RWA_{LA}1$-2 and $RWA_{YW}1$-2) and units 1 and 4 ($RWA_{LA}1$-4 and $RWA_{YW}1$-4). Figure 5.4 illustrates the influence of variations in C_{KL}, C_{MN} and c on the peak side-slip angles developed at the tires on axles 3-2 and 4-3, α_{32} and α_{43}, respectively, and TOF response. Figure 5.5 illustrates the influence of variations in C_{KL}, C_{MN} and c on the peak articulation angles response, γ_1, γ_2 and γ_3.

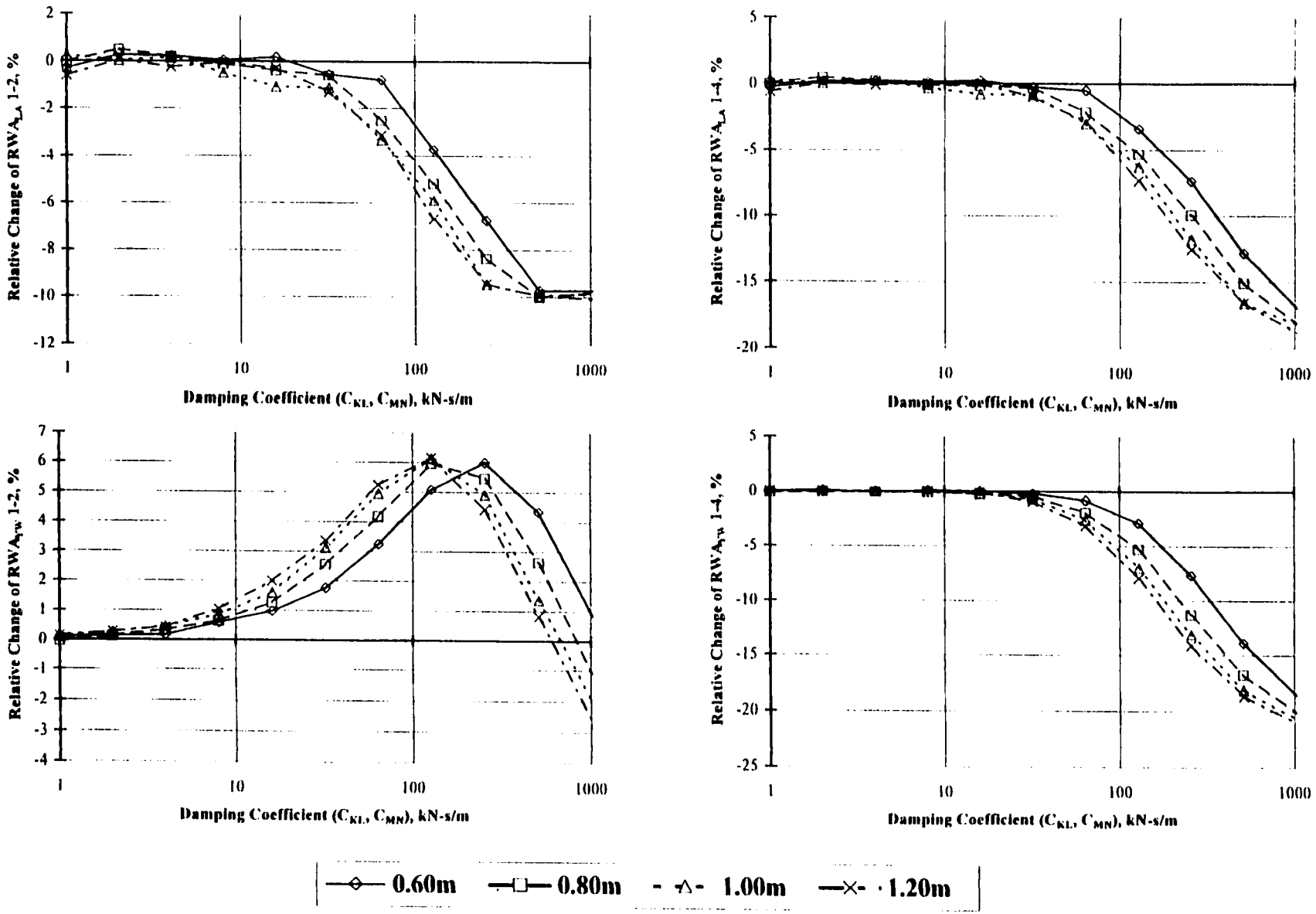

Figure 5.3: **Influence of variations in damping coefficients and parameter 'c' on the rearward amplification response of units 2 and 4.**

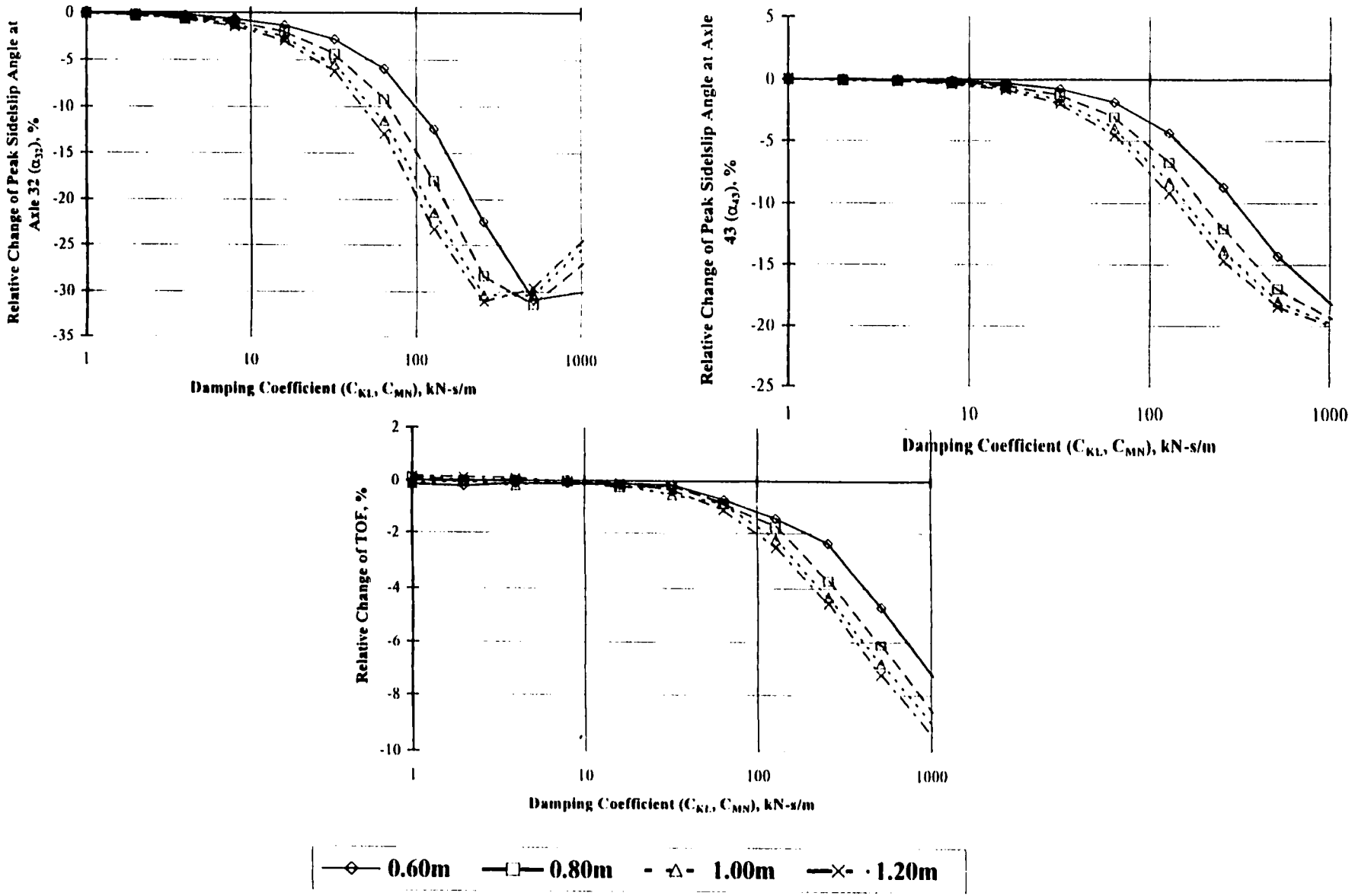

Figure 5.4: Influence of variations in damping coefficients and parameter 'c' on the peak side-slip angles and TOF response.

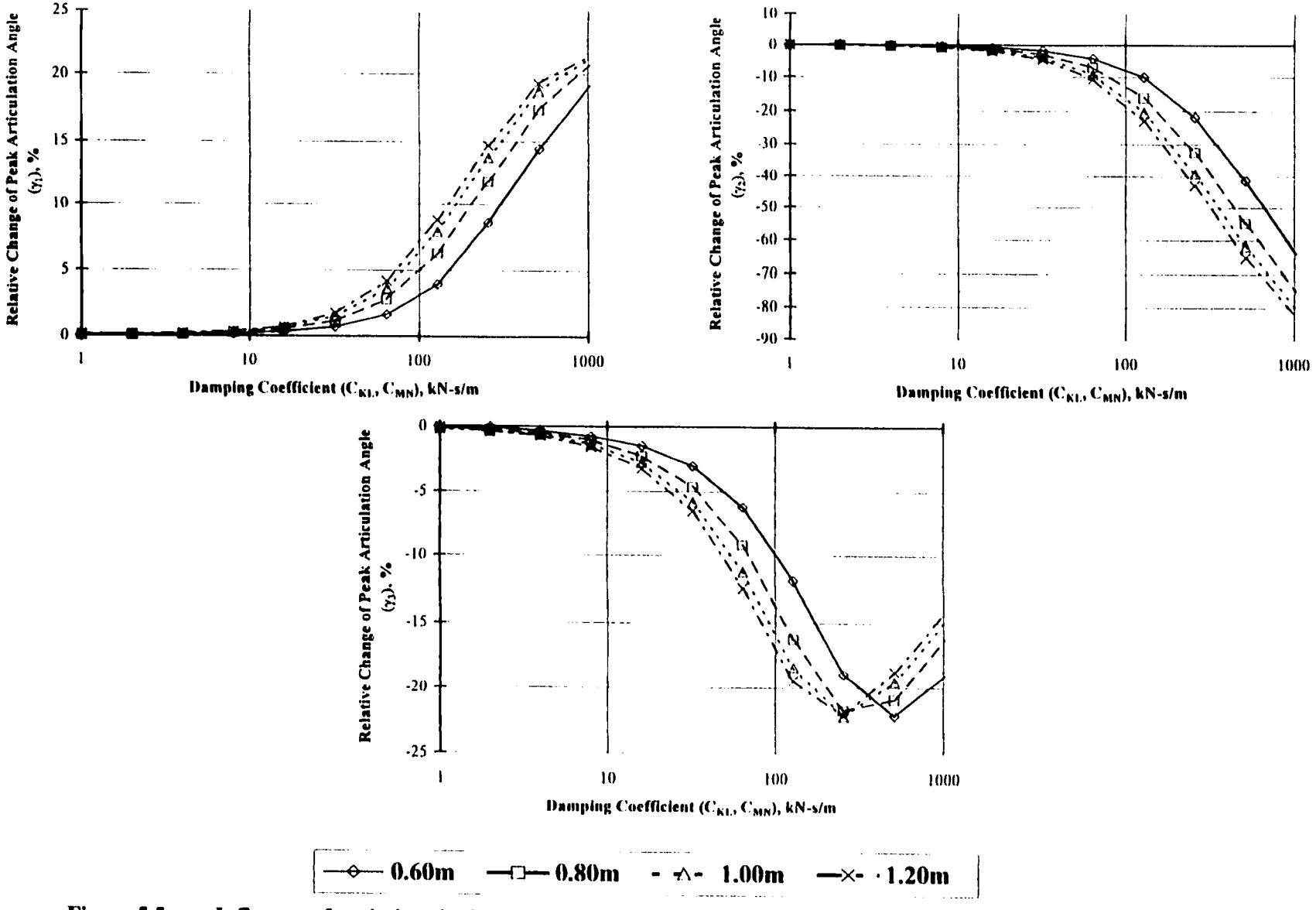

Figure 5.5: Influence of variations in damping coefficients and parameter 'c' on the peak articulation angle response.

The results presented in Figures 5.1 through 5.5 further reveal that an increase in damping coefficients yields considerable improvement in the directional dynamic performance of units 3 and 4. An increase in damping also yields certain reduction in the peak dynamic response quantities of unit 2, while the influence on dynamic response of unit 1 is relatively insignificant. The results show that a lightly damped articulation (C_{KL}, $C_{MN} \leq$ 16kN-s/m) yields insignificant variations in the peak response parameters of the fully loaded A-train double (GCW = 52210 kg), considered in this study, irrespective of the orientation parameter ***c***. Relative changes in terms of both peak lateral acceleration and yaw rate, RWA, peak side-slip and articulation angles, and TOF response of the A-train double combination under a single path-change maneuver are less than ±3.5%, for $C_{KL} = C_{MN}$ = 16kN-s/m. Most significant variations in the response parameters are obtained when the damping coefficients are varied between 64kN-s/m and 512kN-s/m. Although a further increase in articulation damping yields further reductions in some of the dynamic response parameters, the relative change occurs at a lower rate, when C_{KL} and C_{MN} exceed 512kN-s/m. High articulation damping also yields lower articulation angle γ_3, which may affect the maneuverability of the combination. The results further show that an increase in the orientation parameter, ***c***, in conjunction with light damping yields further reductions in most response parameters. It should be noted that an increase in ***c*** offers further reduction in a response parameter, only when the relative change in the same parameter due to damped articulation is negative (damping tends to reduce the peak value of the parameter). When the relative change in a response parameter is positive (damping causes the peak value of the parameter to increase), an increase in ***c*** tends to further deteriorate the performance when viewed in terms of the response parameter

concerned. The response parameters yaw rate of unit 2 (r_2), $RWA_{YW}1$-2, yaw rate of unit 3 (r_3) and side-slip angle at tires on axle 3-2 (α_{32}), shown in Figure 5.2, 5.3, 5.4, and 5.5, respectively, illustrate this behavior.

Integration of damped articulation between units 2 and 3 yields reductions in the peak lateral acceleration response of units 2, 3 and 4 of the combination, as shown in Figure 5.1. For $\mathbf{C_{KL}}$ and $\mathbf{C_{MN}} \geq 512$kN-s/m, and $\boldsymbol{c} = 0.6$m, the damped articulation yields 10-12% reduction in peak Ay_2 and 16-18% reduction in peak values of Ay_3 and Ay_4. The relative change in peak lateral acceleration of unit 1 (Ay_1), however, is less than ±1.5%. High damping tends to increase the peak lateral acceleration response of unit 1, irrespective of the damper orientation.

The damper articulation yields significant reduction in the peak yaw rates of units 3 and 4, in the order of –35% and –18.6%, respectively, for $\mathbf{C_{KL}} = \mathbf{C_{MN}} = 512$kN-s/m, as shown in Figure 5.2. The relative changes in peak yaw rate response of units 1 and 2, however, are observed to be positive, although the changes are below 4%. The peak yaw rate response of unit 2 (r_2) tends to increase with increase in $\mathbf{C_{KL}}$, $\mathbf{C_{MN}}$ and $\boldsymbol{c}$ until $\mathbf{C_{KL}}$ and $\mathbf{C_{MN}}$ approach 256kN-s/m for $\boldsymbol{c} = 0.6$m or until $\mathbf{C_{KL}}$ and $\mathbf{C_{MN}}$ approach 128kN-s/m for $0.8\text{m} \leq \boldsymbol{c} \leq 1.2\text{m}$. The peak r_2 response, however, tends to decrease with further increase in $\mathbf{C_{KL}}$ and $\mathbf{C_{MN}}$, whereas a larger value of $\boldsymbol{c}$ yields additional reduction in r_2. The peak yaw rate response of unit 1, r_1, reduces by approximately –2% when $\mathbf{C_{KL}}$ and $\mathbf{C_{MN}}$ are increased to 128kN-s/m, irrespective of the parameter $\boldsymbol{c}$. A further increase in $\mathbf{C_{KL}}$ and $\mathbf{C_{MN}}$ causes the peak values of r_1 to increase, as shown in the Figure 5.2.

The slight increase in peak value of r_2 when damping coefficients are ≤ 128kN-s/m may be attributed to the moments generated by the damping forces and the inertial

moments of unit 2, which may depend upon the damping coefficients. Figure 5.6 illustrates the influence of the damping coefficient on the damping force developed by the damper 1 of the damped articulation. An increase in the damping coefficient causes significant increase in not only the damping force, but also in the fundamental period of oscillation. It should be noted that the damping force variations shown in the figure are attained under the identical path change maneuver performed at U = 100km/h. The damper 2 also generates forces of similar magnitude, which are out-of-phase with those due to damper 1. Figure 5.7 depicts the time history of the yaw rate response of unit 2 as a function of the damping coefficient, which reveals only minimal effect of the damping coefficient (less that ±4%).

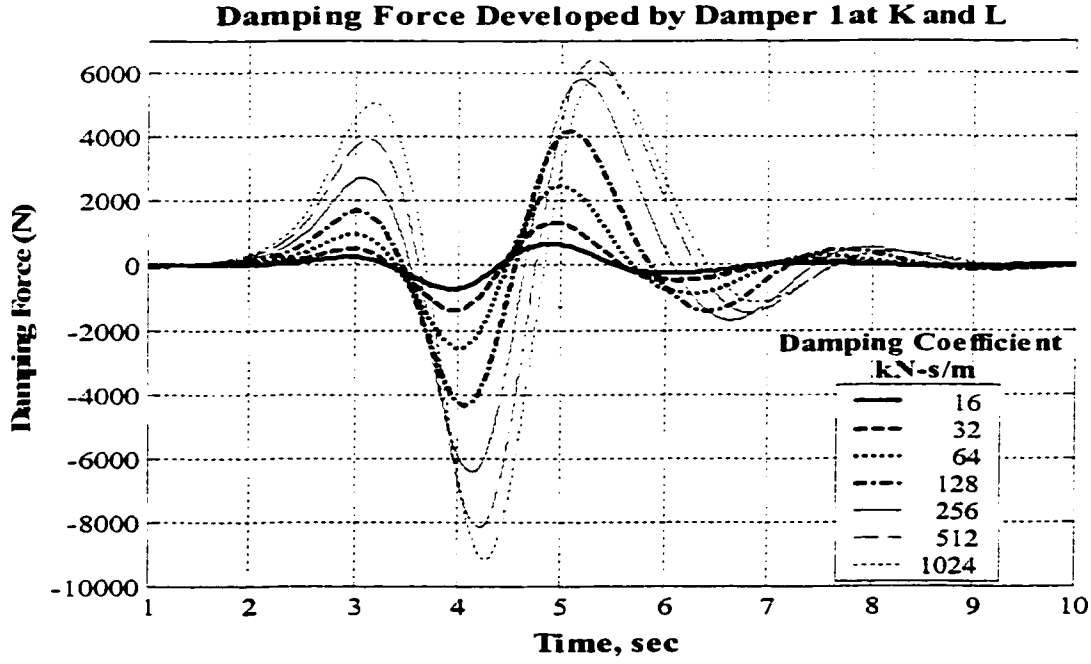

Figure 5.6: Influence of damping coefficient on the damping force developed by damper 1.

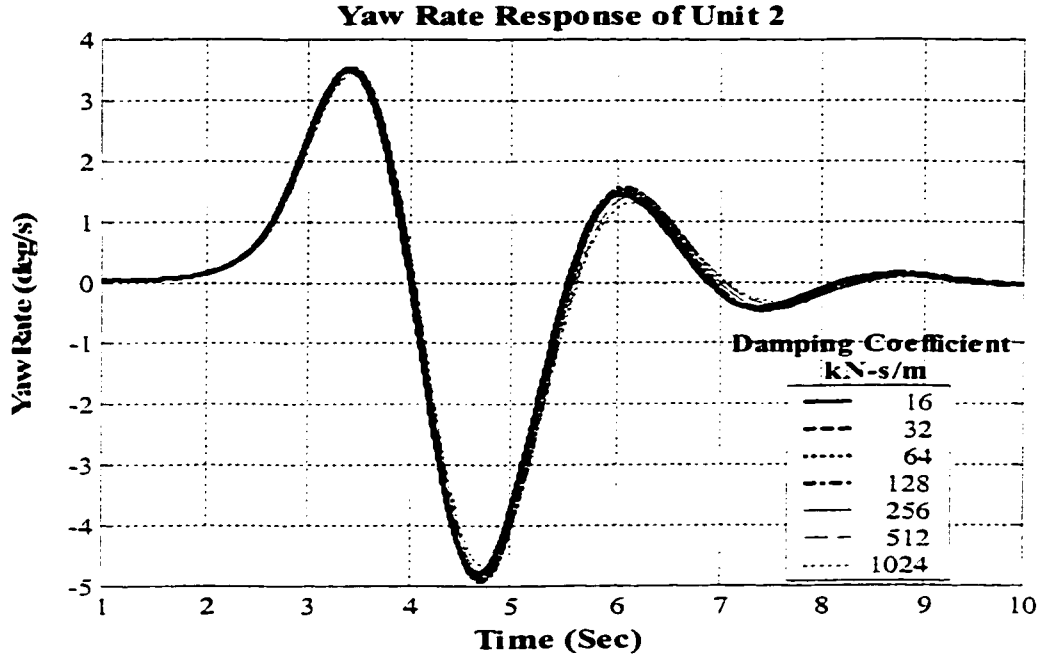

Figure 5.7: Influence of damping coefficient on the yaw rate response of unit 2.

A damped articulation also yields significant reduction in RWA_{LA} response, as shown in Figure 5.3. The RWA_{LA} of unit 2 reduces by approximately –10%, when the damping coefficients are selected as 512kN-s/m, irrespective of the value of parameter ***c*** in the 0.6m to 1.2m range. The RWA_{LA} of unit 4 reduces by –12.5% to –17% when damping coefficients are selected as 512kN-s/m, and parameter ***c*** is in the 0.6m to 1.2m range. A further increase in damping coefficients yields only slight variations in RWA_{LA}. Since $RWA_{YW}1\text{-}2$ is computed from the peak yaw rates of units 1 and 2, the phenomena presented and previously discussed for the yaw rate response of units 1 and 2 causes similar increase in RWA_{YW}, as shown in the Figure 5.3. The decrease in r_1 coupled with an increase in r_2 causes the $RWA_{YW}1\text{-}2$ to increase up to +6%. The $RWA_{YW}1\text{-}4$, however, decreases in the –18.1% to –21% range, when parameter ***c*** is selected between 0.6m and 1.2m at the highest damped coefficients.

The integration of damped articulation tends to reduce both the peak side-slip angles of axles 3-2 (α_{32}) and 4-3 tires (α_{43}), and the transient high-speed offtracking (TOF), as illustrated in Figure 5.4. The peak side-slip angles tend to decrease with increase in damping coefficient and c values. The damping coefficients, ranging from 256kN-s/m to 512kN-s/m, yield most significant reduction (up to –30%) in the peak α_{32}, for all values of c considered in the study. The relative change in the peak α_{43} is obtained in the –18.1% to –19.9% range. A reduction in the peak side-slip angle of the axle tires implies reduced cornering demand on the tires and lesser degree of tire wear. TOF of the combination also decreases with in increase in $\mathbf{C_{KL}}$, $\mathbf{C_{MN}}$ and c. The reduction in TOF is observed within –8%, depending upon the parameter values.

It is interesting to note that the relative change in peak articulation angle between units 3 and 4, γ_3, as shown in Figure 5.5, is similar to the relative change in peak α_{32}, as shown in Figure 5.4, while the reduction in the relative change in γ_3 is up to –22%. As it would be expected and it was found in the preliminary feasibility analysis, γ_2 is strongly affected by the damping coefficients. An increase in damping coefficients and parameter c yields considerably lower peak values for γ_2, while the reductions range from –63.7% to –82.2% for $0.6\text{m} \leq c \leq 1.2\text{m}$. The articulation damping, however, adversely affects the articulation angle between units 1 and 2 (γ_1), as shown in Figure 5.5. An increase in both the damping coefficient and orientation parameter, c, causes the peak value of γ_1 to increase, while peak change is in the order of +20% for $\mathbf{C_{KL}} = \mathbf{C_{MN}} = 1000$kN-s/m and all values of c. From the articulation angle response, it may be deducted that the A-train double with damped articulation undergoes larger relative yaw rotation between units 1 and 2, while the magnitudes of relative yaw rotation between units 2 and 3, and units 3

and 4 decrease, these changes in articulation angles perhaps cause reduction in the rearward amplification, which is a key response for A-train combinations.

5.3 Performance Assessment in terms of Performance Measures

From the parametric study as well as from the preliminary feasibility analysis, it is apparent that the directional response of the A-train double is strongly affected by both damping coefficient and the geometric parameter ***c***. The results of the parametric study further suggest that larger values of damping coefficients and geometric parameter ***c*** yield improved directional performance of the A-train double, when fully-loaded. An examination of the results further reveals that the rate of relative change in response parameters is somewhat lower for damping coefficients exceeding 512kN-s/m. Too high damping yields larger articulation angle γ_1. A value of damping coefficient of 512kN-s/m or slightly higher is thus suggested for the damped articulation. The results also suggest that the orientation parameter in the order of 1.0m yields reasonable performance gains for the A-train double with damped articulation. The potential performance gains of the damped articulation are thus investigated by setting: $\boldsymbol{a}$ = 0.8m, $\boldsymbol{b}$ = 0.38m, $\boldsymbol{c}$ = 1.0m, and $C_{KL} = C_{MN}$ = 660kN-s/m.

Using the baseline vehicle's parameters described in Table 4.1, and by applying the nonlinear yaw plane model for the A-train double which includes the nonlinear dependence between lateral force, self-aligning moment and side-slip angles, the transient, steady-state dynamic responses characteristics of the A-train double combination are obtained for different directional maneuvers. The response

characteristics of the A-train double combination are evaluated for units 1 and 4 in term of the selected performance measures described in chapter 3. The transient response of the A-train double is evaluated in terms of the response time and yaw damping ratio (YDR) performance measures, while the steady-state response is evaluated through understeer coefficient (Ku) and steady-state high-speed offtracking (HOF). The previously named performance measures are obtained under open loop maneuvers, namely, ramp-step and half-sine steer maneuvers, using the methodology described in section 3.2. The dynamic response of units 1 and 4 of the A-train double is also evaluated in terms of rearward amplification (RWA) of lateral acceleration and yaw rate, and the transient high-speed offtracking (TOF) performance measures, derived under a closed loop path-change maneuver.

The computed values of each performance measure of the A-train double with damped articulation are summarized in Table 5.2. For purposes of comparison, Table 5.2 also lists the computed values of each selected performance measures of the vehicle without damped articulation. The table also summarizes the performance gain (loss) for each measure. The evaluated performance measures reported in Table 5.2 are also assessed in relation to the suggested threshold values reported in Table 3.1. The assessment of performance measures revealed that computed values for Ku, HOF, YDR, RWA, and TOF performance measures are within the specified threshold values for both the conventional A-train double and the A-train double with damped articulations, between units 2 and 3.

Table 5.2: **Comparison of performance measures of A-train double with and without damped articulation between units 2 and 3.**

Performance Measures		Damping Coefficient, kN-s/m (C_{KL}, C_{MN})					
		0 (Conventional)		660		% Change	
		Unit 1	Unit 4	Unit 1	Unit 4	Unit 1	Unit 4
Transient Response Time, s		1.3490	1.6780	1.2350	1.7490	-8.45	4.23
Ku, deg.		1.9228	-0.0660	1.9220	-0.0693	-0.04	5.00
U_{cr}, km/h			840.6696		820.1129		-2.45
HOF, m			0.0919		0.0927		0.87
YDR	Lateral Acceleration		0.4102		0.6964		69.77
	Yaw Rate		0.4263		0.5750		34.88
RWA	Lateral Acceleration		1.5929		1.3219		-17.01
	Yaw Rate		1.5942		1.2847		-19.41
TOF, m			0.4360		0.4027		-7.64
Peak Lateral Accel., m/s^2		1.7043	2.7148	1.7138	2.2656	0.56	-16.55
Peak Yaw Rate, deg./s		5.4198	8.6403	5.4420	6.9912	0.41	-19.09
Side-slip Angle, deg.		α_{32}	α_{43}	α_{32}	α_{43}	α_{32}	α_{43}
	Peak values	1.8792	2.4074	1.3409	1.9535	-28.65	-18.85
Articulation Angle, deg.		γ_2	γ_3	γ_2	γ_3	γ_2	γ_3
	Peak values	1.3805	2.4798	0.4257	2.0395	-69.16	-17.76

The results, however, show that the combination with damped articulation prompts unit 1 to respond 8.45% faster and unit 4 to respond 4.23% slower under a ramp-step maneuver, when compared with those of a conventional A-train double combination. While the addition of damped articulation does not affect the understeer coefficient of unit 1, it tends to increase the degree of oversteer for unit 4 and thus the corresponding critical speed is affected as well. Although the oversteer behavior of unit 4 increases by 5%, the critical speed decreases by only –2.45%, which remains well above the operating

forward speed. The steady-state high-speed offtracking (HOF) tends to increase slightly, less than +1%. From these performance measures, it can be concluded that the damped articulation does not affect the steady-state handling performance of the combination.

Although the yaw damping ratios (YDRs) of the conventional vehicle in terms of both lateral acceleration and yaw rate of unit 4 are relatively high (0.41 and 0.43, respectively), the addition of damped articulation tends to further increase the yaw damping ratio performance of the vehicle significantly. YDR in terms of lateral acceleration increases by +69.77% and in terms of yaw rate increases by +34.88%. The rearward amplification (RWA), which is one of the most important performance measure for LCVs and, of greatest concern on the dynamic performance of A-train doubles or triples, can be considerable enhanced by introducing damped articulation between unit 2 and 3 of an A-train double. The results summarized in Table 5.2 suggest that the RWA in terms of lateral acceleration (RWA_{LA}) can be improved by 17%, while that in terms of yaw rate (RWA_{YW}) can be improved by 19.4%. The addition of damped articulation thus offers considerable potentials to enhance the safety dynamic performance of LCVs comprising an A-dolly.

The performance in terms of transient high-speed offtracking (TOF) is also enhanced (reduced by –7.64%) when the damped articulation is introduced. In terms of peak values of both lateral acceleration and yaw rate, unit 1 is subject to increments in both of the measures, which are less that +0.6%. The response measures for unit 4, however, reduce considerably, up to –16.55% for peak lateral acceleration and up to –19.1% for peak yaw rate. The peak values of α_{32} and α_{43}, which may be related to tire wear and cornering demand on tires, also decrease by –28.65% and –18.85%,

respectively. The peak articulation angles between units 2 and 3 (γ_2) and units 3 and 4 (γ_3) further decrease by –69.16% and –17.76%, respectively, with damped articulation.

The potential performance gains of the A-train double combination with damped articulation are further evaluated under a more severe maneuver, consisting of a double path-change maneuver. The computed values of the performance measures derived for a conventional A-train double subject to a double path-change maneuver are summarized in Table 5.3. The parameters that define the double path-change maneuver considered in this study are summarized in Table 3.2. Table 5.4 lists the computed values for the measures derived for conventional and damped A-train doubles, subject to same maneuver performed at a forward speed of 100km/h. Table 5.4 also summarizes the performance gains of the damped articulation.

Table 5.3: Performance measures evaluated for the conventional A-train double under a double path-change maneuver.

		Unit 1	Unit 2	Unit 3	Unit 4
RWA	Lateral Acceleration		1.0582		1.7195
	Yaw Rate		0.9614		1.6087
TOF, m					0.8808
Peak Lateral Acceleration, m/s^2		2.8133	2.9668	3.7936	4.1714
Peak Yaw Rate, deg./s		7.7357	7.4371	9.2578	11.5492

Articulation Angle, deg.	γ_1	γ_2	γ_3
Peak values	2.9679	1.9400	3.2605

Side-slip Angle, deg.	α_{11}	α_{12}	α_{13}	α_{22}	α_{23}	α_{32}	α_{43}
Peak values	2.5370	2.0439	2.3047	2.2418	2.5433	2.9544	3.6590

A comparison of the performance measures evaluated for the conventional A train double under single and double path-change maneuvers, presented in Tables 5.1 and 5.3, respectively, reveals that the double path-change maneuver is a much more demanding maneuver. The peak lateral acceleration values obtained under the double path-change maneuver are at least +48% higher than those obtained during a single path-change maneuver. The corresponding peak values of yaw rates increase by at least +30%, while the peak articulation angles are at least +31% higher. The peak values of side-slip angles and TOF attained during a double path-change are at least +52% and +102% higher than those attained during a single path-change maneuver. The RWA of the A-train double combination also increases when it undergoes a double path-change maneuver. The increments in RWA_{LA} and RWA_{YW}, however, are small, in the order of +9.8% and −9.1%, respectively.

A comparison of performance measures attained for the A-train double with damped articulation with those derived for the conventional vehicle further supports the performance potential gains of the damped articulation between unit 2 and 3. The results summarized in Table 5.4, corresponding to a double path-change maneuver, suggest that the RWA_{LA} and RWA_{YW} can be reduced in the order of −15.1%, when damped articulations are introduced. The corresponding reductions in TOF, $(Ay_1)_{peak}$, $(Ay_2)_{peak}$, $(r_1)_{peak}$, and $(r_4)_{peak}$ are obtained as −9.97%, −1.1%, −9.2%, +0.2%, and −13%, respectively. It should be noted that TOF value of 0.79m is within the suggested threshold of 0.8m, which is proposed for a less severe single path-change maneuver. The damped articulation also yields considerable lower peak values of α_{32} and α_{43}, and the articulation angles of the vehicle subject to double path-change maneuver. A comparison

of the results, presented in Table 5.2 and 5.4, suggest that the performance gains of damped articulation under a double path-change maneuver are slightly smaller in view of those obtained under a single path-change maneuver.

Table 5.4: Comparison of performance measures of A-train double with and without damped articulation between units 2 and 3, under a double path-change maneuver.

Performance Measures		Double path-change					
		Damping Coefficient, kN-s/m (C_{KL}, C_{MN})					
		0 (Conventional)		660		% Change	
		Unit 1	Unit 4	Unit 1	Unit 4	Unit 1	Unit 4
RWA	Lateral Acceleration		1.7195		1.4599		-15.10
	Yaw Rate		1.6087		1.3659		-15.09
TOF, m			0.8808		0.7930		-9.97
Peak Lat. Accel., m/s^2		2.8133	4.1714	2.7827	3.7870	-1.09	-9.22
Peak Yaw Rate, deg./s		7.7357	11.5492	7.7490	10.0633	0.17	-12.87
Side-slip Angle, deg.		α_{32}	α_{43}	α_{32}	α_{43}	α_{32}	α_{43}
	Peak values	2.9544	3.6590	2.3986	3.2210	-18.81	-11.97
Articulation Angle, deg.		γ_2	γ_3	γ_2	γ_3	γ_2	γ_3
	Peak values	1.9400	3.2605	0.7396	2.8975	-61.88	-11.13

5.4 Summary

A comprehensive parametric study is carried out to identify appropriate damping coefficients, C_{KL} and C_{MN}, and damper-orientation parameter, c, for the A-train double combination integrating damped articulation between units 2 and 3 (Case I), which was identified as the more viable concept from the feasibility analysis presented in chapter 4. From the parametric analysis, a set of damping coefficient and geometric parameters is

proposed and a performance assessment of the combination vehicle in terms of the selected performance measures is carried out. The dynamic performance of the A-train double combination with damped articulation is compared to that of the conventional vehicle, which does not included damped articulation at all, to highlight the influence of integrating articulation dampers between units 2 and 3. The potential performance enhancement of the A-train double combination with damped articulation is further evaluated under a more severe maneuver, consisting of a double path-change maneuver. The conclusions made from both parametric and comparative studies are: directional response of the A-train double is strongly affected by both damping coefficient and the geometric parameter ***c***; light damped articulation yields insignificant variations in the peak response parameters of the fully loaded A-train double, considered in this study, irrespective of the orientation of the dampers. Most significant variations in the response parameters are obtained when the damping coefficients are varied between 64kN-s/m and 512kN-s/m. Too high adversely affect the articulation angle between units 1 and 2, γ_1. The rearward amplification (RWA) can be enhanced by 17% in terms of lateral acceleration (RWA_{LA}), while that in terms of yaw rate (RWA_{YW}) can be improved by 19.4%, when parameter a = 0.8m, b = 0.38m, c = 1.0m, and $C_{KL} = C_{MN}$ = 660kN-s/m. The double path-change maneuver is a much more demanding maneuver. The performance gains of damped articulation under a double path-change maneuver are slightly smaller in view of those obtained under a single path-change maneuver.

Chapter 6

Conclusions and Recommendations for Future Research

6.1 General

The use of long combination vehicles (LCVs) has steadily increased during the past few decades owing to relaxations in the weights and dimensions regulations in order to improve truck productivity. The increases in their weights and dimensions coupled with long combinations, such as doubles or triples, have significantly affected the directional performance of such vehicles, mostly in an adverse manner. Many concerns have thus been raised on operational safety and thus the highway safety of LCVs, which have prompted a series of objective assessment of dynamic performance of articulated freight vehicles. The A-train double configurations of LCVs, widely used in North America, are known to exhibit poor dynamic performance in terms of their lateral and yaw stability at highway speeds, and the rearward amplification.

The scope of this dissertation was thus formulated to explore the potential performance benefits of damped articulation concepts in terms of lateral stability and rearward amplification characteristics of an A-train double. The highlights of this

dissertation research and major conclusions drawn are summarized in the following sections.

6.2 Highlights of the Investigation

A nonlinear yaw-plane model of the A-train double combination is developed to study its lateral and yaw directional dynamics. The cornering properties of the tires are characterized using the nonlinear Magic Formula approach, which can predict both lateral forces and self-aligning moments as a function of both vertical load and side-slip angles. The directional dynamics of the A-train double with different distribution of axle loads can thus be performed using the nonlinear model. Two different concepts in viscously damped articulation mechanisms are proposed for possible enhancement in the LCV performance. The first concept consists of integrating a damped articulation mechanism between the first semitrailer (units 2) and the A-dolly (unit 3) of the A-train double, while the second concept proposes the integration of articulation dampers between first and last semitrailers (units 2 and 4) of the vehicle combination. A comprehensive kinematic analysis of each damped articulation concept is developed and their mathematical formulation is then introduced separately into the nonlinear yaw-plane model of the A-train double.

A set of performance measures is selected for objective assessment of potential performance benefits of the damped articulation concepts. A continuous analytical function based upon the Magic Formula is proposed to describe both the single and double path-change directional maneuvers. A path-follower driver-vehicle model is then

developed to describe the closed-loop steering control of the A-train double along the desired path, described using the proposed analytical function. The driver-vehicle model, based upon the preview distance and certain control abilities of the driver, computes the required front wheel steer angle such that the CG of the unit 1 follows the desired path. The potential performance benefits or limitations of the proposed concepts in damped articulations are initially investigated through a feasibility analysis, which highlights the influence of varying the damping coefficient on the performance response of the A-train. The results of the feasibility analysis are analyzed to select the most suited damped articulation concept. The potential performance benefits of the proposed concept are then evaluated in terms of the selected measures.

A parametric study is then performed to select suited damper parameters, and potential benefits are assessed through selected performance measures by comparing the behavior of the A-train double integrating damped articulation with that obtained for a conventional A-train double. A complementary evaluation under a more severe maneuver, double path-change maneuver, is also carried out to assess the performance enhancement of integrating damped articulation between units 2 and 3 of the vehicle combination.

6.3 Conclusions

Following major conclusions are drawn from the results of the study:

- From literature review, it can be concluded that long combination vehicles (LCVs) may jeopardize the highway safety due to increased weights and

dimensions, which may alter the dynamic performance of such vehicles under emergency maneuvers. The A-train double combination exhibits poor lateral stability and excessive rearward amplification at high speeds and standard directional maneuvers.

- The lateral and yaw dynamics of an A-train double combination can be appropriately described by the nonlinear analytical yaw-plane model.

- The directional dynamics of the A-train double is strongly influenced by the nonlinear cornering properties of tires, namely, lateral forces and self-aligning moments, which are known to be nonlinear functions of normal load and side-slip angles. Such nonlinear characteristics can be effectively predicted from the Magic Formula, whose optimized coefficients are computed from vertical load and actual measured data.

- The path coordinates for closed-loop maneuvers, namely, single and double path-change maneuver, can also be accurately described by the Magic Formula, where the coefficients can be defined by additional mathematical relationships.

- The path-follower driver-vehicle model based upon preview strategy can provide front wheel steer angle required to follow a prescribed path through selection of suitable control parameters.

- The steady-state and transient dynamic response of an A-train double can be objectively assessed through performance measures based on transient response time, both steady-state and transient high-speed offtracking, yaw damping ratio, rearward amplification, and peak lateral accelerations and yaw rates.

- Although the directional performance of the A-train double with the proposed damped articulations (Case I and Case II) is well within the suggested threshold values, the damped articulations between units 2 and 3 (Case I) yields considerable improvement in performance measures related to handling, rearward amplification, lateral acceleration and yaw rate response of the vehicle combination. The Case II of damped articulation, on the other hand, yields only slight improvement in some of the performance measures and slight deterioration in the others. The articulation damping between units 2 and 3 (Case I) is thus considered to be feasible.

- For the feasible case (Case I), a lightly damped articulation ($\mathbf{C_{KL}}$, $\mathbf{C_{MN}} \leq$ 16kN-s/m) yields insignificant variations in the peak response parameters of the fully-loaded A-train double, irrespective of the orientation parameter c. Most significant variations in the response parameters are obtained when the damping coefficients are varied between 64kN-s/m and 512kN-s/m. Too high damping yields higher peak articulation angle γ_1.

- From the selected performance measures, it can be concluded that the damped articulation does not affect the steady-state handling performance of the combination.

- The rearward amplification (RWA), which is one of the most important performance measure for LCVs, can be considerable enhanced by introducing damped articulation between unit 2 and 3 of an A-train double.

- The damped articulation also yields significant performance gains under a more severe double path-change maneuver. The magnitudes of the gains, however, are slightly smaller in view of those obtained under a single path-change maneuver.

6.4 Recommendations for Future Research

This dissertation research presents preliminary fundamental investigations on the concepts of damped articulation for A-train double combinations. In view of significant potential benefits of the proposed concepts, as evident from this study, further investigations are extremely essential for practical realization and implementation of damped articulations. Following further investigation may be undertaken in order to assess and maximize the potential performance benefits of damped articulation, and thus the enhancement of yaw and lateral stability of A-trains doubles.

(i) Validation of mathematical models and performance assessments of damped articulation needs to be carried out through real scale tests.

(ii) The design of damped articulations needs to be optimized through formulation and solution of multivariable optimization functions, where the design variables consists of damping coefficients and geometric parameters.

(iii) The investigation considers linear damping characteristics for the articulation. Nonlinear characteristics of damping articulations may offer further performance gains over wide operating conditions and thus should be further explored.

(iv) The performance gains of damped articulation needs to be evaluated as a function of operating conditions, such as fully-loaded, empty and 50% loaded at different forward speeds.

(v) The maneuverability performance of the combination with damped articulation needs to be explored, specifically during relatively tight turns.

(vi) The variation in geometric orientations of dampers should be further explored through kinematics of the spatial linkages together with a yaw-roll plane vehicle model to assess the performance potentials in terms of roll behavior of the vehicle.

(vii) The results of this preliminary investigation revealed that a damped articulation significantly affects the peak articulation angles and side-slip angles of tires. These results suggest that proposed concepts may be further beneficial in enhancing the jackknife behavior and low-speed friction demand of the vehicle. Further systematic investigation may thus be undertaken under simultaneous braking and turning maneuvers.

Bibliography

[1] I.T.E.C. Inc. WebPages:
http://www.itec-inc.com/frames/docs/documnts.htm.
http://www.itec-inc.com/frames/home/index.html.

[2] Norman, I.A, Scharff R. and Corinchock J.A., *"Heavy–Duty Truck System,"* 2nd Edition. Delmar Publishers, ISBN 0–8273–6391–5, 1995.

[3] Fancher, P.S., and Gillespie, T.D., *"Synthesis of Highway Practice 241. Truck Operating Characteristics,"* NCHRP, Transport Research Board, National Research Council, Washington, D.C., 1997.

[4] Fancher, P.S., et al., *"A Factbook of the Mechanical Properties of the Components for Single–Unit and Articulated Heavy Trucks,"* Report No. DOT–HS–807–125. NHTSA. Washington D.C., 1986.

[5] Vlk, F., *"Lateral Dynamics of Commercial Vehicle Combinations: A Literature Survey,"* Vehicle System Dynamics, vol. 11, no. 6, pp. 305–325, 1982.

[6] Huber, L. and Dietz, O., *"Pendelbewegung Von Lastkraftwagen – Anhanger und iher Vereidung,"* VDI–Zeitschrift, vol. 81, no. 16, pp. 459–463, 1937.

[7] Dietz, O., *"Pendelbewegungen an Strassen–Anhangerzugen,"* DKF, Heft 16, 1938.

[8] Dietz, O., *"Uber das Spuren und Pendeln von Lastkraftwagen–Anhangern,"* Atz, vol. 41, no. 15, 1939.

[9] Zeigler, H., *"Die Querschwingungen von Kraftwagenanhagern,"* Ing. – Archiv, vol. 9, no. 2, pp. 96–108, 1938.

[10] Zeigler, H., *"Der Einfluss von Bremsung und Steigung auf die Querschwingungen von Kraftwagenanhagern,"* Ing. – Archiv, vol. 9, no. 2, pp. 241–243, 1938.

[11] Laurien, F., *"Untersuchung der Anhangernseitenschwingungen in Strassinzugen,"* Dissertation, TH. Hannocer, 1955.

[12] Nalecz, A.G. and Genin, J., *"Dynamic Stability of Heavy Articulated Vehicles,"* Int. J. of Vehicle Design, vol. 5, no. 4, pp. 417–426, 1984.

[13] Fancher, P.S., *"The Static Stability of Articulated Commercial Vehicles,"* Vehicle System Dynamics, 14, pp. 201–227, 1985.

[14] Fancher, P.S., *"Directional Dynamics Considerations for Multi–Articulated, Multi–Axled Heavy Vehicles,"* J. of Commercial Vehicles, SAE 1989 Transactions, Section 2, vol. 98, pp. 630–640, 1989.

[15] Billing, A.M., *"Rollover Tests of Double Trailer Combinations,"* Transportation Technology and Energy Division, Ontario Ministry of Transportation and Communications, Report no. TVS–CV–82–114, 1982.

[16] Winkler,C.B. and Bogard, S.E., *"Simple Predictors of the Performance of A–Trains,"* Heavy Vehicle Dynamic and Stability, SAE SP–1002, pp. 145–156, November 1993.

[17] Billing, A.M. and Mercer, W.R.J., *"Demonstration of Baseline Vehicle Performance: A–Train Double,"* Transportation Technology and Energy Branch,

Ontario Ministry of Transportation and Communications, report no. CV–86–03, 1986.

[18] Nordstrom, O., Magnusson, G. and Strandberg, L., *"The Dynamic Stability of Heavy Vehicle Combinations,"* (in Swedish), VTI Rapport No. 9, Statens Vag–och trafikinstitut, Stockolm, 1972.

[19] Nordstrom, O. and Strandberg, L., *"The Dynamic Stability of Heavy Vehicle Combinations,"* International Conference of Vehicle System Dynamics, Blacksburg, Virginia, Report no. 67A, Statens Vag–och trafikinstitut, Linkoping, 1975.

[20] Nordstrom, O. and Nordmark, S., *"Test procedures for the Evaluation of Lateral Dynamics of Commercial Vehicle Combinations,"* Automobile–Insdustrie, vol. 23, no, 2, pp. 63–69, 1978.

[21] El–Gindy, M., *"Dynamic Behavior of a Tractor/Quadaxle Trailer with Variable length Drawbar,"* Int. J. of Vehicle Design, vol. 13, no. 2, pp. 182–200, 1992.

[22] Tong, X., Tabarrok, B., and El–Gindy, M., *"Computer–Based Analysis of the Dynamics Performance of Log Hauling Trucks,"* New Developments in Axles, Steering, Suspension, and Chassis Technology, SAE SP–1128, pp. 55–65. November 1995.

[23] Johnson, D.B and Huston, J.C., *"Nonlinear Lateral Stability Analysis of Road Vehicles Using Liaponov's Second Method,"* SAE, paper no. 841507, 1984.

[24] Wong, J.Y. and El–Gindy, M., *"Computer Simulation of Heavy Vehicle Dynamic Behavior – User's Guide to the UMTRI Models,"* Technical Report No.3, Vehicle

Weights and Dimensions Study, Roads and Transportation Association of Canada, June 1985.

[25] El–Gindy, M. and Wong, J.Y., *"A Comparison of Various Computer Simulation Models for Predicting the Directional Response of Articulated Vehicles,"* Vehicle System Dynamics, 16, pp. 249–268, 1987.

[26] Winkler, C.B., *"Improved Dynamic Performance of Multi–Trailer Vehicles,"* Symposium on the Role of Heavy Freight Vehicles in Traffic Accidents. Vol. 3, OECD, pp. 5–19 to 5–40, 1987.

[27] Rakheja, S., Vallurupalli, R.K., and Woodrooffe, J., *"Influence of Articulation Damping on the Yaw and Lateral Dynamic Response of the Vehicle,"* Heavy Vehicle Systems, Special Series, Int. J. of Vehicle Design, Vol. 2, No. 2, pp. 105–123, 1995.

[28] Kageyama, I. and Saito Y., *"Stabilization of Articulated Vehicles by Semi–active Control Method,"* The Dynamics of Vehicles on Roads and on Tracks, Proceedings of 10th IAVSD Symposium. Supplement to Vehicle System Dynamics, Vol. 17, August 1987.

[29] Winkler, C.B., et al., *"Heavy Vehicle Size and Weight – Test Procedures for Maximum Safety Performance Standards,"* Report No. DOT HS 807 855, UMTRI, Final Report, April 1992.

[30] El–Gindy, M., *"An Overview of Performance Measures for Heavy Commercial Vehicles in North America,"* Int. J. of Vehicle Design, Vol. 16, nos.4/5, pp. 441–463, 1995.

[31] Nix F.P., et al., *"1995 Truck Size and Weight Performance–Base Workshop,"* U.S. Department of Transportation, Comprehensive Truck Size and Weight Study. Report No.4. Prepared by Battelle, January 1996.

[32] Sweatman, P.F., *"Truck Size and Weight System and Outcomes: An International Perspective,"* SAE Technical Paper Series 982820. International Truck & Bus Meeting & Exposition. Indianapolis, Indian. November 16–18, 1998.

[33] Blow, P.W., Woodrooffe, J.H., and Sweatman, P.F., *"Vehicle Stability and Control Research for US. Comprehensive Truck Size and Weight (TS&W) Study,"*. SAE Technical Paper Series 982819. International Truck & Bus Meeting & Exposition. Indianapolis, Indian. November 16–18, 1998.

[34] Ervin, R.D., and Guy, Y., *"The Influence of Weights and Dimensions on the Stability and Control of Heavy-Duty Trucks in Canada,"* UMTRI Report No. 86-35, July 1986.

[35] Leucht, P.M., *"The directional dynamics of the commercial tractor-semitrailer vehicle during braking,"* Society of Automotive Engineering paper No 700371, 1970.

[36] Winkler, C.B., Mallikarjunarao, C, and MacAdam, C.C., *"Analytical Test Plan: Part I – Description of Simulated Models for Parametric Analysis of Heavy Truck Dynamic Stability,"* Report of the University of Michigan Transportation Research Institute, April 1981.

[37] Day, T.D., *"Differences between EDVDS and Phase 4,"* SAE Technical Paper Series 1999–01–0103, reprinted from SP–1407, March 1999.

[38] Segel, L, et al., *"The Mechanics of Heavy–Duty Trucks and Truck Combinations,"* The International Association for Vehicle Design, Chapter 17,

Turning of Single and Multi–Unit Trucks: Findings Derivable from a Linear Analysis, pp. 667–717, 1987.

[39] Fancher, P., Winkler, C., Ervin, R., and Zhang, H., *"Using Braking to Control Lateral Motions of Full Trailers,"* Vehicle System Dynamics Supplement 28 (1998), pp. 462–478.

[40] Pacejka, B.H., and Bakker, E., *"The magic Formula Tire Model,"* Tyre Models for Vehicle Dynamic Analysis, Proceedings 1st International Colloquium on Tire Models from Vehicle Dynamic Analysis, Supplement to VSD, Vol. 21, pp. 1-18. Delft, The Netherlands, October, 1991.

[41] Crolla, D.A., Firth, G., and Horton, D., *"An Introduction to Vehicle Dynamics,"* Department of Mechanical Engineering, University of Leeds, module H1.

[42] Hoffman, M., Fisher, E., and Richter, B., *"The Incorporation of Tire Modes into Vehicle Dynamics,"* Tyre Models for Vehicle Dynamic Analysis, Proceedings 1st International Colloquium on Tire Models from Vehicle Dynamic Analysis, Supplement to VSD, Vol. 21, pp. 49-57. Delft, The Netherlands, October, 1991.

[43] Lidner, L, *"Experience with the Magic Formula Tire Model,"* Tyre Models for Vehicle Dynamic Analysis, Proceedings 1st International Colloquium on Tire Models from Vehicle Dynamic Analysis, Supplement to VSD, Vol. 21, pp. 30-46. Delft, The Netherlands, October, 1991.

[44] Wong, J.Y., *"Theory of Ground Vehicles,"* 2nd ed. 1993 by John Wiley & Sons, Inc., ISBN 0-471-52496-4.

[45] Preston-Thomas, J., *"Measured Characteristics and Dynamic Performance of Two Configurations of Western Canadian Log Truck,"* NRC-CNRC, Technical Report CSTT-HWV-TR-002. 1994/07, pp.18.

[46] Gillespie, T.D., and Winkle, C.B., *"On the Directional Response Characteristics of Heavy Vehicles,"* the Dynamics of Vehicles on Roads and on Tracks, Proceedings 5th VCD-2nd IUTAM Symposium, pp. 165-183, 1997.

[47] El-Gindy, M. and Woodrooffe,, J.H.F. *"Study of Rollover Threshold and Directional Stability of Log Hauling Trucks,"* NRC-CNRC, Technical Report TR-VDL-002. NRCC No. 31274. 1990/02.

[48] Thomson, W.T. and Dillon, M.D., *"Theory of Vibration with Applications,"* 5th ed. 1998 by Prentice-Hall, Inc., ISBN 0-13-651068-X.

[49] Billing, A.M. et al., *"Test of a B-Train Converter Dolly,"* Transportation Technology and Energy Branch, Ontario Ministry of Transportation and Communications, Report no. TVS–CV–82–111, 1983.

[50] Apetaur, M. and Opička, F., *"Assessment of the Driver's Effort in Typical Driving Maneuvers for Different Vehicle Configurations and Managements,"* the Dynamics of Vehicles on Roads and on Tracks, Proceedings 12th IAVSD Symposium, pp. 42-56, 1991.

[51] Kelley, C. R., "*Manual and Automatic Control, A Theory of Manual Control and Its Application to Manual and to Automatic Systems*," John Wiley & Sons, Inc., pp.179-210, 1968.

[52] McRuer, D. T. et al., "*New Results in Driver Steering Control Models*," Human Factors, Vol.19, No.4, pp.381-397, 1977.

[53] MacAdam, C.C., *"Application of an Optimal Preview Control for Simulation of Closed-Loop Automobile Driving,"* The Transactions on Systems, Man., and Cybernetics, Vol. SMC-11, No. 6, June 1981.

[54] Fancher, P.S. and Mathew A., *"A Vehicle Dynamics Handbook for Single-unit and Articulated Heavy Trucks,"* Final Report DOT-HS-807-185, UMTRI-86-37, May 1987.

[55] Segel, L, et al., *"The Mechanics of Heavy–Duty Trucks and Truck Combinations,"* The International Association for Vehicle Design, Chapter 15, Methods of Modeling the Truck Driver, pp. 559–604, 1987.

APPENDICES

Appendix I

EQUATIONS OF MOTION

The equations of motion describing the yaw-plane dynamic of the A-train double with two concepts in articulation damping (Case I and II) are expressed in the matrix form in Equation (I.1). The set of differential equations is solved using numerical integration algorithm, under a steering input δ_f to derive the directional response characteristics of the vehicle combination.

$$[A]\cdot\{\dot{x}\}=[B]\cdot\{x\}+\{MM\} \qquad \textbf{(I.1)}$$

where $[A]$ and $[B]$ are 8x8 matrices of vehicle's inertial properties and geometric parameters. The vector $\{MM\}$ contains the nonlinear tire forces and moments, and damping forces. The matrices $[A]$ and $[B]$ are identical for both cases of articulation damping, while the vector $\{MM\}$ differs for the two concepts. The general structure of the matrices $[A]$ and $[B]$ and vector $\{MM\}$, together with the elements are given below:

$$\begin{bmatrix} A_{11} & A_{12} & A_{13} & A_{14} & A_{15} & 0 & 0 & 0 \\ A_{21} & A_{22} & A_{23} & A_{24} & A_{25} & 0 & 0 & 0 \\ A_{31} & A_{32} & A_{33} & A_{34} & A_{35} & 0 & 0 & 0 \\ A_{41} & A_{42} & A_{43} & A_{44} & A_{45} & 0 & 0 & 0 \\ A_{51} & A_{52} & A_{53} & A_{54} & A_{55} & 0 & 0 & 0 \\ 0 & 0 & 0 & 0 & 0 & 1 & 0 & 0 \\ 0 & 0 & 0 & 0 & 0 & 0 & 1 & 0 \\ 0 & 0 & 0 & 0 & 0 & 0 & 0 & 1 \end{bmatrix} \cdot \begin{Bmatrix} \dot{V}_1 \\ \dot{r}_1 \\ \dot{r}_2 \\ \dot{r}_3 \\ \dot{r}_4 \\ \dot{\gamma}_1 \\ \dot{\gamma}_2 \\ \dot{\gamma}_3 \end{Bmatrix} = \begin{bmatrix} 0 & B_{12} & 0 & 0 & 0 & 0 & 0 & 0 \\ 0 & B_{22} & 0 & 0 & 0 & 0 & 0 & 0 \\ 0 & B_{32} & 0 & 0 & 0 & 0 & 0 & 0 \\ 0 & B_{42} & 0 & 0 & 0 & 0 & 0 & 0 \\ 0 & B_{52} & 0 & 0 & 0 & 0 & 0 & 0 \\ 0 & 1 & -1 & 0 & 0 & 0 & 0 & 0 \\ 0 & 0 & 1 & -1 & 0 & 0 & 0 & 0 \\ 0 & 0 & 0 & 1 & -1 & 0 & 0 & 0 \end{bmatrix} \cdot \begin{Bmatrix} V_1 \\ r_1 \\ r_2 \\ r_3 \\ r_4 \\ \gamma_1 \\ \gamma_2 \\ \gamma_3 \end{Bmatrix} + \begin{Bmatrix} MM_1 \\ MM_2 \\ MM_3 \\ MM_4 \\ MM_5 \\ 0 \\ 0 \\ 0 \end{Bmatrix}$$

$$A_{11} = m_1 + m_2 + m_3 + m_4 \; ; \qquad A_{12} = -X_{1A} \cdot (m_2 + m_3 + m_4)$$

$$A_{13} = -X_{2A} \cdot (m_2 + m_3 + m_4) - X_{2B} \cdot (m_3 + m_4) \; ; \qquad A_{14} = -X_{3B} \cdot (m_3 + m_4) - X_{3C} \cdot m_4$$

$$A_{15} = -X_{4C} \cdot m_4 \; ; \qquad A_{21} = A_{12} \; ; \qquad A_{22} = I_1 + (X_{1A})^2 \cdot (m_2 + m_3 + m_4)$$

$$A_{23} = X_{1A} \cdot X_{2A} \cdot (m_2 + m_3 + m_4) + X_{1A} \cdot X_{2B} \cdot (m_3 + m_4)$$

$$A_{24} = X_{1A} \cdot X_{3B} \cdot (m_3 + m_4) + X_{1A} \cdot X_{3C} \cdot m_4 \; ; \qquad A_{25} = X_{1A} \cdot X_{4C} \cdot m_4$$

$$A_{31} = A_{13} \; ; \qquad A_{32} = A_{23}$$

$$A_{33} = I_2 + (X_{2A})^2 \cdot m_2 + (X_{2A} + X_{2B})^2 \cdot (m_3 + m_4)$$

$$A_{34} = (X_{2A} + X_{2B}) \cdot (X_{3B} \cdot (m_3 + m_4) + X_{3C} \cdot m_4)$$

$$A_{35} = (X_{2A} + X_{2B}) \cdot X_{4C} \cdot m_4$$

$$A_{4j} = A_{j4} \qquad (j = 1, 2, 3)$$

$$A_{44} = I_3 + (X_{3B})^2 \cdot m_3 + (X_{3B} + X_{3C})^2 \cdot m_4 \; ; \qquad A_{45} = (X_{3B} + X_{3C}) \cdot X_{4C} \cdot m_4$$

$$A_{5j} = A_{j5} \qquad (j = 1, 2, 3, 4) \; ; \qquad \textit{and}$$

$$A_{55} = I_4 + (X_{4C})^2 \cdot m_4$$

$$B_{j2} = -A_{j1} \cdot U \qquad (j = 1, 2, 3, 4, 5)$$

The elements of forces and moments vector, $\{MM\}$, for Case I of articulation damping are derived as:

$$MM_{11} = \sum_{i=1}^{4} \sum_{j=1}^{3} F_{ij} + F_{KL} \cdot (\cos \beta_1 - \sin \zeta_1) - F_{MN} \cdot (\cos \beta_2 - \sin \zeta_2)$$

$$MM_{21} = X_{11} \cdot F_{11} - \sum_{j=2}^{3}\left(X_{1j} \cdot F_{1j}\right) - X_{1A} \cdot \left(\sum_{i=2}^{4}\sum_{j=1}^{3} F_{ij}\right) + \sum_{j=1}^{3} M_{1j} -$$
$$X_{1A} \cdot \left[F_{KL} \cdot (\cos\beta_1 - \sin\zeta_1) - F_{MN} \cdot (\cos\beta_2 - \sin\zeta_2)\right]$$

$$MM_{31} = -X_{2A} \cdot \left(\sum_{i=2}^{4}\sum_{j=1}^{3} F_{ij}\right) - \sum_{j=1}^{3}\left(X_{2j} \cdot F_{2j}\right) - X_{2B} \cdot \left(\sum_{i=3}^{4}\sum_{j=1}^{3} F_{ij}\right) + \sum_{j=1}^{3} M_{2j} -$$
$$(X_{2A} + X_{2B}) \cdot \left[F_{KL} \cdot (\cos\beta_1 - \sin\zeta_1) - F_{MN} \cdot (\cos\beta_2 - \sin\zeta_2)\right] -$$
$$c \cdot (F_{KL} \cdot \sin\beta_1 - F_{MN} \cdot \sin\beta_2)$$

$$MM_{41} = -X_{3B} \cdot \left(\sum_{i=3}^{4}\sum_{j=1}^{3} F_{ij}\right) - \sum_{j=1}^{3}\left(X_{3j} \cdot F_{3j}\right) - X_{3C} \cdot \sum_{j=1}^{3} F_{4j} + \sum_{j=1}^{3} M_{3j} +$$
$$a \cdot (F_{KL} \cdot \sin\zeta_1 - F_{MN} \cdot \sin\zeta_2) + b \cdot (F_{KL} \cdot \cos\zeta_1 - F_{MN} \cdot \cos\zeta_2)$$

$$MM_{51} = -X_{4C} \cdot \sum_{j=1}^{3} F_{4j} - \sum_{j=1}^{3}\left(X_{4j} \cdot F_{4j}\right) + \sum_{j=1}^{3} M_{4j}$$

The elements of forces and moments vector, $\{MM\}$, for Case II of articulation damping are derived as:

$$MM_{11} = \sum_{i=1}^{4}\sum_{j=1}^{3} F_{ij} + F_{KL} \cdot (\cos\theta_1 + \cos\zeta_1) + F_{MN} \cdot \left(\sin\left(\theta_2 - \frac{\pi}{2}\right) + \sin\left(\zeta_2 - \frac{\pi}{2}\right)\right)$$

$$MM_{21} = X_{11} \cdot F_{11} - \sum_{j=2}^{3}\left(X_{1j} \cdot F_{1j}\right) - X_{1A} \cdot \left(\sum_{i=2}^{4}\sum_{j=1}^{3} F_{ij}\right) + \sum_{j=1}^{3} M_{1j} -$$
$$X_{1A} \cdot \left[F_{KL} \cdot (\cos\theta_1 + \cos\zeta_1) + F_{MN} \cdot \left(\sin\left(\theta_2 - \frac{\pi}{2}\right) + \sin\left(\zeta_2 - \frac{\pi}{2}\right)\right)\right]$$

$$MM_{31} = -X_{2A} \cdot \left(\sum_{i=2}^{4} \sum_{j=1}^{3} F_{ij} \right) - \sum_{j=1}^{3} \left(X_{2j} \cdot F_{2j} \right) - X_{2B} \cdot \left(\sum_{i=3}^{4} \sum_{j=1}^{3} F_{ij} \right) + \sum_{j=1}^{3} M_{2j} -$$

$$\left(X_{2A} + X_{2B} \right) \cdot \left[F_{KL} \cdot \left(\cos \theta_i + \cos \zeta_1 \right) + F_{MN} \cdot \left(\sin \left(\theta_2 - \frac{\pi}{2} \right) + \sin \left(\zeta_2 - \frac{\pi}{2} \right) \right) \right] -$$

$$c \cdot \left[F_{KL} \cdot \sin \theta_1 - F_{MN} \cdot \cos \left(\theta_2 - \frac{\pi}{2} \right) \right]$$

$$MM_{41} = -X_{3B} \cdot \left(\sum_{i=3}^{4} \sum_{j=1}^{3} F_{ij} \right) - \sum_{j=1}^{3} \left(X_{3j} \cdot F_{3j} \right) - X_{3C} \cdot \sum_{j=1}^{3} F_{4j} + \sum_{j=1}^{3} M_{3j} -$$

$$\left(X_{3B} + X_{3C} \right) \cdot \left[F_{KL} \cdot \cos \zeta_1 + F_{MN} \cdot \sin \left(\zeta_2 - \frac{\pi}{2} \right) \right]$$

$$MM_{51} = -X_{4C} \cdot \sum_{j=1}^{3} F_{4j} - \sum_{j=1}^{3} \left(X_{4j} \cdot F_{4j} \right) + \sum_{j=1}^{3} M_{4j} +$$

$$a \cdot \left[F_{KL} \cdot \cos \zeta_1 + F_{MN} \cdot \sin \left(\zeta_2 - \frac{\pi}{2} \right) \right] + b \cdot \left[F_{KL} \cdot \sin \zeta_1 - F_{MN} \cdot \cos \left(\zeta_2 - \frac{\pi}{2} \right) \right]$$

Appendix II

STEADY-STATE HIGH-SPEED OFFTRACKING (HOF) ANALYSIS

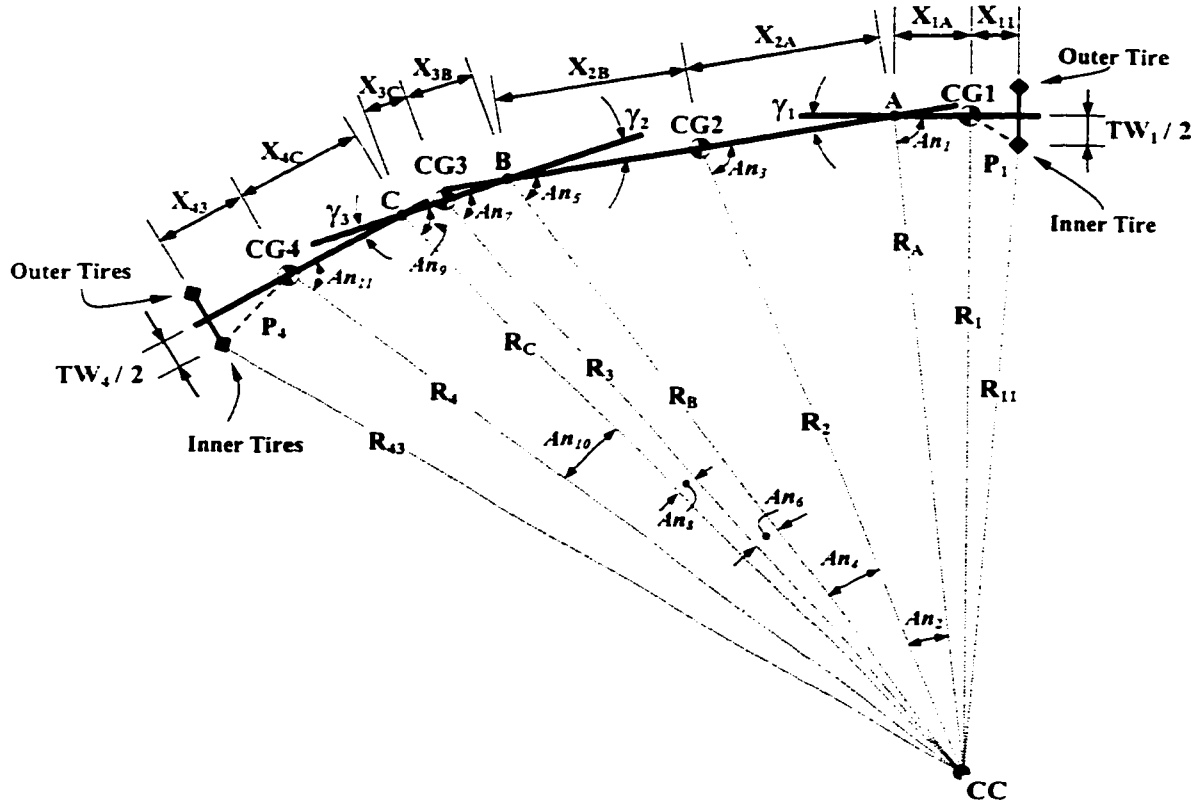

Figure II.1: A-train double during a steady-state turning maneuver.

The steady-state high-speed offtracking of the A-train double is defined as the difference between the turning radii of front and rearmost axles, R_{11} and R_{43}, shown in Figure II.1. The HOF of the vehicle combination has been evaluated assuming linear cornering properties of tires [54, 55]. The present analysis involves nonlinear tire forces and moments, and damping forces. The reported method thus cannot be applied for analysis of HOF of the A-train double.

In this study, the HOF is analyzed from the steady-state response behavior of the nonlinear yaw-plane model and the geometric parameters of the vehicle. The turn radius

R_1 of the steady-state path followed by the CG of the leading unit (unit 1) is initially estimated from the steady-state yaw rate response, such that:

$$R_1 = \frac{U}{r_1} \tag{II.1}$$

The turning radius of the inboard tires of the front axle is then evaluated from the geometry of unit 1.

$$R_{11} = \sqrt{R_1^2 + P_1^2 - 2 \cdot R_1 \cdot P_1 \cdot \cos\left\{\pi/2 - \arctan\left[\frac{OW_1/2}{X_{11}}\right]\right\}} \tag{II.2}$$

where OW_1 is the overall track width of the front axle and

$$P_1 = \sqrt{X_{11}^2 + (OW_1/2)^2}$$

The turn radius of the articulation joint **A**, R_A, and CG of unit 2, R_2, are then evaluated as:

$$\begin{aligned} R_A &= \sqrt{R_1^2 + X_{1A}^2} \\ R_2 &= \sqrt{R_A^2 + X_{2A}^2 - 2 \cdot R_A \cdot X_{2A} \cdot \cos\{\pi - \gamma_1 - An_1\}} \end{aligned} \tag{II.3}$$

where

$$An_1 = \arctan\left[\frac{R_1}{X_{1A}}\right]$$

The turn radius of the articulation joint **B**, R_B, and CG of unit 3, R_3, are then evaluated as:

$$R_B = \sqrt{R_2^{\,2} + X_{2B}^{\,2} - 2 \cdot R_2 \cdot X_{2B} \cdot \cos\{\pi - An_3\}}$$
$$R_3 = \sqrt{R_B^{\,2} + X_{3B}^{\,2} - 2 \cdot R_B \cdot X_{3B} \cdot \cos\{\pi - \gamma_2 - An_5\}} \qquad \textbf{(II.4)}$$

where

$$An_2 = \arcsin\left\{\frac{X_{2A}}{R_2} \cdot \sin[\pi - \gamma_1 - An_1]\right\};$$
$$An_3 = \gamma_1 + An_1 - An_2;$$
$$An_4 = \arcsin\left\{\frac{X_{2B}}{R_B} \cdot \sin[\pi - An_3]\right\}; \quad \text{and}$$
$$An_5 = An_3 - An_4$$

The turn radius R_C and R_4 of the articulation joint **C** and CG of unit 4, respectively, are expressed as:

$$R_C = \sqrt{R_3^{\,2} + X_{3C}^{\,2} - 2 \cdot R_3 \cdot X_{3C} \cdot \cos\{\pi - An_7\}}$$
$$R_4 = \sqrt{R_C^{\,2} + X_{4C}^{\,2} - 2 \cdot R_C \cdot X_{4C} \cdot \cos\{\pi - \gamma_3 - An_9\}} \qquad \textbf{(II.5)}$$

where

$$An_6 = \arcsin\left\{\frac{X_{3B}}{R_3} \cdot \sin[\pi - \gamma_2 - An_5]\right\};$$
$$An_7 = \gamma_2 + An_5 - An_6;$$
$$An_8 = \arcsin\left\{\frac{X_{3C}}{R_C} \cdot \sin[\pi - An_7]\right\}; \quad \text{and}$$
$$An_9 = An_7 - An_8$$

The turn radius of the inboard tire on the rearmost axle, R43, is finally evaluated from the geometry of unit 4, and expressed as:

$$R_{43} = \sqrt{R_4^2 + P_4^2 - 2 \cdot R_4 \cdot P_4 \cdot \cos\left\{\pi - An_{11} - \arctan\left[\frac{OW_4/2}{X_{43}}\right]\right\}} \qquad \textbf{(II.6)}$$

where

$$An_{10} = \arcsin\left\{\frac{X_{4C}}{R_4} \cdot \sin\left[\pi - \gamma_3 - An_9\right]\right\};$$

$$An_{11} = \gamma_3 + An_9 - An_{10}; \quad \text{and}$$

$$P_4 = \sqrt{X_{43}^2 + (OW_4/2)^2}$$

The high-speed steady-state offtracking (HOF) of the vehicle combination is then evaluated from:

$$HOF = R_{11} - R_{43}$$

If ***HOF*** is positive, the inner tires of the axle$_{43}$ follow a path whose radii is smaller that the radii described by the path followed by the inner tire of the axle$_{11}$. The rearmost tires of the last unit are thus observed to be inboard respect to the tire of the front axle of Unit 1. On the other hand, if ***HOF*** is negative, the inner tires of the axle$_{43}$ follow a path whose radii is greater than the radii described by the path followed by the inner tire of the axle$_{11}$. The rearmost tires of the last unit are thus observed to be outboard with respect to the tire of the front axle of Unit 1.